Universidade de Lisboa

Instituto de Geografia e Ordenamento do Território

Spatial modelling of the Temperature at the Top of Permafrost in Cierva Point (Antarctic Peninsula)

Sara Ramos Marín

Dissertação orientada pelo Prof. Dr. Gonçalo Brito Guapo Vieira e coorientada pelo Dr. Gabriel Alejandro Goyanes

Mestrado em Sistemas de Informação Geográfica e Modelação Territorial Aplicados ao Ordenamento

2018

Universidade de Lisboa

Instituto de Geografia e Ordenamento do Território

Spatial modelling of the Temperature at the Top of Permafrost in Cierva Point (Antarctic Peninsula)

Sara Ramos Marín

Dissertação orientada pelo Prof. Dr. Gonçalo Brito Guapo Vieira e coorientada pelo Dr. Gabriel Alejandro Goyanes

Júri:

Presidente: Professor Doutor Eusébio Joaquim Marques dos Reis do Instituto de Geografia e Ordenamento do Território da Universidade de Lisboa.

Vogais:

- Professor Doutor Gonçalo Brito Guapo Teles Vieira do Instituto de Geografia e Ordenamento do Território da Universidade de Lisboa.
- Professor Doutor Marc Oliva i Franganillo do Departamento de Geografia da Universidad de Barcelona.

2018

Acknowledgements

The completion of this master thesis has been much more than analysing data and writing an ordinary dissertation, it has been an opportunity to get involved in the world of permafrost research and polar science.

I would like to thank my supervisor, Professor Gonçalo Vieira, for trusting me for the development of this research and for giving me the chance to discover the beautiful area of Cierva Point to collect the data in-situ. Stepping in "the end of the world" and getting in contact with the Antarctic territory allowed me to better understand the importance of monitoring the impacts of climate change in such sensitive environment and empowered my motivation to carry out this study.

Many thanks to Gabriel Goyanes, who accompanied me on the journey and supported me in every adventure working on field. Without his patience, Antarctic experience and drone pilot skills, I would not have been able to get all the fundamental data indispensable to carry out this work.

Special acknowledgments to the Portuguese Polar Program 2017/18 (PROPOLAR) for funding this research and facilitating the logistics that make possible the larger scale project about "Permafrost and Climate Change in the Antarctic Peninsula" (PTDC/AAG-GLO/3908/2012 – FCT, Portugal). Also, to Ana Salomé for all the support provided during my trip to Antarctica and for her great skills to handle any kind of incident.

Thanks as well to the project "Impact of Recent Climate Warming on Active-Layer Dynamics, Permafrost, and Soil Properties on the Western Antarctic Peninsula" (ANT-6900673) from the National Science Foundation (USA), in which the boreholes used in this work were installed. On the framework of this project, Prof. James Bockheim and Dr. Kelly Wilhelm provided the shallow borehole data for the years from 2012 to 2014.

Always thankful with my father, Miguel Ramos, who introduced and guided me on my first steps into the world of polar sciences, with the passion and enthusiasm of who devoted his life to the research in Antarctica. Thanks as well to my mum, the one that stands my anxiety and always have the magic words to keep me calm in the most stressful situations.

Finally, yet important, thanks to all my colleagues, teachers and friends that helped me during the last two years, either with advice, knowledge or encouragement.

TABLE OF CONTENTS

TABLE OF FIGURES

TABLE OF CHARTS

TABLE OF EQUATIONS

Abstract

The Western Antarctic Peninsula (WAP) has shown complex reactions to climate change in the last decades. To evaluate the changes occurring in these environments, permafrost and active layer monitoring and modelling are essential. In this dissertation, the characteristics of the ground temperature regime are analysed and the spatial distribution of the "Temperature at the Top of Permafrost" (TTOP) in Cierva Point (Danco Coast, WAP) is estimated using topo-climatic information over an area of 0.65 km^2. With the results, the climate sensitivity of permafrost in this area and the potential impact of small climate change in its extent are evaluated.

A first evaluation of the temperature regimes allowed to determine the temperature and depth of the permafrost table and the ground thermal offset using observed borehole and climate data from nine different monitoring sites, in selected periods from 2012 to 2018. The top of permafrost was observed at depths of 0.4, 1 and 5m and the temperature at these depths was observed to be -1.4 ºC, -2.6 ºC and 1.2 ºC in these locations. For the monitoring boreholes where the top of permafrost was not reached, the depth of the top of permafrost was estimated to range between 0.4 and 5 m with temperatures ranging between -0.2 ºC and -2.6 ºC.

The results were used together with topographic data to implement the spatial TTOP model using a Geographical Information System (GIS)-based methodology to implement a high-resolution model (1 x 1 m grid cell) that allows a further insight into the spatial characteristics of permafrost.

Permafrost was estimated to be present in nearly 88% of the area and the lower TTOP values were found at high altitudes and unconsolidated soil or peat areas covered by moss. The highest TTOP results were found at low altitudes, bare surfaces and concave areas. Bare surfaces increase exposure to solar radiation during the summer and the concavity of the terrain promotes higher snowpack accumulation during the winter, which acts as a good thermal insulator hindering ground energy loses.

In the areas where the mean temperature at the top of permafrost was found to be higher than 0 ºC, permafrost is absent and the TTOP stands for the temperature at the base of the seasonal freezing layer.

An increment of the TTOP was observed in case of a hypothetical long-term increase of 1 ºC in the MAAT and the results suggest the disappearance of nearly 50% of the current modelled permafrost area. Ground temperatures resulted to be more sensitive to the temperature increment at bare ground surfaces and/or concave sites. The less sensitive areas were the ones covered by moss formations as well as the most convex.
Permafrost degradation in Cierva Point, which is an Antarctic Specially Protected Area, may lead to significate impacts in the local ecosystem.

Keywords: Permafrost, Active layer, temperature regime, Western Antarctic Peninsula, TTOP.

Resumo

Durante as últimas décadas, a região ocidental da Península Antártica manifestou reações complexas às mudanças climáticas e as suas causas ainda não foram completamente compreendidas. Na segunda metade do século XX, foi observada uma tendência de aquecimento na Península Antártica. Contudo, a partir do início do século XXI, observou-se uma tendência para o arrefecimento em algumas regiões da Península. Com o objetivo de avaliar os efeitos destas reações nos ambientes livres de gelo da região, é importante a monitorização e modelação do *permafrost* e da camada ativa. O *permafrost* é definido como solo permanentemente congelado (mantém a temperatura a/ou abaixo de 0 ºC durante pelo menos dois anos). A camada compreendida entre a superfície do solo e o topo do *permafrost*, e que congela e descongela sazonalmente, é designada como "camada ativa".

Nesta dissertação, são analisadas as caraterísticas do regime térmico do solo em Cierva Point (Costa de Danco Coast, Península Antártica Ocidental), numa área com 0.65 km^2 e apresenta-se um mapa da distribuição espacial da Temperatura no Topo do Permafrost (TTOP), usando dados topoclimáticos observados e modelizados. Com os resultados, é avaliada a sensibilidade climática do *permafrost* e o potencial impacte que mudanças na temperatura média anual poderão causar na sua extensão.

Inicialmente, foi desenvolvida uma análise do regime térmico do solo em nove locais com diferentes caraterísticas usando dados climáticos e de temperaturas do solo observados de 2012 a 2018 em perfurações instaladas na área de estudo. Esta análise, permitiu a determinação da espessura e da variabilidade interanual da camada ativa, da temperatura e profundidade do topo do *permafrost*, e finalmente, do *offset* térmico do solo (diferença de temperatura entre a superfície do solo e o topo do *permafrost*) nestes nove locais. O topo do *permafrost* (TOP) foi encontrado em três dos nove locais com diferentes caraterísticas a 0,4, 1 e 5 m de profundidade e com temperaturas de -1.4 ºC, -2.6 ºC e 1.2 ºC, respetivamente. Contudo, os dados mostraram que a presença de *permafrost* é possível em oito dos nove locais, embora a profundidades maiores que aquelas de algumas perfurações, que apenas se encontram na camada ativa. As temperaturas no topo do *permafrost* estimadas nestes nove locais variam entre -0,2 ºC e -2,6 ºC. Em geral, o topo do *permafrost* foi observado a maior profundidade em locais com afloramentos rochosos, seguindo-se os depósitos não consolidados e os substratos orgânicos formados por musgos.

Os resultados da análise do regime térmico foram utilizados, em conjunto com dados topográficos, para a implementação de um modelo espacial da "Temperatura no Topo do *Permafrost*" (TTOP) em toda a área de estudo, usando uma metodologia baseada nos Sistemas de Informação Geográfica (SIG). Para a implementação do modelo *TTOP*, foram determinadas relações estatísticas entre os fatores topográficos e os parâmetros que constituem o modelo usando como base os dados observados nos nove locais. O *software* SPSS Statistics 25 foi o utilizado para estimar as correlações estatísticas entre fatores topográficos e parâmetros observados e para determinar as relações matemáticas existentes entre eles. Mais tarde, as relações estatísticas encontradas foram espacialmente computadas sob a área de estudo mediante o *software* ArcMap 10.4, e finalmente aplicou-se a equação do modelo sob a área de estudo completa.

O resultado foi um modelo TTOP de alta resolução (1 m) que oferece pela primeira vez uma perspectiva da distribuição espacial do *permafrost* em Cierva Point. Os resultados do modelo *TTOP* ilustram os valores mais baixos (até -6.2 ºC) em solos orgânicos ou pouco consolidados cobertos por musgos e em altitude, do que em áreas de menor altitude de rocha nua, húmidas e em terrenos côncavos

Os valores da Temperatura no Topo do *Permafrost* modelizada mais elevados (superiores a 0 ºC e até 3,5 ºC), encontraram-se em áreas mais baixas, húmidas e com topografia côncava. Nestas áreas, os valores resultantes representam, efetivamente, a temperatura na base do solo gelado sazonal.

Embora a profundidade do topo do *permafrost* seja desconhecida, os resultados mostram que o *permafrost* deverá estar presente em 88% da área de estudo, estando ausente especialmente em setores com solo nú em altitudes inferiores a 120 m e com topografia côncava.

O modelo espacial desenvolvido foi ainda usado para identificar a potencial sensibilidade do *permafrost* face a um cenário hipotético de aumento da temperatura média anual do ar de longo prazo de 1 ºC, considerando estáveis os restantes fatores como a precipitação, a neve, a humidade do solo, a distribuição dos musgos, etc. Os resultados indicam um significativo aumento na temperatura no topo do *permafrost*, correspondendo a um valor médio de +1.2 ºC, e o possível desaparecimento das condições para a manutenção do *permafrost* em cerca de 50% da área com *permafrost* na atualidade. A área com permafrost, ficaria então reduzida a cerca de 43% da área de estudo. Os setores mais sensíveis a esta mudança de temperatura são

as áreas localizadas a menor altitude, caraterizadas por superfícies nuas e/ou elevados valores de concavidade topográfica. As áreas menos sensíveis ao impacte do aumento de temperatura são as com cobertura de musgos, pois estes atuam como isolante térmico, assim como as áreas com topografia convexa.

A dinâmica do *permafrost* é especialmente importante em Cierva Point, que é uma Área Especialmente Protegida no quadro do Sistema do Tratado para a Antártida (ASPA), devido à presença de uma colónia de pinguins *Gentoo*, assim como de coberturas de líquenes e musgos. A redução da área com *permafrost* poderá influenciar significativamente o ecossistema local, pelos seus impactes na hidrologia e consequentemente, na flora. As propriedades impermeáveis do *permafrost* promovem o escoamento de água nos horizontes superficiais do solo ou à superfície, bem como a formação de pequenas lagoas temporárias. O descongelamento do *permafrost*, poderá induzir o aumento da infiltração em profundidade, reduzindo a água disponível para a vegetação.

Keywords: *Permafrost*, camada ativa, regime de temperaturas, Península Antárctica Ocidental, TTOP.

Acronyms

CALM: Circumpolar Active Layer Monitoring.

DSM: Digital Surface Model.

DZAA: Depth of Zero Annual Amplitude.

ECV: Essential Climate Variable.

GCOS: Global Climate Observing System.

GST: Ground Surface Temperature.

GTN-P: Global Terrestrial Network for Permafrost.

IPA: International Permafrost Association.

IPCC: Intergovernmental Panel on Climate Change.

MAGST: Mean Annual Ground Surface Temperature.

MaxAST: Maximum Annual Surface Temperature.

MDAT: Mean Daily Air Temperature.

MinAST: Minimum Annual Surface Temperature.

Toffset: Thermal offset.

TSP: Thermal State of Permafrost.

TTOP: Temperature at the Top Of Permafrost.

TWI: Topographic Wetness Index.

UNEP: United Nations Environmental Programme.

UNFCC: United Nations Framework Convention on Climate Change.

WAP: Western Antarctic Peninsula.

WMO: World Meteorological Organization.

ZAA: Zero Annual Amplitude.

1 Introduction

1.1 Objectives

The main objective of this dissertation is to characterize the permafrost in Cierva Point (Western Antarctic Peninsula) and evaluate its climate sensitivity by assessing the main potential impact of small climate changes in the permafrost extent of this ice-free environment area. In order to achieve this goal, we analysed the area's ground temperature regime and created a GIS-based spatial model of the Temperature at the Top Of Permafrost (TTOP) based on statistical relations between certain topographic factors and locally computed TTOP parameters from climate observed data.

This work is included on the larger-scale framework of permafrost research in the ice-free terrestrial environments of Western Antarctic Peninsula, which aim to evaluate permafrost dynamics and its linkages to recent climate changes through systematic and long-term monitoring and modelling of ground and climate properties. The project is conducted by the CEG/IGOT team of the University of Lisbon, within the ANTPAS/SCAR expert group.

1.2 An overview of Permafrost and its global significance

1.2.1 WHAT IS PERMAFROST?

Permafrost is ground at or below the freezing point of water (0°C, 32°F) for at least two consecutive years (Brown et al., 1998). Permafrost forms in cold climates generally distinct by long winters without much of snow and short, dry and cold summers. In regions with such this climate, some of the ground frozen during the winter will not completely thaw during the summer; therefore, a permanent frozen layer will form and continue to grow downward gradually each year constituting the permafrost (Péwé, 1979).

Permafrost is distributed on Earth covering great stretches of land at high latitudes and altitudes in both hemispheres. In the Northern Hemisphere, permafrost occupies about 24% of the exposed land area in the Arctic and sub-Arctic, including large areas in Russia, Alaska and Canada. In the Southern Hemisphere, permafrost occurs in most ice-free regions of Antarctica (Schaefer et al., 2012; Bockheim et al., 2012). Alpine permafrost may exist at high altitudes in much lower latitudes, being present in the high mountains of South America, Central Asia, the United States and Europe (Péwé, 1979).

1.2.2 DISTRIBUTION OF PERMAFROST

Permafrost regions are classified into zones based on its spatial distribution. *"Continuous permafrost"* zones have permafrost underlying 90-100% of the land area; *"discontinuous permafrost"* zones have 50-90% of permafrost; and *"sporadic permafrost"* around the 10-50%. *"Isolated patches"* refer to regions where permafrost underlies less than 10% of the land area (Schaefer et al., 2012). Permafrost also occurs subsea on the continental shelves of the surrounding continent of the Arctic Ocean and Antarctica.

In the Northern Hemisphere permafrost occurs almost continuously in large areas, being normally absent under lakes and rivers that do not freeze to the bottom (Péwé, 1979). The location of the boundary of the continuous permafrost zone variates around the world because of regional climate controls. In areas characterized by warmer climates, permafrost occurs only in sheltered locations, usually with a north aspect (in the Northern Hemisphere) or south aspect (in the South Hemisphere), creating *discontinuous, sporadic* or *isolated permafrost*.

In the Southern Hemisphere, most of the Antarctic continent is overlain by glaciers and liable to basal melting (Zoltikov, 1962). The exposed ice-free land of Antarctica is extensively underlain with permafrost, some of which is liable to warming and thawing along the coastline (Campbell & Claridge, 2009).

Figure 1 represents the distribution of different types of permafrost in both South and North hemispheres.

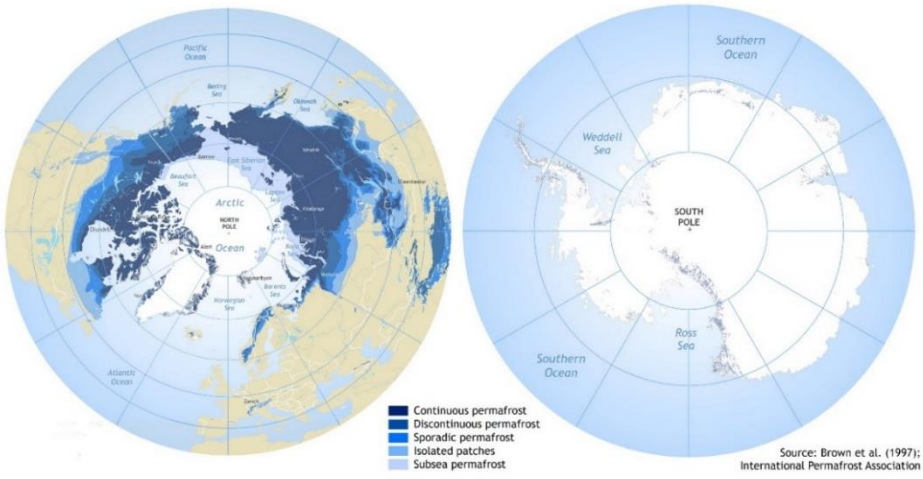

Figure 1. Distribution of permafrost in the North (left) and South (right) hemispheres (Brown et al., 1997).

1.2.2 PERMAFROST STRUCTURE AND THERMAL REGIME

The vertical structure of permafrost is determined by the ground temperatures at different depths and is represented in Figure 2.

When permafrost is present in areas not overlain by ice, it occurs beneath a layer of soil, rock or sediment, which freezes and thaws annually, which is called the *active layer* (Staff, 2014). The active layer generally starts thawing in spring after snow melt and may stay thawed until autumn, while its maximum depth is reached in late summer. It begins to refreeze in autumn with the onset of winter and is completely frozen by late winter or early spring (Schaefer et al., 2012).

The *active layer thickness* is the annual maximum thaw depth at the end of the summer. It depends mainly on the moisture content, being thinner in wet, organic sediments and thicker in well-drained gravels or bedrock. Active layer thickness can be less than 30 cm in continuous permafrost along the Arctic coast and the Antarctic continent, where values range generally from 0.2 to 0.7 m, occasionally with >0.9 m in coastal sites and with very shallow active layers (<0.1 m) at high elevation sites (Vieira et al., 2010). The active layer thickness usually reaches 2 m or more in discontinuous permafrost of Southern Siberia, and several meters in the European Alps and on the Qinghai-Tibetan Plateau (Schaefer et al., 2012). In the Antarctic Peninsula, the active layer thickness was found to be greater than 0.9 m on monitored sites at unconsolidated materials in the South Shetlands Islands, and around 0.3 m in Deception Island (Vieira et al., 2010).

Under the active layer, permafrost occurs at the depth where the maximum annual temperature remains below 0 ºC, and is bounded on the top by the *Top of Permafrost (TOP)* and on the bottom by the *Base of Permafrost (BOF)* (Schaefer et al., 2012).

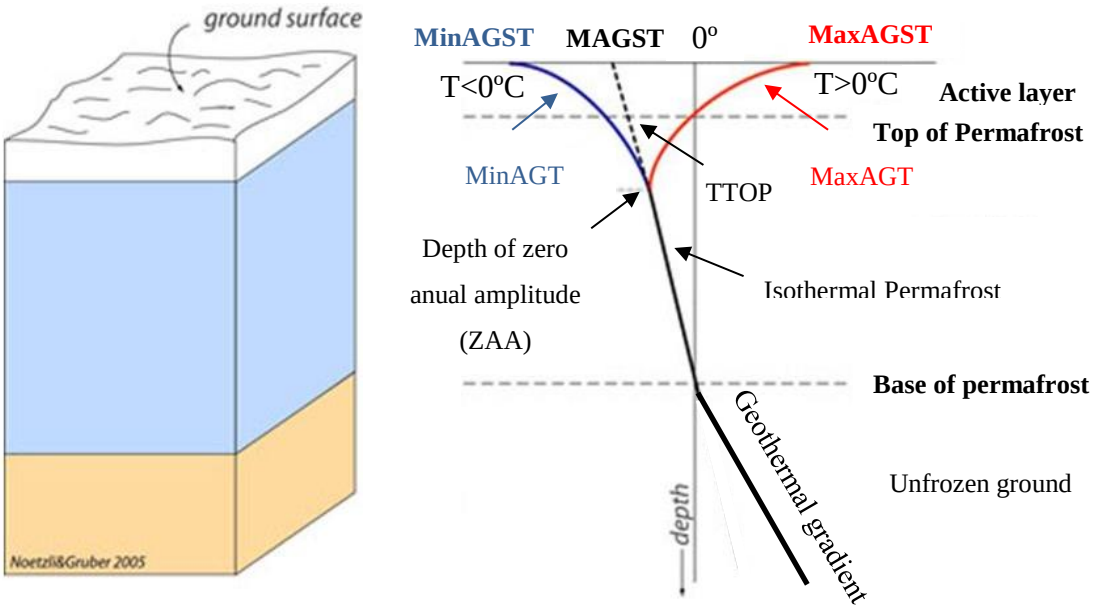

Figure 2. Permafrost vertical structure defined by its ground thermal regime- trumpet curve (modified from: Cassie, n.d.).

The annual variations of air temperature from winter to summer is revealed in the active layer and in the few first meters of the permafrost. In this layer, the ground temperature profile over a temperature to depth graph (Figure 2), presents three different curves that represent the variation of ground temperature with depth. The red curve represents the *Maximum Annual Ground Temperature* (MaxAGT), the dotted line represents the *Mean Annual Ground Temperature* (MAGT) and the *Minimum Annual Ground Temperature* is represented by the blue curve (MinAGT).

The MaxAGT decreases with depth being the depth at which the maximum annual temperature reaches 0º C considered the base of the active layer, and the top of permafrost, which is known as *Temperature at the Top Of Permafrost (TTOP).* The point where the red curve crosses the ground surface represents the *Maximum Annual Ground Surface Temperature (MaxAGST).*

The MinAGT increases with depth being and the point where the blue curve crosses the ground surface represent the *Minimum Annual Ground Surface Temperature (MinAGST).*

The MAGT can either increase or decrease depending on a positive or negative ground *thermal offs*et. The thermal offset's magnitude is the difference between the mean annual ground temperature at the top of permafrost and the MAGST, and it depends on the soil thermal properties.

The point where the dotted line crosses the surface represents the *Mean Annual Ground Surface Temperature (MAGST).*

Despite the curve of the MAGT being often considered linear for simplification of the modelling, Goodrich (1978) showed that the MAGT warming at depth is not linear, but offsets to progressively lower values at depth within the active layer (Smith & Riseborough, 1996).

Under the surface, the seasonal ground temperature signal becomes smaller with depth due to the thermal balance between the heat flow from the Earth's interior and that flowing outward into the atmosphere. When the amount of geothermal heat reaching the permafrost equals the heat lost to the atmosphere, the permafrost temperature reaches equilibrium and becomes seasonally stable at the depth of *Zero Annual Amplitude* (ZAA) (Péwé, 1979). The temperature at the Z depth is known as the *Temperature at the depth of Zero Annual Amplitude* (TZAA). Because the maximum temperature at the top of permafrost is 0 ºC, no significant phase change occurs at lower depths, such that soil thermal properties below the active layer remain relatively constant. For practical purposes, the temperature at the top of permafrost should be close to the temperature measured at the depth of zero annual amplitude (Smith & Riseborough, 1996).

Below the ZAA depth, the temperature of permafrost does not change seasonally, and hence this layer is named *isothermal permafrost* (Delisle, 2007). In the isothermal permafrost layer, the temperature increases steadily under the influence of heat from the Earth's interior until overpassing 0 ºC due to the geothermal gradient. This point constitutes the *base of permafrost (BOP)* (Péwé, 1979).

1.2.3 CONTROLLING FACTORS IN PERMAFROST: CLIMATE, WATER BODIES, SOLAR RADIATION, VEGETATION AND SNOW

The distribution and thickness of permafrost are directly affected by climate, ground properties and geothermal gradient, topography, snow, vegetation and water cover (Péwé, 2016).

- Air temperature and climate

Air temperature is the dominant variable controlling global permafrost distribution and climate and it directly affects the thickness of the permafrost layer. When the climate warms to a mean annual air temperature above 0 °C, the position of the *top of permafrost* will be lowered by thawing. As the climate becomes colder or warmer, the temperature of the permafrost respectively rises or declines, resulting in changes in the position of the bottom of permafrost. Generally, the colder the climate, the thicker the permafrost layer (Péwé, 2016).

Considering the relation of the ground characteristics with atmospheric temperatures, permafrost may be considered as a good indicator of climate sensitivity.
Seasonal variability in shallow ground temperature reflects variability in air temperature at the short-term but becomes increasingly muted with depth. Permafrost temperatures at deeper depths reflect variability in climate conditions at longer time scales due to the slow diffusion of heat through permafrost. Below the ZAA depth, where the permafrost temperature has no seasonal variation, permafrost temperatures reflect long-term climate variations (Schaefer et al., 2012).

- Ground properties and geothermal gradient

The rate at which the base or top of permafrost change depends not only on the magnitude of climatic fluctuation but also on the ground's composition, properties and ice content, since these factors determine the ground's thermal conductivity (Péwé, 2016). If the mean annual air temperature is identic in two different areas, the permafrost layer will be thicker where the conductivity of the ground is higher and the geothermal gradient is lower.

- Topography and solar radiation

The slope and aspect of the ground also influence permafrost formation and active layer thickness. South-facing hillslopes in the Northern Hemisphere, as well as north-facing slopes in the Southern Hemisphere, receive more incoming solar energy per unit area than other slopes and therefore they get warmer. For instance, in the North Hemisphere, permafrost is usually absent in the regions of discontinuous permafrost in south facing slopes while shaded north facing slopes may develop continuous permafrost (Schaefer et al., 2012)

- Vegetation

Vegetation and soil organic matter can also influence permafrost formation and active layer thickness.

Their effects often result in large variability in active layer thickness within the space of a few meters (Humlum, 1998a). Shading by vegetation and the insulating effect of a thick organic layer, reduces the solar energy absorbed by the soil, resulting in shallower active layers than bare exposed soil (Shur & Jorgensen, 2007).

- Snow cover

After the air temperature, local snow thickness and characteristics are the dominant variables controlling global permafrost distribution (Schaefer et al., 2012) as they influence heat flow between the ground and the atmosphere (Péwé, 2016). Any location with annual average air temperatures below freezing can form permafrost (Humlum, 1998b; Stocker-Mittaz et al. 2002). However, depending on the snow accumulation and other environmental factors, permafrost may even be present in regions with mean annual air temperature as high as 2 °C or absent where annual average air temperature is as low as -20 °C (Jorgensen et al., 2010).

Snow is a good thermal insulator as it is composed by air and ice crystals in its volume. This fact often results in ground temperatures 5 to 20 °C higher than winter air temperatures and permafrost temperatures 3 to 6 °C higher than the mean annual air temperature. Snowpack thickness, timing and duration, hence influence ground temperature (Zhang, 2005; Jorgensen et al., 2010).

- Water bodies

Finally, bodies of water such as lakes, rivers, and the sea show a noticeable effect on the distribution of permafrost. A deep lake that does not freeze to the bottom during the winter will be underlain by a zone of thawed material. Small, shallow lakes that freeze to the bottom each winter are underlain by a zone of thawed material, but the thawed zone normally does not completely penetrate the surrounding permafrost extent (Péwé, 2016).

1.2.4 TYPICAL LANDFORMS IN PERMAFROST ENVIRONMENTS

Permafrost processes manifest themselves in large-scale landforms, such as thermokarst phenomena, polygonal ground and pingos. In addition, there are many features caused in large part by frost action that are common but not restricted to permafrost areas, such as solifluction (frost creep and flow) and frost-sorted patterned ground.

The main geomorphic features present in permafrost environments are described below (Péwé, 2016):

- Polygonal ground

One of the most common geomorphic features associated with permafrost is the relief pattern on the surface of the ground, usually called "*polygonal ground"*, or "*tundra polygons"*. This pattern appears with the formation of a network of shallow troughs delineating 3 to 30 m diameter polygons and occurs as the result of winter freezing and spring thawing. In winter, the soil becomes brittle and cracks due to the contraction in response to cold temperatures. In spring, meltwater fills the cracks and consequently freezes forming ice wedges (Dick, 2012). Season after season, the cracks and ice wedges increase in diameter and depth. From the air perspective, the tundra will show a pattern of cracks looking like honeycombs (Figure 3).
In many areas of the continuous permafrost zone, drainage follows the troughs of the tops of the ice wedges forming the polygons; and at ice wedge junctions, melting may occur to form small pools. The joining of these small pools by a stream causes what is known as *beaded drainage* (Figure 4). Such drainage evidences the presence of perennially frozen, fine-grained sediments cut by ice wedges (Péwé, 1979).

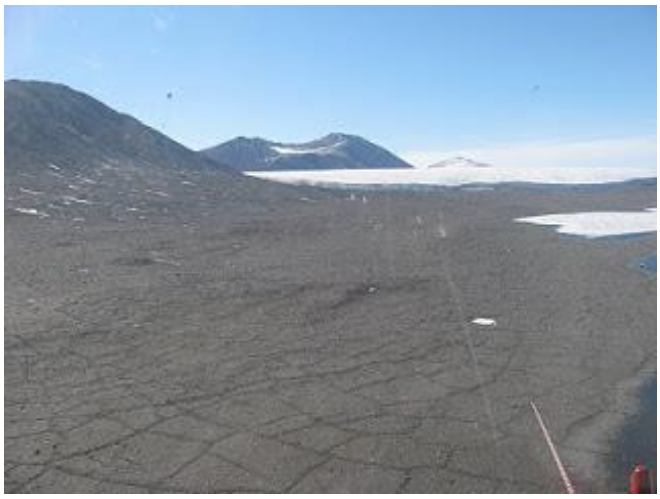

Figure 3. Helicopter view from of the *polygonal ground* in the F6 camp on Lake Fryxell in Taylor Valley (McMurdo, Dry Valleys region, Antarctica) (Ball, 2010).

Figure 4. *Tundra polygons* and *beaded drainage* on the north slope in the Arctic National Wildlife Refuge, Alaska (Shaw, 2015).

- Thermokarst

The thawing of permafrost creates thermokarst topography, an irregular surface containing mounds, sinkholes, caves, tunnels and steep-walled ravines resulting from the melting of ground ice (Péwé, 1979).

Thawed depressions filled with water are known as *thermokarst lakes* (Figure 5) and are widespread in permafrost regions, especially in those underlain with permanently frozen silt. They can appear on hillsides or even on hilltops and are good indicators of ice-rich permafrost (Péwé, 1979).

Figure 5. Circular thermokarst lakes in peatlands, Hudson Bay Lowlands, Manitoba. Natural Resources Canada (de Schutter, 2004).

- Pingos

Other landforms linked to permafrost are *pingos*, which are ice-cored circular or elliptical hills of frozen sediments or bedrock. Pingos can reach dimensions up to 60 m high and 450 m in diameter. They can occur in the continuous permafrost zone, especially in the tundra. They are much less outstanding in the forested area of the discontinuous permafrost zone. Frequently they are cracked on top with summit craters formed by thawing massive ice (Figure 6) (Péwé, 1979).

Figure 6. Open system *pingo* in upper Eskerdalen, 35 km east of Longyearbyen, Svalbard, Norway. Photo: Hanne Christiansen (Ingólfsson, 2008).

- Patterned ground

Intense and repeated freezing and thawing throughout the year produces small-scale patterned ground. This phenomenon tends to stir and sort granular sediments, forming circles, stone nets, and polygons a few centimetres to 6 m in diameter (Figure 7) (Péwé, 1979). These features require a cold climate besides a ground composed by some fine-grained soils and high water content, but they do not necessarily need to be underlained by permafrost. However, permafrost constitutes a non-permeable substrate that keeps the soil water content available for freezing.

Figure 7. Sorted circles 2–3 m in diameter with gravel borders about 0.25 m high, Broggerhalvoya, NW Spitsbergen (Hallet, 2013).

- Solifluction

In areas underlain by an impermeable layer of seasonal frozen ground, the active layer is often saturated with water and becomes easily deformable. The progressive downslope movement of water saturated soil under the action of gravity and frost is called *solifluction*. This material moves in a semifluid condition and results in lobe-like and sheet-like flows of soil on slopes. The pattern formed on the ground because of this phenomenon is known as *solifluction lobes and sheets* (Figure 8). An outstanding feature of solifluction is the mass transport of material over low-angle slopes (Péwé, 1979).

Figure 8. *Solifluction lobes* on the Ulu Peninsula, James Ross Island, Antarctica (Bethan, 2017).

1.3 Global and regional impacts of permafrost dynamics in a global warming scenario

Permafrost and its dynamics are important components of the cryosphere as well as the Earth system as a whole. These dynamics interact with ecosystems and climate on various spatial and temporal scales.

Climate change is expected to have considerable effects above and below ground climate being the main reason for the modifications of the structure and distribution of permafrost (Schaefer, 2014). The combination of complex permafrost-ecosystem-climate interactions in a warming world could exacerbate the overall impacts of permafrost dynamics to the Earth system. The feedbacks resulting from these interactions range from local impacts on ecosystem processes, to complex influences on global scale biogeochemical cycling (Grosse et al., 2016).

1.3.1 GLOBAL IMPACTS OF PERMAFROST DYNAMICS

Global concerns on permafrost dynamics are related with the Earth's carbon cycle. The most recent studies investigating the permafrost carbon pool size estimate that 1035 Gt of carbon is stored in the frozen organic soil in the northern circumpolar permafrost region (Schuur, 2015). The rest of Earth's biomes, excluding the Arctic and boreal regions, are thought to contain around 2,050 Gt carbon. This pool may cause climate impacts at the global scale upon thaw and mobilization (Schuur et al., 2015). This is, if permafrost thaws where carbon pools are present, the stored carbon may be released in the form of carbon dioxide and methane, which are powerful greenhouse gases that would again contribute to an increased rate of warming constituting a feedback loop (Schaefer, 2014).

In Antarctica, permafrost shows lower carbon content and its contribution to greenhouse gas fluxes is minor at a global scale (Turner et al., 2009). The contribution of Antarctic permafrost might have even the opposite effect than Arctic permafrost because recently deglaciated terrain, or areas with a thickening active layer, may function in the intermediate to long-term as carbon sinks due to increased biomass from colonization by new plant species and microbial communities (Vieira et al., 2010)

1.3.2 REGIONAL IMPACTS OF PERMAFROST DYNAMICS

Local and regional consequences of changes in permafrost dynamics vary from changes in the ecosystem's vegetation, fauna, hydrology and terrain, to costly infrastructural damages and economic costs (Grosse et al., 2016).

- Ecosystem disturbances: vegetation, hydrology, and fauna.

  Plant life can be supported only within the active layer since growth can occur only in soil that is fully thawed for some part of the year. Therefore, plant growth and rooting zones are largely restricted to the active layer, since roots cannot penetrate the frozen ground beneath (Ullrich, 2016). Because of this, the dominant ecosystems in permafrost regions are boreal forests and tundra. Sedges, shrubs, mosses and lichens dominate tundra vegetation while evergreen spruce, fir and pine, as well as the deciduous larch or tamarack dominate boreal forests.

  In the Arctic, boreal forests occur in the southern regions and tundra up in the north (Schaefer et al., 2012). The tundra in Antarctica occurs mainly close to the coastline, while cold deserts occur in the mainland and at high altitude (Lopez-Terril, 2014). In mountainous permafrost regions, forests dominate at lower elevations and tundra at higher elevations (Schaefer et al., 2012).

  Regarding the hydrology and fauna in permafrost regions, permafrost is impermeable to water, so rain and melt water accumulate on the surface forming numerous lakes and wetlands. These lakes and wetlands are favourable to migratory birds from around the world, which use them as summer breeding grounds (Schaefer et al., 2012). However, permafrost constitutes also limitations for fauna requiring subsurface homes, as building dens and burrows in the frozen ground beneath the surface is often harsh. Other species dependent on plants and animals, such as bacteria, have their habitat constrained by the permafrost as well. One gram of soil from the active layer may include more than one billion bacteria cells. However, the number of bacteria in permafrost soil is much lower varying typically from 1 to 1000 million per gram of soil (Hansen, 2017). Permafrost degradation may disturb ecosystems and change species composition, modifying wildlife habitats and migration (Schaefer, 2012).

The main ecosystem factor affected by degrading permafrost will be the local hydrology, which will suffer changes with wetlands and lakes forming in continuous permafrost and disappearing in discontinuous permafrost (Smith et al., 2005).

- Terrain disturbances: Topography and slope stability

Climate change is expected to increase erosion rates along the Arctic and Antarctic coastline (Schaefer, 2012). As much of the structural stability in mountain ranges can be attributed to glaciers and permafrost, thawing permafrost in steep mountain terrain increases the risk of rock falls and landslides (Harris et al. 2001). Talus and rock faces cemented together by ice in mountainous permafrost zones can form rock glaciers that creep downhill at velocities of centimetres to several meters per year (Figure 9).

Figure 9. Rock and talus debris flowing downhill in a rock glacier near McCarthy, Alaska (photo: Isabelle Gärtner-Roer) (Schaefer et al., 2012).

If temperatures increase, ice on the permafrost will deform more easily of even thaw, resulting in an increase of collapse risk, landslides and rock glacier flow (Schaefer et al., 2012).

- Infrastructure:

Thawing permafrost is structurally weak, resulting in foundational settling that can damage or even destroy infrastructure as buildings, roads, pipelines, railways, and power lines (Figure 10). Infrastructure failure can have dramatic environmental consequences, as seen in the 1994 breakdown of the pipeline of the Vozei oilfield in

Northern Russia, which resulted in a spill of 160,000 tons of oil, the world's largest terrestrial oil spill (Schaefer et al., 2012).

Permafrost regions in the North Hemisphere are more vulnerable to damage as it counts with more infrastructure and population than the South Hemisphere permafrost regions. However, the effect of climate change on subsidence on Antarctica is of major concern, particularly in coastal areas with abundant ground ice, since despite the small total area of infrastructure in Antarctica, financial investments are substantial (Vieira et al., 2010).

Figure 10. Irregular settling due to permafrost thaw destroyed this apartment building in Cherski, Siberia (photo: Vladimir Romanovsky, in Schaefer et al., 2012).

The impacts of the permafrost-ecosystem-climate feedbacks mentioned above have significantly raised the awareness for this component of Earth's cryosphere in the view of stakeholders, decision makers, and the public over the last few years (Grosse et al., 2016).

Moreover, although widespread changes to permafrost usually take centuries, the *Intergovernmental Panel on Climate Change* (IPCC) report estimates that "by the mid-21st century the Arctic and alpine air temperatures will increase at roughly twice the global rate and the area of permafrost in the Northern Hemisphere will decline by 20-35%" (IPCC, 2007). Additionally, the *United Nations Environmental Programme* (UNEP, 2012) suggests the depth of thawing could increase by 30-50% by the year 2080.

In recognition of this importance, permafrost has been added as an *Essential Climate Variable* (ECV) in the *Global Climate Observing System* (GCOS) of the *World Meteorological*

Organization (WMO). Consequently, permafrost now requires broad-scale research and systematic observations to support the IPCC and *United Nations Framework Convention on Climate Change* (UNFCC) in their assessments of the state of the global climate system and its variability (Grosse et al., 2016).

To understand the status and dynamics of permafrost, the monitoring of ground temperature and active layer thickness are needed. Other observations include sample drilling, remote sensing to detect changes in land surface characteristics and measurements of surface subsidence or heave (Schaefer et al., 2012).

1.4 Global Permafrost Monitoring

The creation of national permafrost monitoring networks was considered by the IPCC as one of the key steps to understand the potential impacts of permafrost dynamics in a climate-changing world affected by global warming (Grosse et al., 2016).

Currently, there are two global networks to monitor permafrost: the Thermal State of Permafrost (TSP) network, which coordinates measurements of permafrost temperature; and the Circumpolar Active Layer Monitoring (CALM) network, which coordinates measurements of active layer thickness in both polar regions as shown in Figure 11.

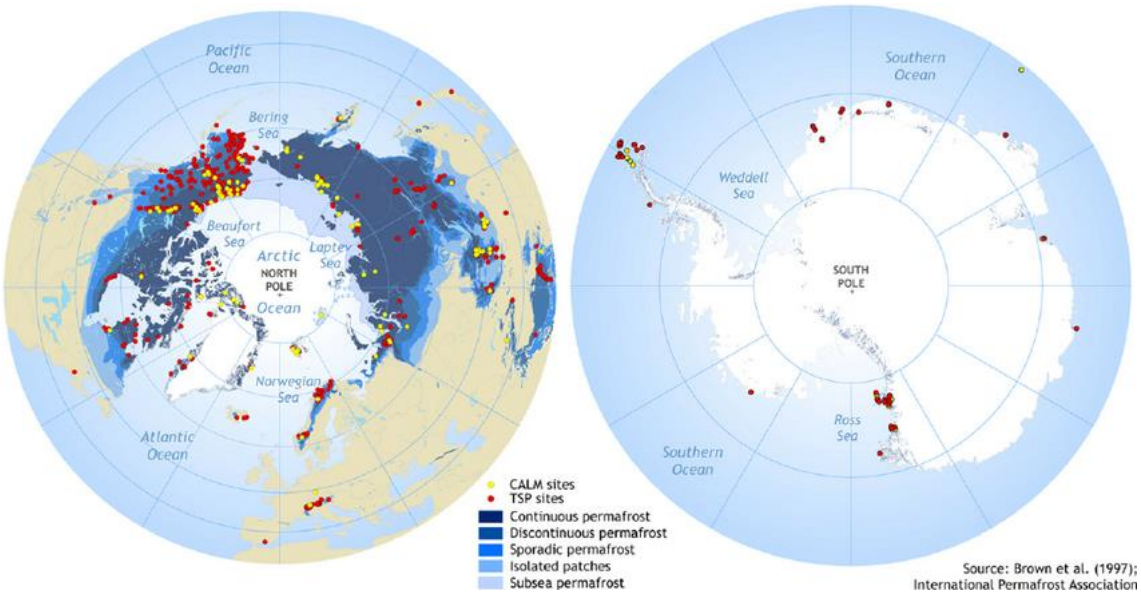

Figure 11. Circumpolar Active Layer Monitoring (CALM) network and Thermal State of Permafrost (TSP) network distribution (Schaefer, 2014).

The TSP and CALM networks are the two components of the Global Terrestrial Network for Permafrost (GTN-P). The GTN-P was initiated by the International Permafrost Association (IPA) to organize and manage a global network of permafrost observations for detecting, monitoring and predicting climate change, and was implemented under the GCOS and its associated organizations. The IPA currently coordinates international development and operation of the TSP and CALM networks for the GTN-P (Schaefer et al., 2012).

The TSP network measures permafrost temperature using boreholes. Boreholes vary in depth from a few meters to a hundred meters and deeper, with a string of temperature sensors at multiple depths. Newer boreholes are automated, but manually lowering a single sensor probe down a borehole to measure temperature is still common. The oldest boreholes have operated since the middle of the 20th century, with several decades of permafrost temperature observations. The TSP network includes approximately 1357 boreholes mostly located in the Arctic, also includes boreholes in the European Alps, Antarctica and the Qinghai-Tibetan Plateau (GNT-P, 2018).

The CALM network measures active layer thickness or maximum annual thaw either mechanically using a probe, or electronically with a vertical sequence of temperature sensors. The probe is a metal rod sunk into the ground until it hits the hard top of permafrost. The active layer depth is measured on the rod and recorded. To account for high spatial variability,

researchers generally probe the active layer on a specified 1 km or 100 m grid. A 252-sites network presently exists under the CALM Network (GNT-P, 2018), some of which have been measuring active layer thickness since the 1990s (Schaefer et al., 2012).

Most stations in TSP and CALM are nationally or regionally funded and operated by independent research teams. TSP and CALM coverage are limited because installation and maintenance costs restrict sites to regions with reasonable access by truck, plane or boat. The research teams in the GTN-P have made tremendous progress, but evaluation of overall permafrost status in a region or country is still very difficult because of the non-standard observations and limited coverage of the TSP and CALM networks, due to a limited and irregular funding (Schaefer et al., 2012). Moreover, international collaboration on data collection and analysis is still a great challenge to overcome in this advancing scientific problem of global concern. The willingness of scientists to share data and to participate in data management strategies is as well a crucial requirement for scientific advancement (Papale et al., 2012)

Specially during the International Polar Year (IPY) in 2007-08, the Antarctic region received great efforts to increase the spatial coverage of the existing permafrost-monitoring network and installing boreholes deeper than the depth of ZAA (Figure 12) all around the continent (Vieira et al., 2010). About 350 new boreholes for temperature monitoring were established globally and a considerable number of active layer depth observations were collected during this year (Biskaborn et al., 2015). Meteorological stations were as well installed close to some boreholes in order to evaluate ground–atmosphere coupling (Vieira et al., 2010).

Efforts of the IPA and the GTN- P at the end of the IPY resulted in reports on the thermal state of permafrost in high latitudes and high altitudes which were called the “IPA snapshot” and published in a special issue of the journal *Permafrost and Periglacial Processes* (Christiansen et al., 2010; Romanovsky et al., 2010a; Smith et al., 2010; Vieira et al., 2010; Zhao et al., 2010).

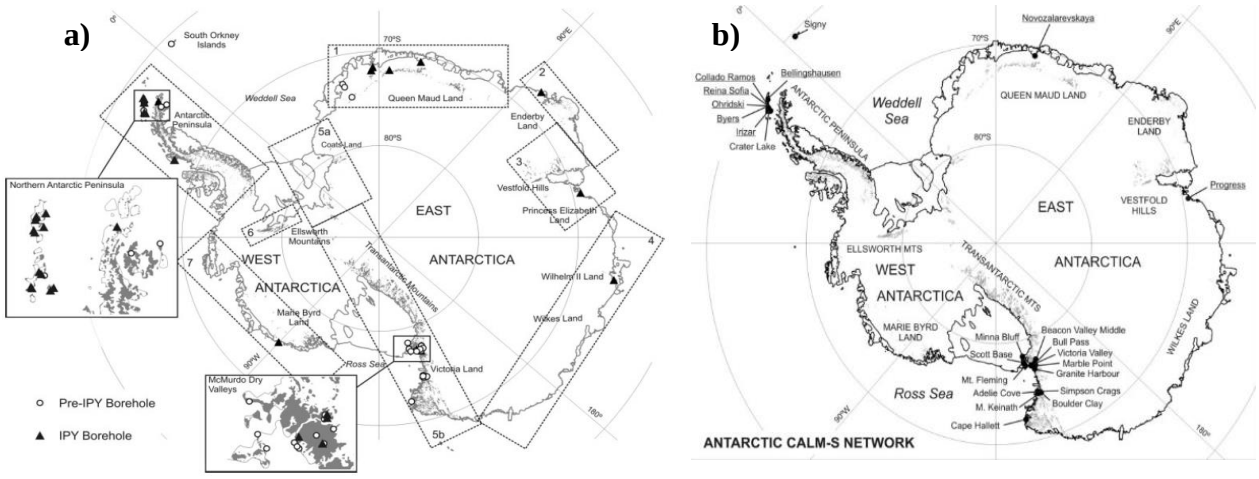

Figure 12. **a)** Antarctic permafrost monitoring boreholes (pre-and IPY installation) in relation to soil regions according to Greene et al. (1997): 1. Queen Maud Land; 2. Enderby Land; 3. Vestford Hills; 4. Wilkes Land; 5a nd b. Transantarctic Mountains; 6. Ellsworth Mountains; 7. Marie Byrd Land; 8. Antarctic Peninsula; **b)** Antarctic Circumpolar Active Layer Monitoring Network (CALM). New sites installed during the IPY are underlined (Vieira et al. 2010).

1.5 Permafrost in Antarctica

Antarctica, with an area of 14 million km^2, is the world's largest continent, yet exposed ground on which permafrost soils occur covers a mere 49,000 km^2 (Fox and Cooper, 1994 in Campbell & Claridge, 2009). Despite occupying only 0.36% of the Antarctic region, permafrost is present beneath virtually all ice-free terrain, such as the Antarctic Peninsula and the Transantarctic Mountains, except at the lowest elevations of the maritime Antarctic and sub-Antarctic islands (Vieira et al., 2010).

Existing studies on permafrost and active-layer dynamics in Antarctica were summarized in Vieira et al. (2010). However, in the last years, the Antarctic Peninsula has been the ice-free region receiving greater permafrost research interest as is one of the areas of the currently affected by the greatest air warming (Guglielmin, 2011).

1.5.1 CLIMATE, ECOSYSTEM AND SENSITIVITY TO CHANGE

The climate of Antarctica embraces the most extreme cold conditions on Earth. Whereas the climate is oceanic in the coastal areas of West Antarctica, it is continental in Central and East Antarctica. As a rule, temperatures decrease with distance inland. The average winter

temperatures range around -20°C and -30°C along the coasts and -60°C to -70°C inland on the continent (Umweltbundesamt, 2016). The lowest temperature recorded on site (-89.6°C) was measured at the Russian research station Vostok in eastern Antarctica in 1983 (Campbell & Claridge, 2009).

The mean annual precipitation over Antarctica averages around 50 mm per year, with less falling inland and most in coastal locations. The precipitation normally falls as snow, and little is available for direct soil moistening in the continental part of Antarctica because of ablation and evaporation (Campbell & Claridge, 2009).

Regarding the ecosystem, the soils in Antarctica have been referred as "Cold Desert Soils" (Campbell and Claridge, 1969), with the exception of the ice-free areas of the Antarctic Peninsula, where plant life including lichens, mosses and some grasses are more abundant. Biodiversity inland in the continent is extremely low, and diminishes with increasing severity of climatic conditions. The occurrence of terrestrial biota is sporadic, being found only in very small areas where there is enough water, light and warmth, as well as shelter from the wind.

Terrestrial ecosystems in this harsh environment are extremely fragile. A review of the impacts of human activities and the susceptibility of the land systems to disturbance was carried out for the Ross Sea region (Campbell, 2001), and showed that disturbances from human activities are long-lasting. Physical disturbances to the soils could be persistent for hundreds of years, or in the most arid zones (where recovery processes are negligible), could even be permanent. Chemical contaminations may also persist in the absence of significant leaching. Permafrost is equally dramatically and rapidly disturbed when physical disturbance takes place. Less clear, however, are the future impacts of global climate change. From the 1950's until 1999, a distinct warming trend was observed in the Antarctic Peninsula region, while recent data reports a cooling trend in the North of this peninsula and the East Antarctic region since then (Turner et al., 2016; Campbell and Claridge, 2006).

1.5.2 PERMAFROST DISTRIBUTION

Permafrost research in Antarctica has been increasing significantly since Bockheim (1995) developed the first permafrost map of Antarctica (Figure 13), proposing that discontinuous and continuous permafrost boundaries correspond to mean annual air temperatures of −1°C and −8°C, respectively.

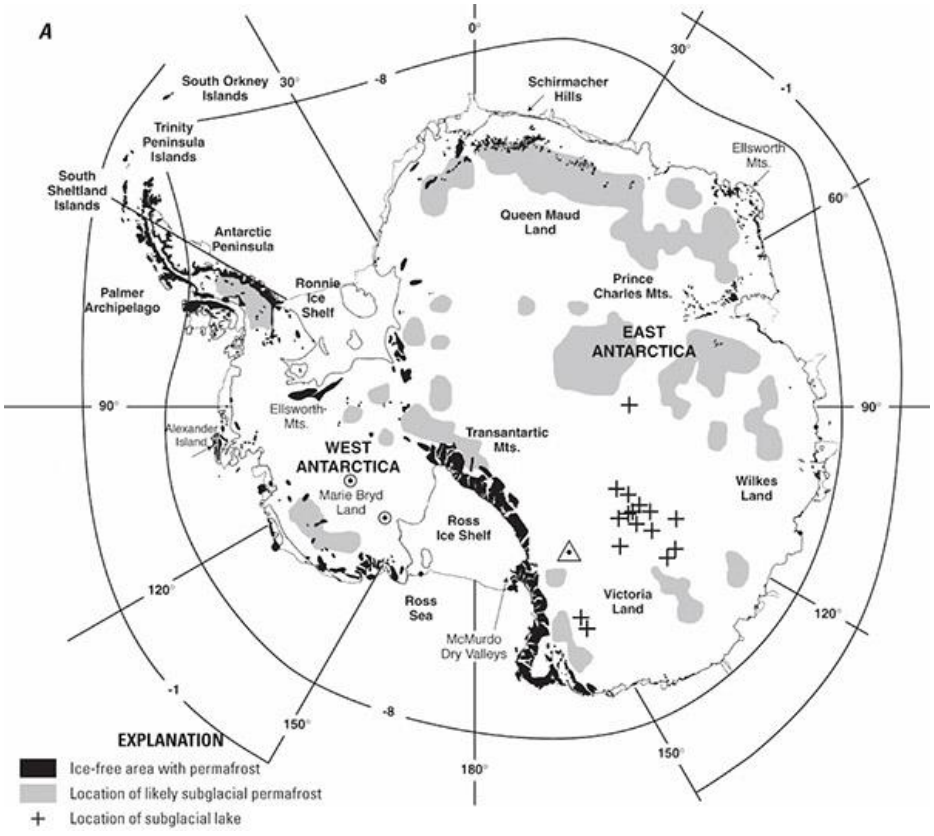

Figure 13. General permafrost distribution map in the Antarctic (modified from Bockheim, 1995).

The permafrost table is at greatest depth in the warmer west and northern regions of Antarctica, and diminishes in depth inland with increasing latitude and altitude. However, the depth of the permafrost table also varies from site to site at small scales because of the local differences in the substrate type and in the exposition to solar radiation that varies with topographic shading, aspect, snow cover, surface colour and roughness (Campbell and Claridge, 2009).

Later on, results obtained during the IPY on the thermal state of permafrost and the active layer in the WAP showed the South Shetland Islands near sea-level region, as an area near the climatic boundary of permafrost. Permafrost temperatures range from −0.4 to −3.1°C along the WAP, where the greatest rate of warming (ca. 2.4–3.4 °C) has occurred from 1950 to 2000 (Bockheim et al., 2013). Therefore, the WAP was reported as the one with the highest sensitivity to climate change in the Antarctic continent (Vieira et al., 2010).

Permafrost temperatures were much lower in continental Antarctica: from the coast to the interior and with increasing elevation, they ranged between -13.4 ºC and -18.7 ºC in Northern Victoria Land, from -17.5 ºC to -22.6 ºC in the McMurdo Dry Valleys, and down to -23.7 ºC in high elevation on Mount Fleming (Ross Island). The snapshot obtained during the IPY shows that the range of ground temperatures in the Antarctic is even greater than in the Arctic (Vieira et al., 2010).

1.5.3 RELEVANCE OF PERMAFROST RESEARCH IN WESTERN ANTARCTIC PENINSULA: A REVIEW.

Despite the Transantarctic Mountains being the ice-free region of the Antarctic where systematic permafrost research has been conducted for the longest time, it was the Antarctic Peninsula region receiving greater permafrost research interest and efforts during the IPY in 2007-08 (Vieira et al., 2010).

The reason is because, the WAP was considered as "one of the areas of the world currently affected by the greatest air warming and provides a unique opportunity to understand the impacts of climate change on permafrost and its related ecosystems" (Guglielmin, 2011).

Along the WAP, the mean annual air temperature showed an increment of around 3.4 °C during the second half of the 20th century, making the region one of the world's climate warming "hotspots" (Vaughan et al., 2003; Turner et al., 2005, 2009). These changes in climate were possibly linked to shifts of the Antarctic Circumpolar Current to the south (Böning et al., 2008), which resulted in a 40% decrement in sea-ice coverage in the Bellingshausen Sea (Ducklow et al., 2008; Stammerjohn et al., 2008) and in the disintegration of ice shelves along the WAP (Cook and Vaughan, 2010).

However, more recent studies (Turner et al., 2016) found that the warming signal is more complex than previously accounted and report a cooling in the north of the Antarctic Peninsula since 2000.

The complexity of the reaction in this region to climate change is still poorly understood. Permafrost properties and seasonal thaw-layer dynamics are considered two key indicators of climate change in the polar region (Anisimov et al., 1997; Burgess et al., 2000). Therefore, in order to evaluate the consequences of climate change in the terrestrial environments dominated by the presence of permafrost in the WAP, permafrost and active layer dynamics monitoring and modelling is essential.

On one hand, monitoring is possible though the TSP and CALM network of permafrost temperature and active layer monitoring sites set up in some areas of the WAP.

Especially during the IPY, several national projects focused their efforts in the Antarctic Peninsula and led to the installation of new boreholes (see Figure 14a): two intermediate, one shallow, 11 surface and 25 under 2m deep ground temperature boreholes. These included activities by Argentina, Brazil, Bulgaria, Italy, Portugal, Russia, Spain, Switzerland and the

UK (e.g. Ramos et al., 2009 a,b; Ramos and Vieira, 2009; Vieira et al., 2007, 2008, 2009; Vieira 2009; de Pablo et al., 2010).

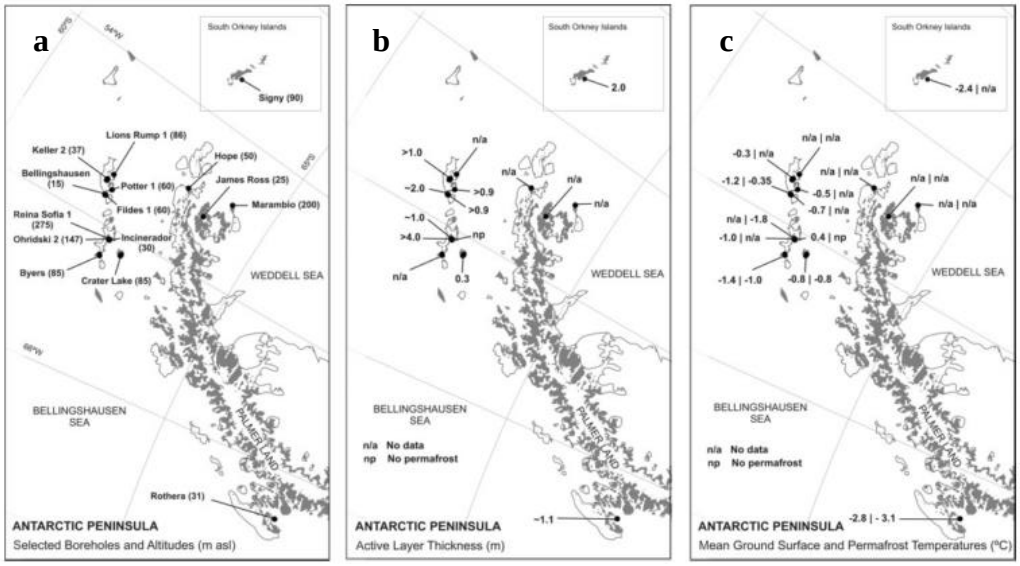

Figure 14. a) Permafrost monitoring boreholes installed in the Antarctic Peninsula during the IPY. b) Active-layer thickness for selected boreholes. c) Mean ground surface and permafrost temperatures for selected boreholes (Vieira et al., 2010).

Still, during the last decade, after the IPY, the permafrost research activity has kept ongoing in the area and the number of boreholes has continued increasing. The data belonging to the temperature monitoring in these boreholes has been used for the publication of several papers on the characterization of the active layer dynamics and permafrost thermal state in the WAP, such as Hauck et al. (2007), Ramos and Vieira (2009), Vieira et al. (2010), Bockheim et al. (2013), de Pablo et al. (2014), Wilhelm & Bockheim (2016), Ferreira et al. (2017), Ramos et al. (2017).

Results of these studies show that permafrost temperature ranges from −0.4 to −3.1 °C along the western Antarctic Peninsula region and the warming rate between 1950 and 2000 ranged around 2.4–3.4 °C (Bockheim et al., 2013). This warming has resulted in the continuous degradation of permafrost. For instance, reports prior to 1980 showed that permafrost was present at a depth of 0.25 to 0.35 m in organic soils near Palmer Station (64°46′S; 64°04′W), but currently, permafrost is absent or near thawing in the upper 14 m. In the South Shetland Islands, thawing of permafrost has resulted in increases in active-layer thicknesses and in thermokarst features such as debris flows and active-layer detachment slides. Several low-elevation boreholes show the presence of permafrost with temperatures close to 0 ºC, especially beneath diamictons or in sedimentary materials. Such is the case at Bellingshausen,

Byers Peninsula or Crater Lake amongst others. On Deception Island, where the substratum is of volcano-sedimentary origin with extremely high insulation properties and ice-rich permafrost occurs almost down to sea level (Vieira et al., 2010).
Bedrock temperatures from Hurd Peninsula (Livingston Island) suggest that the continuous permafrost boundary is probably at ca. 150 m a.s.l. (Vieira et al., 2009).
The permafrost was found to be ice-cemented at high altitudes on the WAP. At low elevations, sporadic permafrost is especially unstable due to the disequilibrium of the frozen bodies with current climatic conditions (Bockheim et al., 2013). The lowest coastal terrain near sea level is considered to be essentially permafrost free, but an altitudinal limit for continuous permafrost in bedrock has not been identified with confidence (Vieira et al., 2010). Observed permafrost temperatures and active layer thickness in different points of the WAP are shown in Figure 14b and Figure 14c.

In spite of the monitoring expansion efforts and research interest in permafrost in the WAP during the last years, due to the scarce of monitoring boreholes in the remotest areas, permafrost and active layer dynamics in the WAP is still poorly understood and efforts and research here must keep going on to understand its relation with recent climate change. This climate changes can have consequences for infrastructure, especially at the low elevations, where 25 scientific stations exist in the Antarctic Peninsula region. Warming may also have an impact in the sensitive ecosystems of maritime Antarctica (Bockheim et al., 2013).

2 Study Area

Cierva Point (lat. 64°10'S, long. 60°57'W) is an ice-free peninsula about 1 km long in north to south direction and 1.5 km wide in east to west direction, mainly exposed to the north. The peninsula (Figure15) stands on the south side of Cierva Cove, located at the north end of Hughes Bay in the Danco Coast of Western Antarctic Peninsula. The climate is cold oceanic, with a mean annual air temperature of ci. -3 °C, being 4.3 ºC and -20 ºC the maxima and minima recorded from 2012 to 2018. The estimated annual precipitation ranges from 400 to 1100 mm and winter snow depths can exceed 1 m. However, during the summer most of the snow in glacier-free areas completely melts (Wilhelm, 2016b). As a result, some temporary ponds form at mid-altitudes (Figure 15).

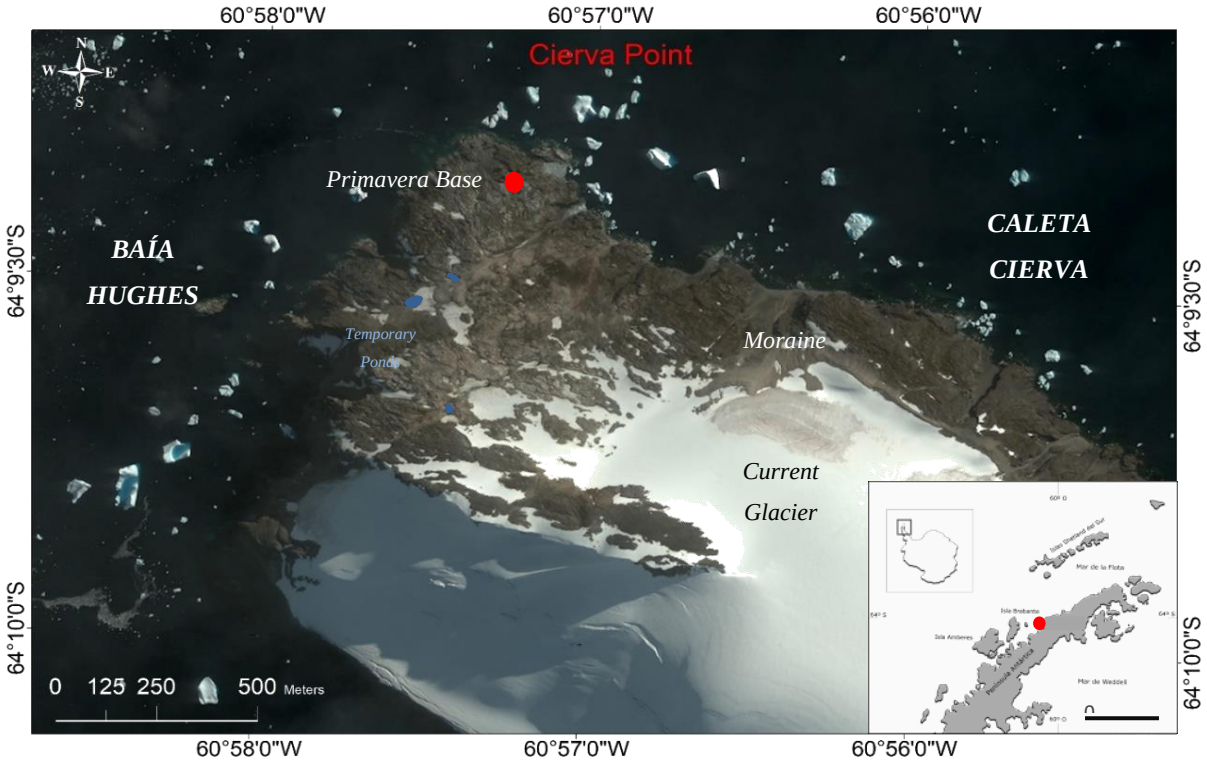

Figure 15. Cierva Point ice-free peninsula, Hughes Bay (Danco Coast, Western Antarctic Peninsula) (Base Image source: Google Earth, resolution: 2.4 m).

The area taken in consideration in this work is a small sector of the Cierva Point peninsula. It covers an area of 0.65 km^2, restricted to the ice-free terrain, excluding areas of permanent snow accumulations and temporary ponds (Figure 16).

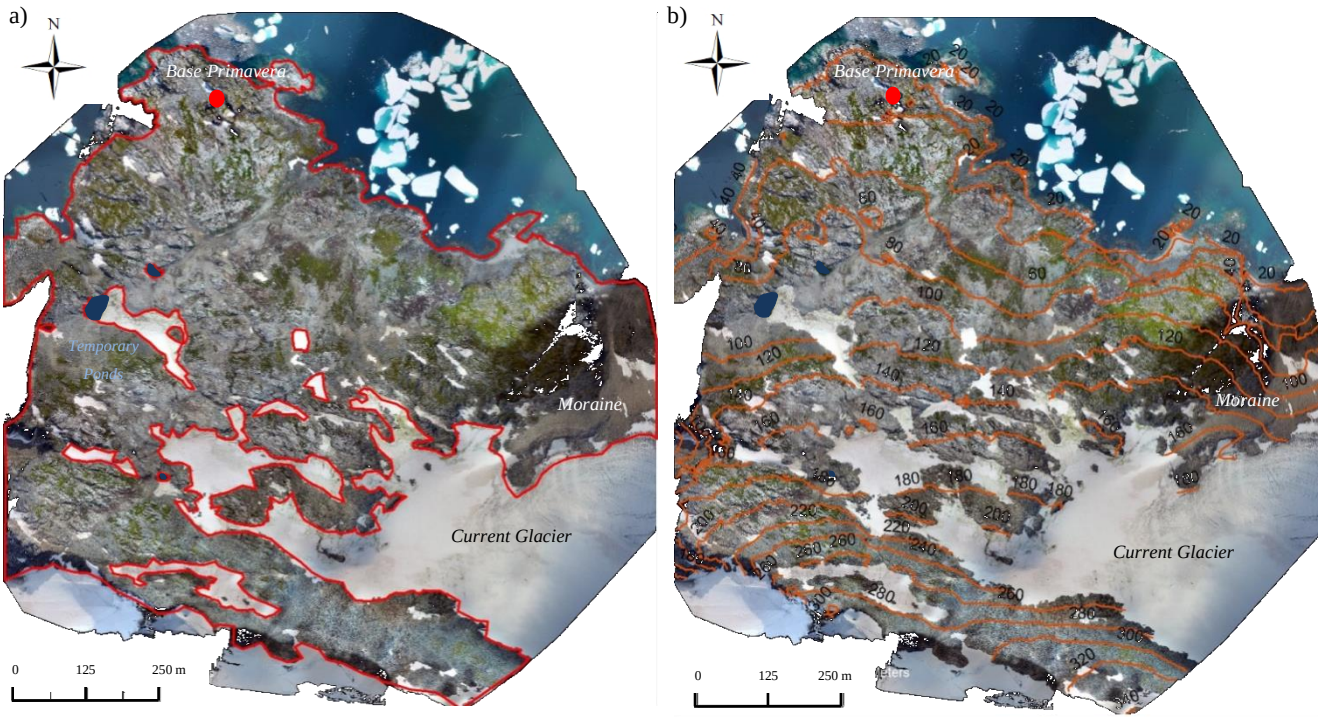

Figure 16. Cierva Point study area. a) Orthomosaic with indication of the ice-free terrains analysed in the modelling (red line), b) Contour lines with altitude in meters (source: mosaic from UAV aerial imagery. Resolution: 6.5 cm).

The Cierva Point Peninsula shows a rugged relief that culminates at 340 m elevation in a sharp ridge. Most of the peninsula is glacierized with rock outcrops occurring mostly close to sea-level on the north side of the peninsula or in its NW tip (Figure 15). Polished bedrock, striations, and chatter marks on bedrock throughout the peninsula show the effects of glacial erosion on the ice-free areas (Wilhelm, 2016b), while at some locations, recent moraine accumulations occur. The northern and lowest elevation sector of Cierva Point is dominated by deposits of granite debris and boulders and peat areas covered by significant moss (*Polytrichum strictum* and *Chorisodontium aciphyllum*) accumulations up to 0.8 m deep (Wilhelm, 2016b).

Most deglaciated slopes are north facing showing high solar radiation inputs, especially during the summer (Bockheim et al., 2013). Bedrock benches in the north slopes of Cierva Point show the presence of unconsolidated materials with soils derived from bedrock weathering and from glacial deposits. Slopes vary from 0 to 20% on benches and from 30 to 60% on bedrock cliffs (Wilhelm, 2016a).

The bedrock in Cierva Point is of intrusive igneous origin. The northernmost area is mainly constituted by granodiorites, the middle of the peninsula (uphill and to the south) is dominated by feldspar granites and the eastern side, along with the southern peaks, is dominated by basalts containing olivine and quartz (Wilhelm, 2016b).

In the NW area of the peninsula, at low elevation close to the shore, stands the Argentinian Antarctic Station "Primavera" that supports scientific research (Figure 16)
Cierva Point is an Antarctic Specially Protected Area (ASPA) within the Antarctic Treaty as it guests a large Gentoo penguin (*Pygoscelis papua*) colony, as well as different types of lichens and mosses. The lowest elevations of Cierva Point are characterized by ornithogenic soils due to penguin activity.

Several shallow boreholes (1.2-4.3 m) and a deep borehole (15 m) were drilled in Cierva Point in 2012 by research teams from the University of Wisconsin-Madison and the University of Lisbon (CEG-IGOT) in order to monitor the ground temperature at different depths. The existing data series from 2012 to 2018, which although discontinuous in some boreholes, allows for a very detailed analysis of the ground thermal regime and is an excellent data set for modelling the thermal regime and permafrost in the area.
The borehole data for the period 2012-2014 has been analysed by Wilhelm (2016a) to characterize the thickness of the active layer and to model conductive energy transfer in different soil types.

However, little is still known about the climate sensitivity linked to regional air and ground surface warming in this area. The availability of longer more recent borehole data up to 2018 presents a good opportunity for modelling the thermal regime and permafrost distribution in the region, being them considered as climatically sensitive variables used for determining the permafrost thermodynamics in the area and evaluate its impact on ecosystem processes.

3. Methodology

In order to estimate the temperature and distribution of permafrost, different distribution models relying both in statistical and physical approaches have been applied so far in polar and mountain regions. Physical-based approaches (Ferreira et al., 2016) have assessed the TTOP model using freezing and thawing indexes, n-factors and thermal conductivity of the ground, as factors representing ground-atmosphere interactions and providing a framework to understand the ground thermal regime and permafrost temperature distribution. Other methods have been developed for determining the spatial distribution of permafrost using GIS-based empiric-statistical permafrost models (e.g. Etzelmüller et al., 2006). Such modelling was calibrated with ground temperature observations, and used non-parametric correlations and logistic regression modelling to estimate the spatial permafrost probability based on single independent variables (Lewkowicz and Ednie, 2004; Brenning et al., 2005).
In this investigation, the aforementioned studies, together with others mentioned along this dissertation, gave us the insights to create a methodology that allows increment the scarce existing knowledge about the permafrost distribution and climate sensitivity of Cierva Point.

The method followed to achieve the objectives of this investigation was divided in two main steps.
Initially, the ground thermal regime of 9 sites with different ground characteristics and topographical conditions was analysed. In these locations, ground and air temperature records were available from 2012 to 2018, although with significant observational gaps. The ground temperature records, taken every 4 hours, were obtained from thermistor strings in boreholes with depths ranging from 1.2 m to 15 m. Air temperatures at 4-hour intervals, were measured from 7 air temperature sensors and a meteorological station located close to the boreholes.
Using the ground temperature records, the local ground thermal regime was analysed in the different monitoring sites. This allowed to determine the inter-annual variability of the active layer, the observed or estimated temperature and depth of the top permafrost and the ground thermal offset for each site. Subsequently, the analysis of the air and ground temperatures allowed determining the parameters needed to develop the TTOP model for the 9 borehole sites.

The outputs of the local ground thermal regime and local parameters were subsequently used together with ground, topographic and spatial data as inputs to implement a GIS-based spatial *TTOP model* all over the study area using statistical relations between the inputs.

The TTOP model predicts the mean annual ground temperature at the depth of the *top of the permafrost*, or the base of seasonal freezing if permafrost is absent, using relatively simple parameters representing key climate and terrain factors influencing the ground thermal regime (Way, 2016).

The ground and air temperature data used for the model were obtained from the *in situ* measurements aforementioned. The spatial data used for the elaboration of a *digital surface model* (DSM) that constitutes the base for the spatial modelling, comes from UAV aerial imagery and D-GPS control points collected in the field.

The main software tools used for the development of this methodology were: Excel (for the data and thermal regime analysis); SPSS Statistics (for statistical analysis); Pix4D Mapper (for the creation of the orthomosaic and DSM through aerial imagery); and ArcMap 10.4 (for the spatial model implementation).

3.1 Data Collection and analysis

3.1.1 GROUND TEMPERATURE MONITORING

The ground temperature records, measured every 4 hours, were obtained from 9 thermistor strings in boreholes with depths ranging from 1.2 to 15 m.

The boreholes were drilled in the summer of 2012 by a field team of the Universities of Wisconsin-Madison and Lisbon and spatially distributed over Cierva Point, as explained in Wilhelm & Bockheim (2016). Sites were selected based on different geomorphic ground settings. The descriptions of each site are summarized in Table 1 and their spatial distribution is shown in Figure 17.

Site Name	Elevation (m)	X coordinate (m)	Y coordinate (m)	Ground Type	Substrate class	Max Depth (m)	Thermistor depths (cm)	Notes
Site 1: Permafrost	198	599632.3	2883337.6	Granite	Bedrock	15	20, 40, 80, 120,160, 200, 250, 300, 350, 400, 500, 550, 600, 700, 800, 1000, 1250, 1500	Permafrost at 5 m
Site 2: Summit	336	599836.5	2883057.0	Basalt	Bedrock	1.8	5, 15, 40, 60, 80, 100, 120, 140, 160, 180	No permafrost in the dataset
Site 3: BelowSummit	318	599721.2	2883083.3	Pigmatitic K-Spar Granite	Bedrock	1.8	5, 15, 40, 60, 80, 100, 120, 140, 160, 180	No permafrost in the dataset
Site 4: Saddle	290	599505.9	2883142.7	Gelifluction Lobe	Unconsolidated Soil	1.2	5, 15, 40, 60, 80, 100, 120	No permafrost in the dataset
Site 5: Moraine	166	600018.3	2883484.3	Glacial Moraine	Unconsolidated Soil	1.8	5, 15, 40, 60, 80, 100, 120, 140, 160, 180	Permafrost at 1 m
Site 6: Midslope	137	599883.8	2883588.9	Granodiorite	Bedrock	1.4	5, 15, 40, 60, 80, 100, 120, 140	No permafrost in the dataset
Site 7: MossRock	71	599279.4	2883872.4	Granodiorite	Bedrock	1.8	5, 15, 40, 60, 80, 100, 120, 140, 160, 180	No permafrost in the dataset
Site 8: MossMoss	71	599284.1	2883871.9	40cm of moss with peat substrate over granite	Peat	1.8	5, 15, 40, 60, 80, 100, 120, 140, 160, 180	Permafrost at 0.4 m
Site 9: Lowdeep	43	599350.6	2884022.2	Granodiorite	Bedrock	4.3	5, 15, 40, 60, 80, 100, 120, 140, 160, 180, 200, 250, 300, 350, 400, 430	No permafrost in the dataset

Table 1. Ground temperature monitoring boreholes in Cierva Point. Monitoring boreholes where presence of permafrost was observed are highlighted in red. Elevation is shown in meters above the ellipsoid WSG84.

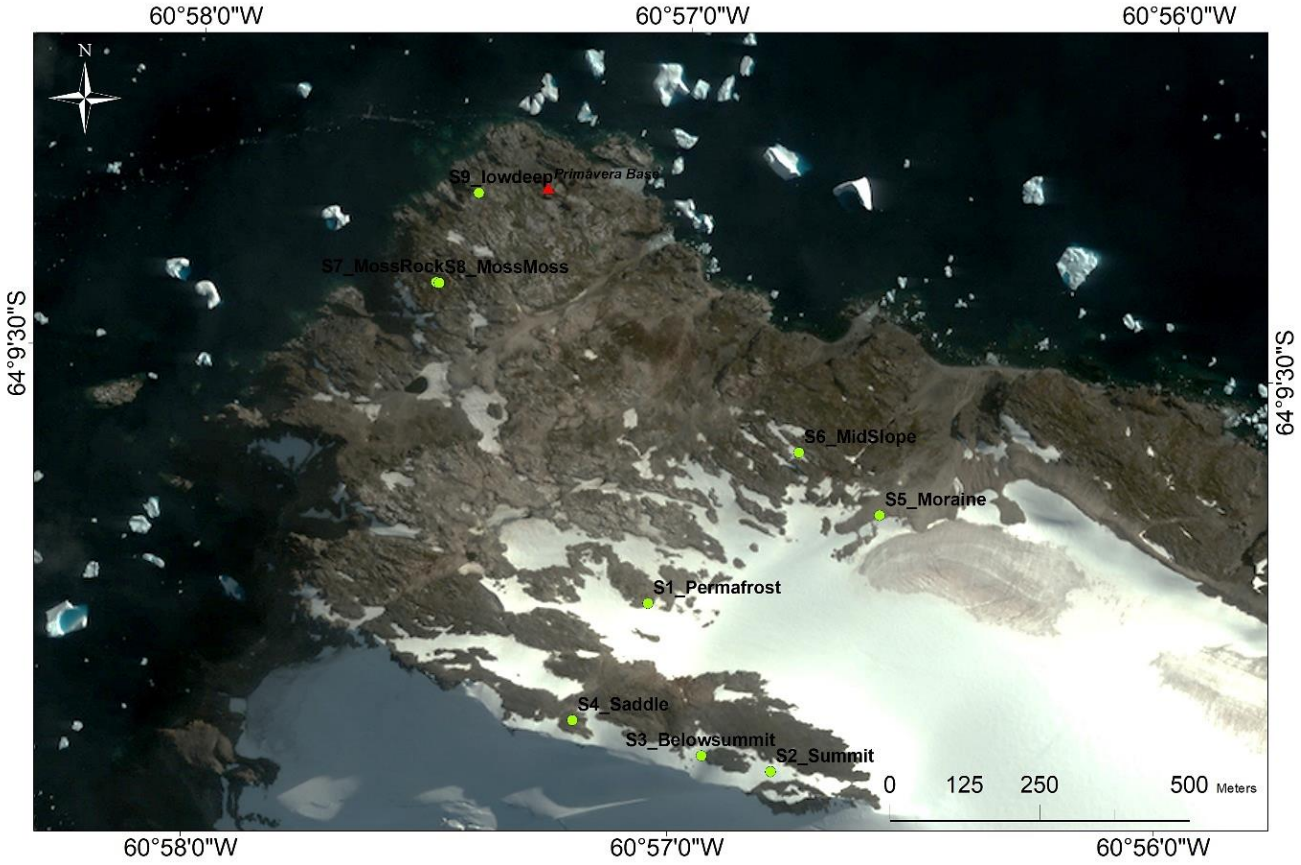

Figure 17. Ground temperature boreholes distribution over Cierva Point. (Base image: Google Earth, resolution: 2.4m)

In March 2012, strings containing miniature temperature loggers (iButton, Model DS1922L, Maxim Integrated, San Jose, CA) were placed inside the boreholes, cased in sealed, air-filled, pvc pipes with an outer diameter of 5 cm. Temperature was recorded every four hours at the depths indicated in Table 1. The iButton temperature sensors used in this study (Figure 18a) show an accuracy of ±0.5 °C.

Temperatures in the shallow boreholes were recorded until February 2017, with data downloaded and the loggers reset at the end of each summer between February and April. Unfortunately, the dataset over this period is not continuous, showing several gaps in different boreholes at various depths. In February 2017, the thermistors for all the shallow boreholes were removed and the thermistors of the deepest borehole (Site1-Permafrost) were replaced with a higher accuracy thermistor-chain (GeoPrecision, model M-log5W-DALLAS) (Figure 18b), being this the only borehole recording ground temperatures up to March 2018.

The GeoPrecision thermistors show a standard resolution of ±0.065 ºC and an accuracy of ±0.25 ºC. The sensors were calibrated in an ice-bath following manufacturer instructions and the final accuracy was reduced to ±0.1 ºC.

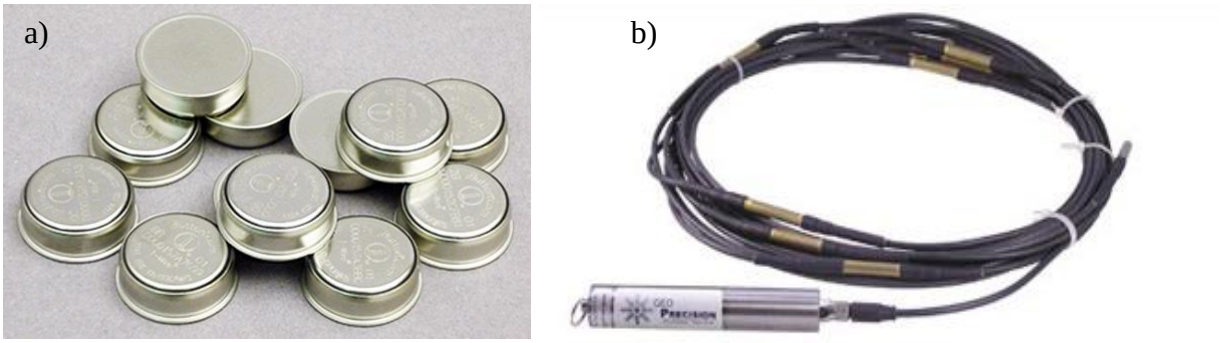

Figure 18. a) iButton ground/air thermistors. b) Ground temperature GeoPrecision thermistor strings.

Besides the higher resolution of these sensors, the main advantage of the replacement was the possibility of download the data via wifi communication with the thermistors using a computer without the necessity of annually extracting the sensors from the borehole, as well as the much higher capacity of the memory of the datalogger, allowing hourly measures for a period of 5-years and a much higher battery life, lasting up to 3 years without maintenance.

With these data, we computed and plotted the daily mean ground temperatures over the full dataset (Figure 19a). When analysing the mean daily ground temperatures to time curve, we observed an abrupt change in Site1 records at all the depths after the thermistor's replacement (Figure 19b) in February of 2017. GeoPrecision thermistors were considered to give closer values to real temperatures, as they are more accurate than the iButtons. In order to normalize the dataset and correct the abrupt difference in the temperature measurement from 2017, the shift value, which was similar at all depths, showing an average of -0.2 ºC, was subtracted to the 2012-2017 data. Since the ibuttons had been replaced several times, without other shifts

detected, we assume that the error is due to smaller precision of the ibuttons when compared to the Geoprecision device.

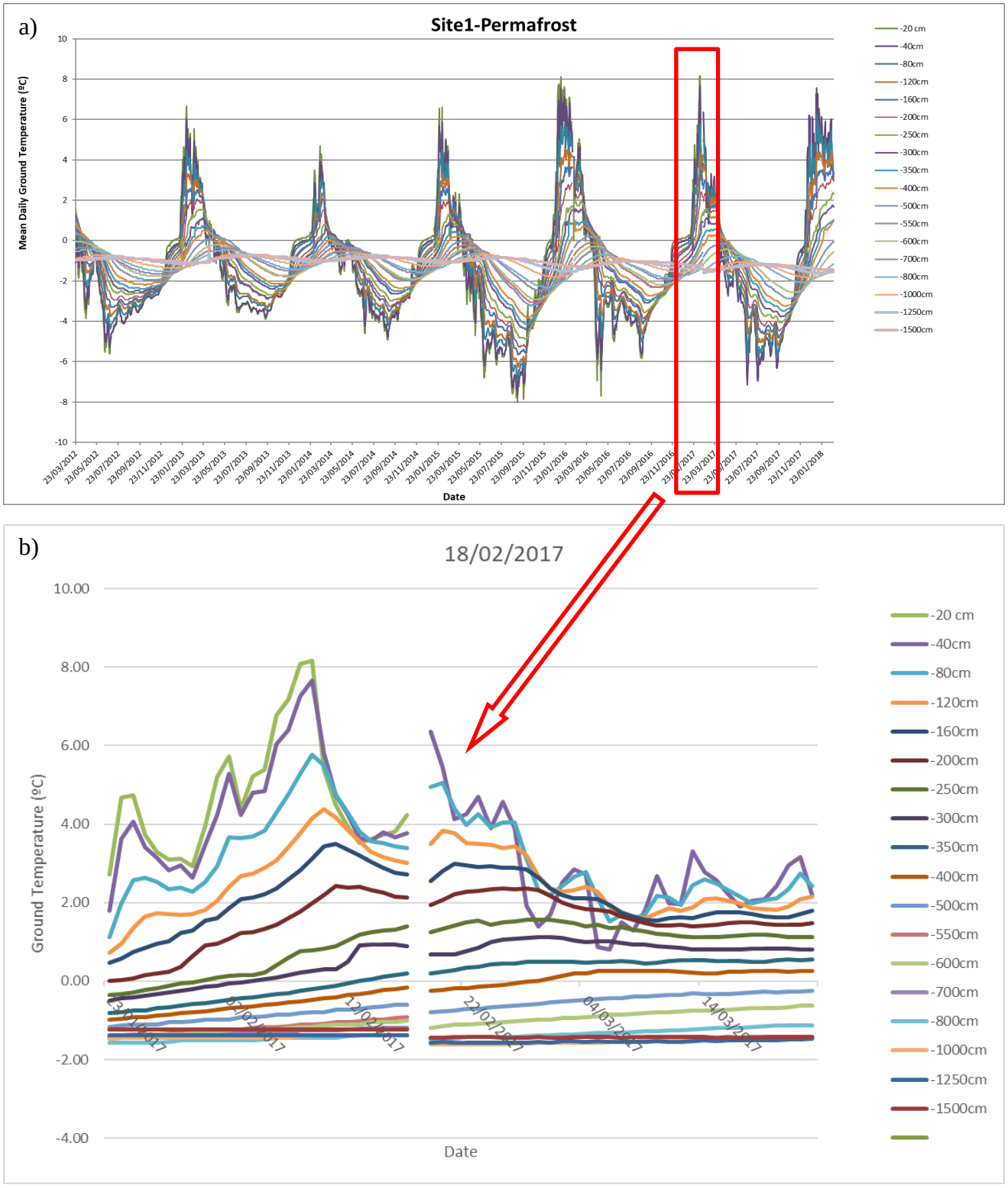

Figure 19. a) Mean daily ground temperatures measured in Site 1-Permafrost borehole from 2012 to 2018. b) Differences in temperatures recorded after 18/Feb/17 thermistor replacement, from iButton to GeoPrecision.

Moreover, the dataset was analysed in order to identify and clean outliers due to anomalies or sensor manipulation during the data downloading tasks, which were usually found only a few days every year, between February and April.

Daily ground temperatures and the gaps in the datasets for each borehole are shown in Figure 20, evidencing the issues during the 6-year period from March 2012 to February 2018. For the analysis, only the periods that included a complete thawing-freezing annual cycle with continuous records of air and ground temperatures for all the boreholes were used for the analysis of the thermal regimes and TTOP modelling.

A complete annual air freezing-thawing cycle was defined as per Lewkowicz et al. (2012), considering it as the period from the beginning of one year's autumn (March-April in the Southern Hemisphere), when the mean daily air and surface temperatures drop durably below 0 ºC (freezing period), to the end of next summer (next March-April), after the mean daily air and surface temperatures have been durably positive on the cumulative degree-day time curves (thawing period). This ensures that the entire cold and warm season is captured in the calculation. Dates for thawing and freezing cycles in our specific case study are designated later on in next section 3.1.2.

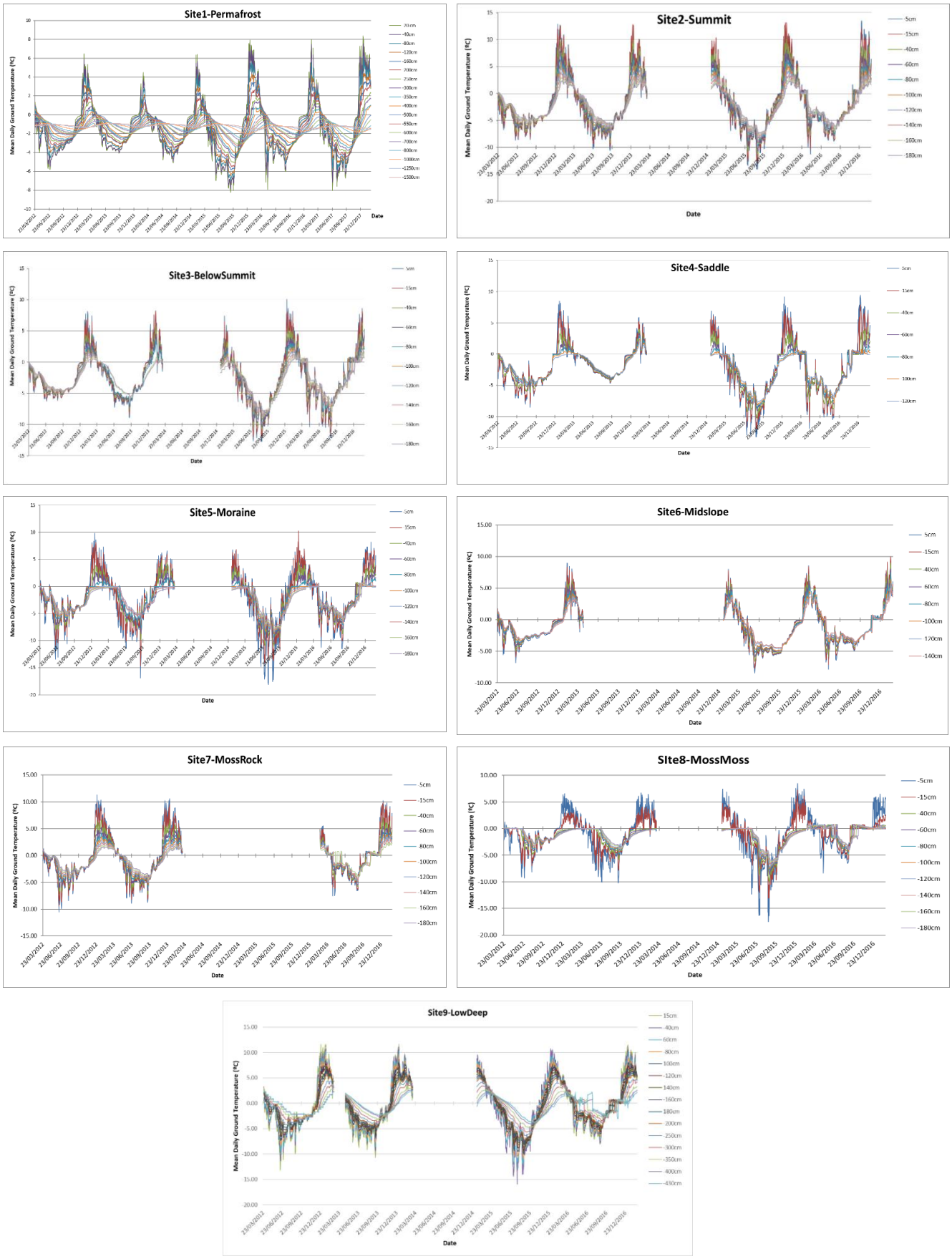

Figure 20. Mean daily ground temperatures in Cierva Point boreholes from 2012 to 2018. Note the different data gaps.

3.1.2 AIR TEMPERATURE MONITORING

Within a distance of approximately 2 m from each borehole, air and surface temperature iButton miniloggers were installed to monitor temperatures at 8 sites (due to the short distance between boreholes 7 and 8, just one common air temperature logger was installed). The distribution of air temperature miniloggers is represented in Figure 21.

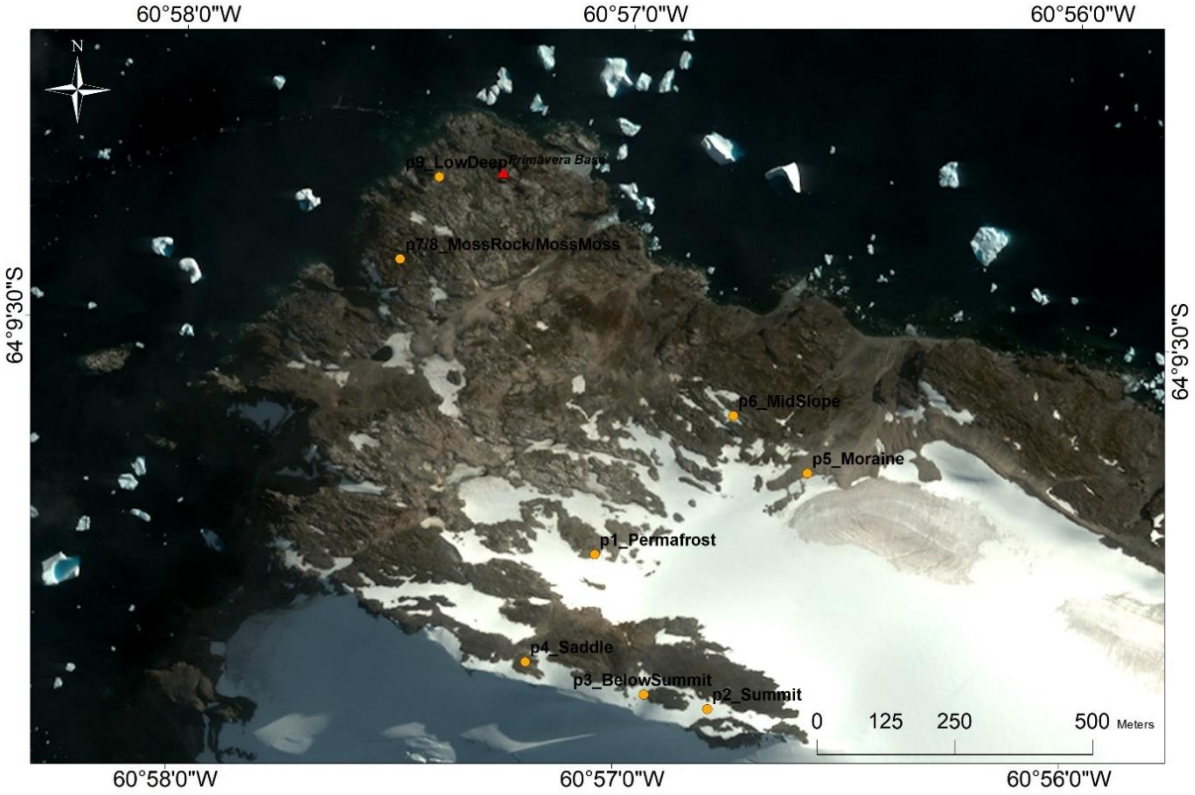

Figure 21. Air temperature miniloggers distribution in Cierva Point. (Base image: Google Earth, resolution: 2.4m).

The air temperature miniloggers were attached to a pole 1.5m above the surface within a solar shield as explained in Wilhelm & Bockheim (2016) and recorded almost continuous data from 09/03/2012 to 10/03/2014, when they were removed.

A meteorological station installed a few meters from the Site1-Permafrost borehole, recorded climate data until 25/03/2018. The meteorological station is based in a Campbell Scientific CR1000 logger powered by a 12V, 155 amp/hour deep cycle battery and a 90W, 12V solar panel (BP590J, BP Solar). It has six instruments recording atmospheric conditions (Wilhelm & Bockheim, 2016): an air temperature probe (109-L, Campbell Scientific), a relative humidity probe (HMP-45C, Vaisala), a pyranometer (LI200X-L, LI-COR) which recorded solar radiation, an anemometer (05103, R.M. Young) which recorded wind speed and direction, and a tipping bucket rain gauge (TE525WS, Texas Electronics). In the end of the

summer (between late February and early April) of each season, thermistor data were downloaded and the loggers reset.

The dataset for all the sites was explored in order identify and omit main outliner values due to sensor manipulation during the data downloading tasks (usually few days every year between February and April). Mean daily air temperature (MDAT) fluctuations and available data for each site after the data exploration and correction are shown in Figure 22.

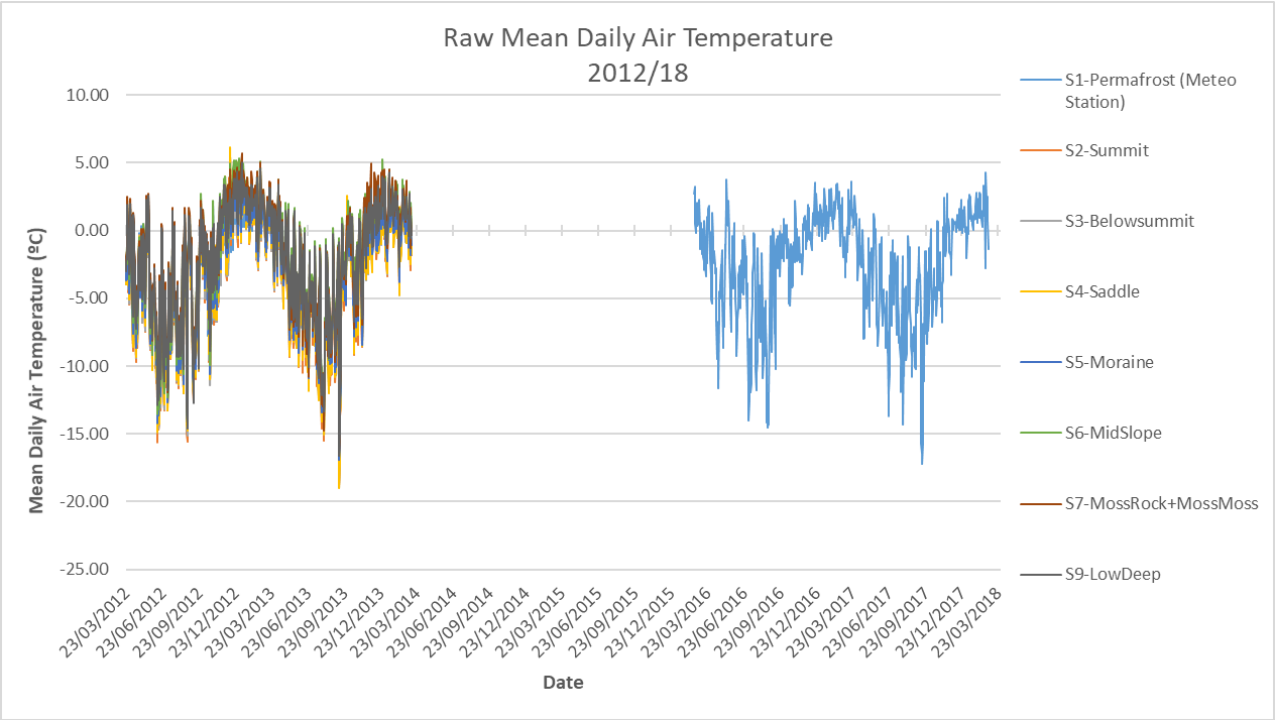

Figure 22. Mean daily air temperatures in the monitoring sites of Cierva Point.

As observed in Figure 22, the dataset for the entire sites except of Site1 is limited to the period from March 2012 to March 2014.

The periods determined as complete freezing-thawing annual cycles between 2012 and 2018 are shown in the PERIOD column of Table 2. However, only years 1 and 2, which are the cycles having complete ground and air temperature records (green tick, grey coloured) were used for the analysis of the thermal regime and TTOP modelling.

In site 6, ground temperature records for year 2 are missing, as an exception, only year1's dataset will be used in this site for the computation of the thermal regime and TTOP modelling.

				S1-Permafrost		S2-Summit		S3-Belowsummit		S4-Saddle		S5-Moraine		S6-MidSlope		S7-MossRock		S8-MossMoss		S9-LowDeep	
		PERIOD	DAYS	Ground T°	Air T°	Ground T°	Air T°	Ground T°	Air T°	Ground T°	Air T°	Ground T°	Air T°	Ground T°	Air T°	Ground T°	Air T°	Ground T°	Air T°	Ground T°	Air T°
Year 1: 2012/13	Freezing season	23-Mar-12 03-Dec-12	364	√	√	√	√	√	√	√	√	√	√	√	√	√	√	√	√	√	√
	Thawing season	04-Dec-12 22-Mar-13																			
Year 2: 2013/14	Freezing season	23-Mar-13 21-Nov-13	352	√	√	√	√	√	√	√	√	√	√	X	√	√	√	√	√	√	√
	Thawing season	22-Nov-13 10-Mar-14																			
Year 3: 2014/15	Freezing season	10-Mar-14 02-Dec-14	386	√	X	X	X	X	X	X	X	X	X	X	X	X	X	X	X	X	X
	Thawing season	03-Dec-14 31-Mar-15																			
Year 4: 2015/16	Freezing season	01-Apr-15 25-Nov-15	378	√	X	√	X	√	X	√	X	√	X	√	X	X	X	√	X	√	X
	Thawing season	26-Nov-15 13-Apr-16																			
Year 5: 2016/17	Freezing season	14-Apr-16 01-Nov-16	356	√	X	X	X	X	X	X	X	X	X	X	X	X	X	X	X	X	X
	Thawing season	02-Nov-16 05-Apr-17																			
Year 6: 2017/18	Freezing season	06-Apr-17 13-Dec-17	369	X	X	X	X	X	X	X	X	X	X	X	X	X	X	X	X	X	X
	Thawing season	14-Dec-17 ≈10-Apr-18																			

Table 2. Availability of air and ground temperature dataset over the full thawing and freezing cycles from 2012 to 2018. Years 1 and 2 are the only thawing and freezing cycles with a complete dataset for both air and ground temperatures (green checks, grey shaded). Years 3,4, and 6 have missing data for either ground or air temperature during 30 or more days during the freezing/thawing cycle.

3.1.3 AERIAL IMAGERY AND D-GPS GROUND CONTROL POINTS

For the implementation of a spatial TTOP model, spatial information of the area is mandatory to spatialize the model and to derive the terrain and topographic parameters influencing in the model's parameters. Consequently, we built up a *Digital Surface Model* (DSM) of the area to constitute the base for the spatial modelling. UAV aerial imagery and D-GPS ground control points collected in the field were processed using Pix4D Mapper software to create a *DSM* and an orthomosaic.

In late March 2018, we performed seven UAV flights over the study area using a DJI-Phantom 3 Advanced drone. The flights were carried out at altitudes between 200 and 380 meters above the sea level and following the flight plans shown in Figure 23, using the Android app Pix4Dcapture. The flights provided 1792 aerial images in .jpeg format, with an 80% overlap, taken by a DJI-FC300S (RGB) camera covering around the 90% of the desired area. Some examples of images captured during the flights and are shown in Figure 24. Unfortunately, due to a UAV malfunction which led to the loss of the UAV, a small area was not surveyed.

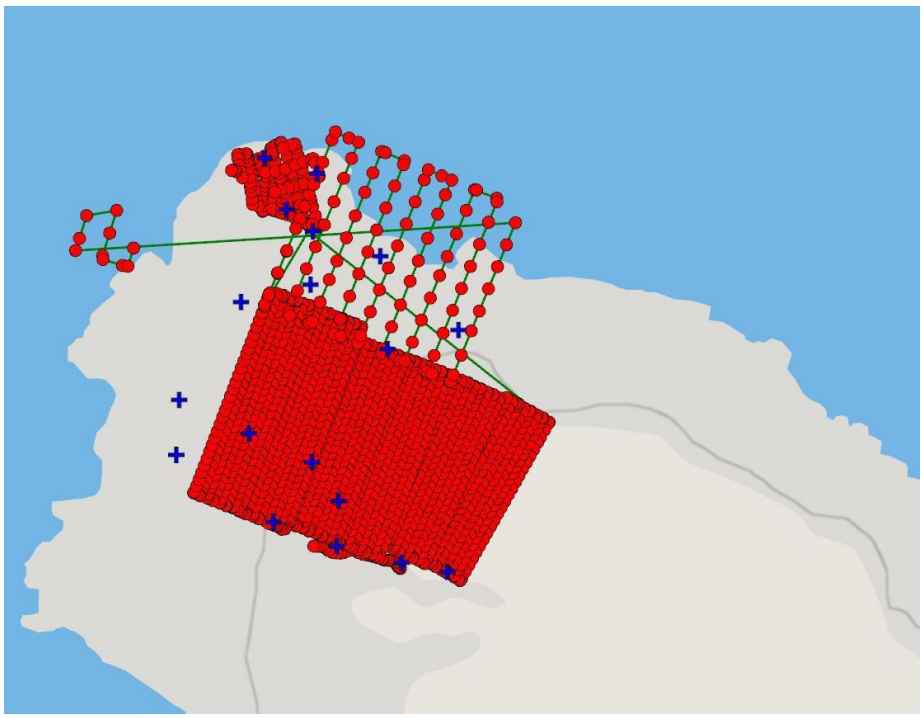

Figure 23. Flight plans and photo shot locations of the UAV surveys conducted in Cierva Point with an overlap of 80% (Source: Pix4DMapper software processing).

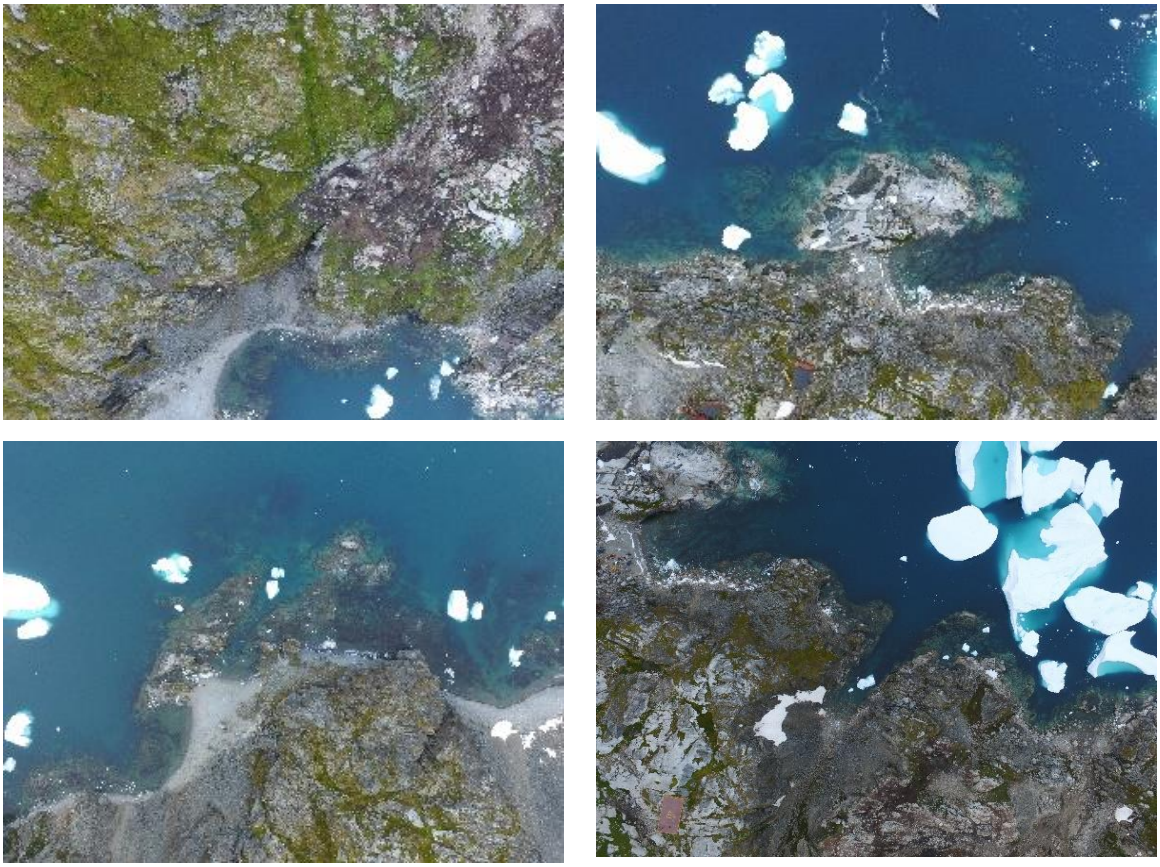

Figure 24. Example of images taken by the DJI-FC300S (RGB) in Cierva Point using the Phantom 3 Advanced UAV.

These images were processed in *Pix4D Mapper* for the construction of a high-resolution mosaic (i.e. assemblymen of all the images acquired over the area into a single georeferenced 2D/3D model by computing automated approaches to detect the same features on adjacent images).

In order to improve the geometry and accuracy of the final model, we developed a georectification process previous to the mosaic implementation, still in Pix4D. In this process, the coordinates of 18 D-GPS control points collected on singular geographical features on the terrain were introduced in the software and were manually associated to the exact related pixel point on the images. The ground control points were collected using a D-GPS Trimble equipment constituted by a GPS rover and receiver Trimble R4 GNSS (in RTK mode) and a controller Trimble JUNO T41 Handheld.

The final Pix4D outputs after the georeferencing and processing were a very high-resolution ortophotomosaic and a DSM covering a total land area of 1.063 km^2 with a resolution of 6.51 cm and a mean RMS error of 0.665 m (Figure 25a and b). This RMS error reflects the steep slope in such a small area and also limitations associated to the different flight altitudes, which originated problems in the DSM reconstruction.

The raw mosaic and DSM created in Pix4D were afterwards processed in ArcMap 10.4 in order to clip them to the restricted area of study of 0.65km^2 (avoiding permanent snow cover and ponds as shown in Figure 16) and to improve visualization (Figures 26a and b). The resolution of the models derived from the DSM is 1 m.

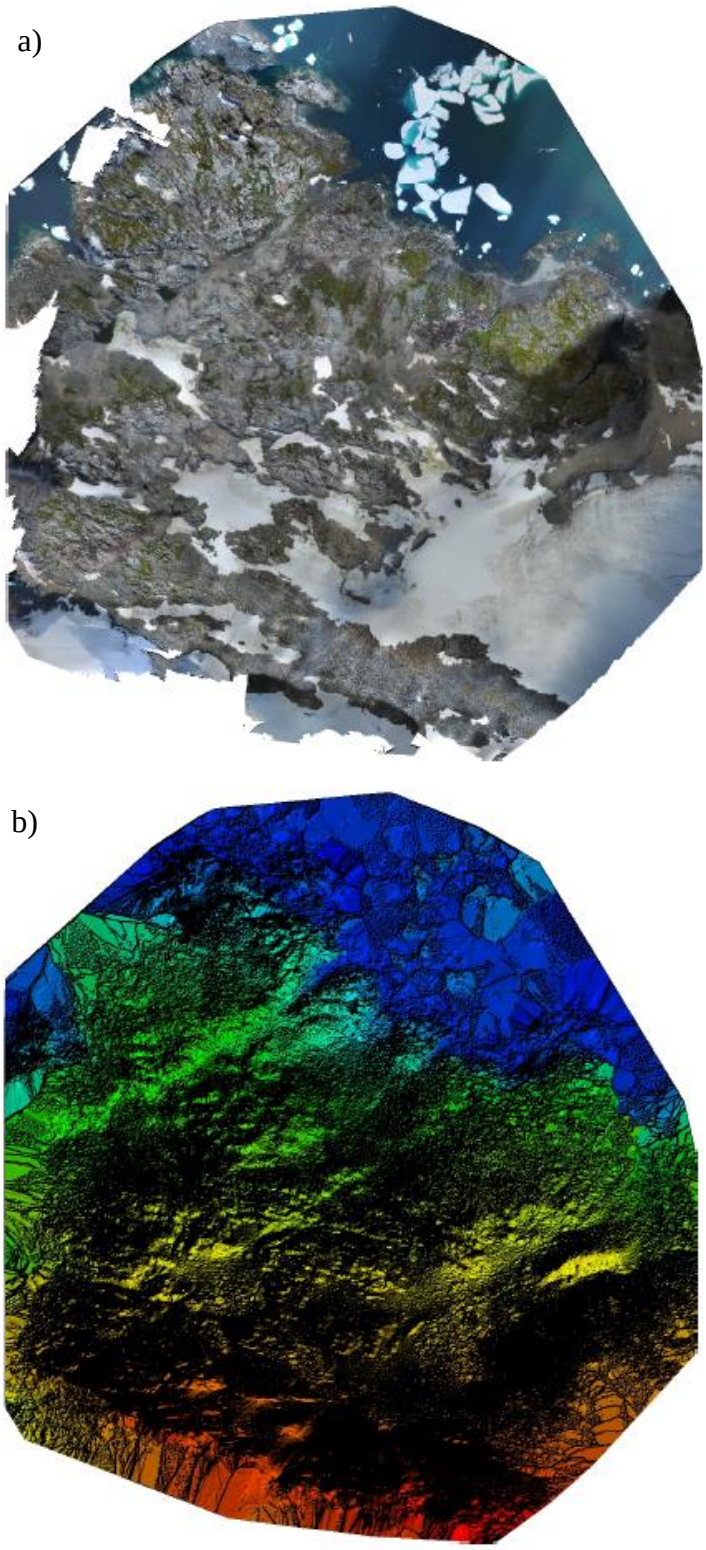

Figure 25. a) Resulting orthophoto mosaic of the area of study made using UAV aerial images. b) Digital Surface Model of the study area. (Font: Pix4D software processing. Resolution: 6.51cm).

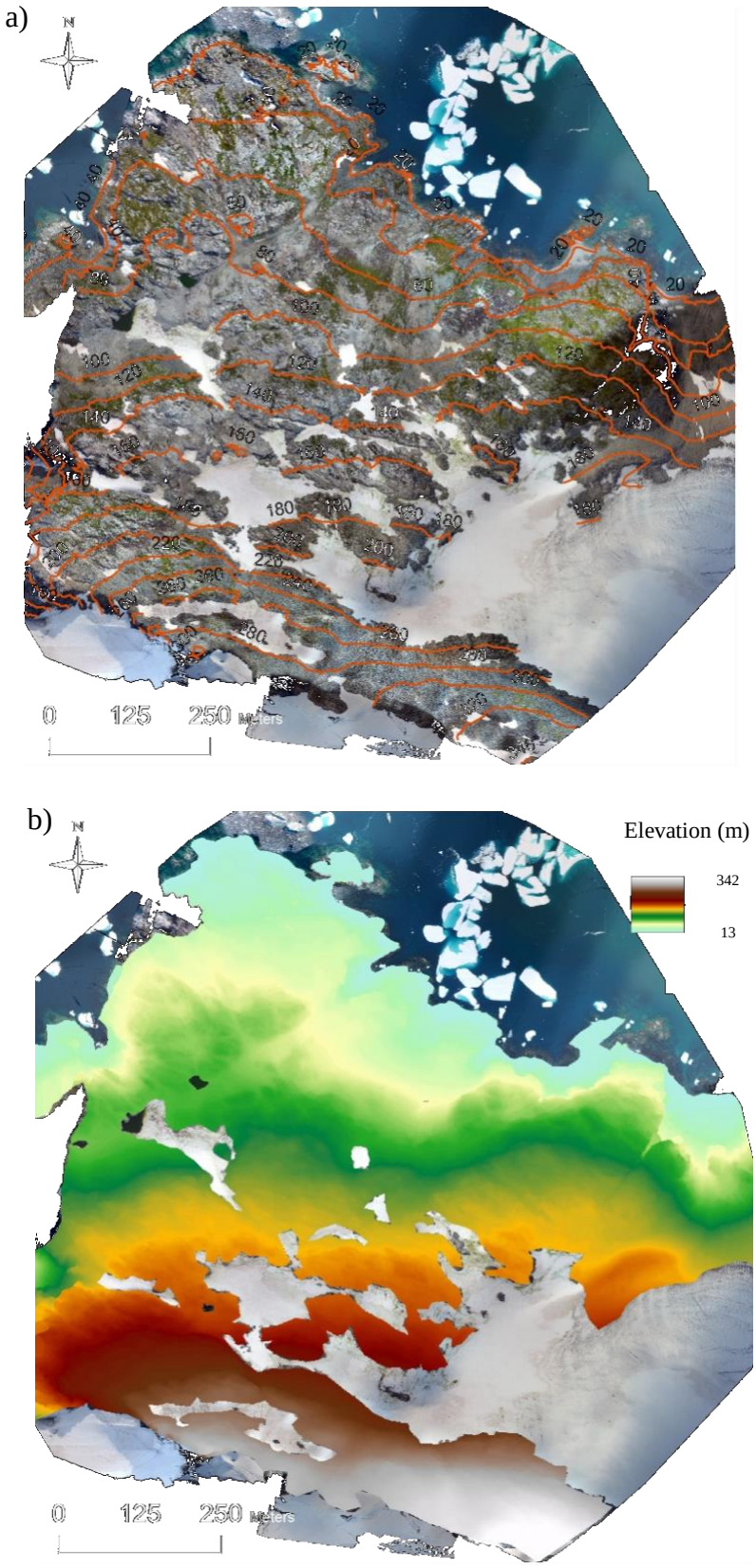

Figure 26. a) Ortophotomosaic with contour lines and clipped to the area of study. b) DSM clipped to the area of study. Altitudes in both maps are expressed in meters above the ellipsoid WSG84 (Font: ArcMap 10.4 processing. Resolution: 6.51cm).

A summary of the characteristics, type, sources and format of all the types of input data is presented in Table 3.

Data	Characteristics	Input format	Source	Analysis/ processing	Format after analysis
Ground Temperature	Discontinuous records from 2012 to 2018 taken every 4h.	Text (.txt)	9 boreholes with ground temperaure monitoring thrmistors	Data explortion, erasing of outliners, conversion to .xlsx, computation of MDGT	Excel sheet (.xlsx)
Air Temperature	Discontinuous records from 2012 to 2018 taken every 4h.	Text (.txt)	7 air temperaure monitoring thrmistors and 1 meteorological station	Data explortion, erasing of outliners, conversion to .xlsx, computation of MDAT	Excel sheet (.xlsx)
GPS coordinates and alttitude of 9 monitoring sites	Taken in situ in March 2018	Text (.txt)- Cartesian coordinates	Measured on field using D-GPS	Conversion to .xcls, spatial spotting of sites over a basemap	Excel sheet (.xlsx)
Aerial Images	1792 aerial images taken in situ in March 2018	Image (.jpeg)	UAV flight performance	Image processing in Pix4D, ortophotomap and DSM computation	DSM (raster), Ortophotomal (.tiff)
Ground GPS Countrol Points	Taken in situ in March 2018	Text (.txt)- Cartesian coordinates	Measured on field using D-GPS	Mosaic and DSM georeferencing through "ground truthing"	

Table 3. Summary of available data used for the analysis of the thermal regime and TTOP local and spatial modelling.

3.2 Analysis of the local ground thermal regimes

In order to understand the ground thermal regimes and the presence or absence of permafrost, it was conducted a graphical and analytic evaluation of the thermal regime for all the monitored sites using the observational data available.

For each borehole, all the parameters that characterize the ground temperature *"trumpet profile"* were estimated (Figure 2): *Maximum Annual Ground Temperature* (MaxAGT); *Minimum Annual Ground Temperature* (MinAGT); *Mean Annual Ground Temperature* (MAGT), *Depth of Zero Annual Amplitude* (ZAA), *depth at the Top Of Permafrost* (TOP),

Temperature at the Top Of Permafrost (TTOP) and *Mean Annual Thermal Offset* between the TOP and the surface (Toffset).

For computing these parameters, the observed ground temperatures of years 1 and 2 (Mar2012-Mar2014) were considered, as they are the only years with a complete dataset for the whole freezing-thawing period in all sites (see Table 2 section 3.1.2).

Firstly, the two-year's average values of MaxGAT, MinGAT and MAGT in all depths for each borehole were determined (Annex A1). Then these values were plotted in a ground temperature to depth graphs to determine each borehole's thermal *"trumpet profile"* as exemplified in Figure 27.

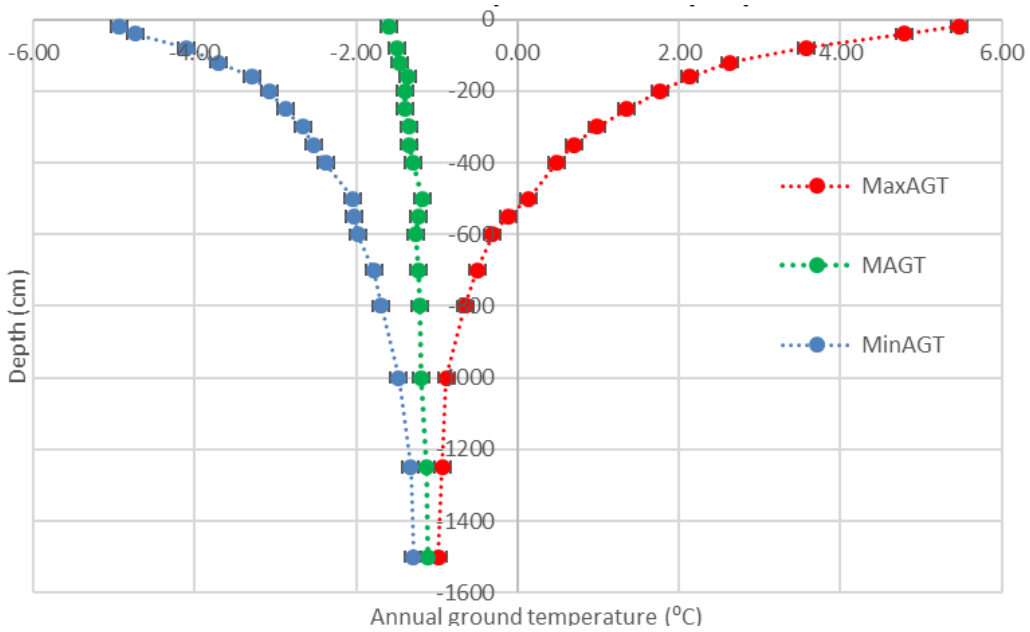

Figure 27. Ground temperature to depth plot of the maximum (red), mean (green) and minimum (blue) annual ground temperatures constituting a borehole's "trumpet profile".

When estimating each borehole's ground trumpet profile, one must account for that the MAGT profile is not strictly linear but is offset to progressively lower values at depth within the active layer (Goodrich, 1978). Therefore, the best-fit to the observed data for the MAGT was not estimated as a strictly linear function but by adjusting the best curve to the observed data.

On the other hand, MinAGT and MaxAGT values, respectively increase or decrease with depth, following a non-linear function (Figure 2). Eventually, the ground temperature reaches the equilibrium and becomes seasonally invariable below the ZAA point. At this depth, known as "depth of zero annual amplitude", values for MinGAT, MaxGAT and MAGT are considered infinitesimally equal (Péwé, 2016).

Considering the behaviour explained above, the MinAGT and MaxAGT functions were approximated by minimum least square polynomial regressions. We have individually selected the most suitable polynomial degree of regressions for MinGAT and MaxGAT in terms of two facts: the regression curve with the highest value of local adjustment to the observed range of data (higher R^2 values); and the regression curves whose trend tends to cross together with MAGT at a common ZAA point. Values for local residuals, standard error and R^2 of each estimation were determined as well.

For the boreholes where the depth of observations does not allow plotting the complete thermal regime's trumpet profile until reaching the Top of Permafrost (sites 2, 3, 4, 6, 7 and 9), the thermal profile was estimated down to the ZAA point by adjusting the most suitable least-squares regression curves to the available extent of the observed data.

It is important to highlight that the regression curves for MinGAT and MaxGAT parameters should just be considered as good estimators locally, at lower depths than the ZAA depth. Below this depth, the temperature of permafrost becomes seasonally invariable (Delisle, 2007) and increases steadily with depth following the MAGT tendency until reaching the base of permafrost (0 ºC) (Péwé, 1979).

Once we had the graphs of all site's ground thermal profiles, we determined the observed values (sites 1, 5 and 8) and the estimated by curve adjustment values (sites 2, 3, 4, 6, 7 and 9) of the following parameters: depth of the Top of Permafrost (depth value when MaxGAT = 0 ºC), Temperature at the Top of Permafrost (MAGT at the depth when MaxGAT = 0 ºC), depth and temperature at the ZAA point (depth and MAGT values when the three functions cross together), Mean Annual Ground Surface Temperature (MAGST), and the active layer's thermal offset (computed as the difference between TTOP and MAGST (Burn and Smith, 1988).

The ground surface temperature is a key parameter for the calculation of the MAGST and thus, for the calculation of the thermal offset as well. However, often ground surface temperature is not easy to measure due to the radiative and convective energy flows at the surface and difficulty in keeping the sensor in the same position. Because of these difficulties, nominal surface temperature measurements are often taken a few centimetres below the surface (Riseborough, 2003). In this work, because no data was available on temperature at the surface to empirically determine MAGST values for each borehole, corresponding values are based on data measured at 5 cm depth under the ground surface (i.e. the depth of the shallowest thermistor in all the boreholes).

3.3 TTOP Model implementation

Once analysed the ground temperature regimes profiles for the 9 specific locations, the next step was the implementation of the TTOP model.

The TTOP model predicts the mean annual ground temperature at the depth of the *top of the permafrost*, or at the base of the seasonal freezing and thawing layer, if permafrost is absent, using relatively simple parameters representing key climate and terrain factors influencing the ground thermal regime (Way, 2016).

The TTOP model was first computed and validated for the 9 locations, where observational temperature data is available. In a second stage, we spatialized the model all over the area of interest using statistical relations between topographic factors and the previously computed local TTOP model parameters, in a GIS-based environment.

3.3.1 TTOP MODEL'S THEORY

The TTOP model was developed by Smith & Riseborough (1996) to estimate the equilibrium temperature at the top of the permafrost at local or regional spatial scales. It constitutes a functional model of the relationship between permafrost and climate. It accommodates the geographical variations of climatic, surface and soil factors controlling the ground thermal regime and is a useful tool to analyse the impacts of climate change on ground temperatures (Smith & Riseborough, 1996).

Analysing the responses of permafrost to climate requires an appropriate characterization of the permafrost-climate system. Following Lachenbruch et al. (1988), the permafrost-climate

relationship can be depicted by the temperature regime at four levels: *(1) the temperature at standard screen height; (2) the temperature at the snow surface; (3) the temperature at the ground surface; (4) the temperature at the top of permafrost.*

Differences in mean temperature values at each of these levels are due to the variation trough time of heat transfer coefficients with temperatures through the different layers of the system. In the lower atmosphere, turbulent transfer varies diurnally and seasonally between stable and unstable conditions. Heat conduction at ground level varies between frozen and thawed states. The presence or absence of the snow cover determines if heat transfer right above the ground surface is predominantly conductive or convective. Heat transfer processes occurring at this interface and within the buffer layer are complex, implicating radiative influxes, turbulence, conduction, evaporation, and transpiration of living vegetation (Smith & Riseborough, 1996).

The TTOP model uses the temperature regime at the top of permafrost (state 4) as the best level to study the climate-permafrost linkages, relating ground temperatures to the annual cycle of atmospheric temperatures. Between ground and atmospheric temperatures, the model takes into account the effects of local soil properties and surface conditions such as vegetation and snow cover, being the first considered as the greatest local influence on permafrost temperatures followed by the surface snow cover and vegetation (Smith & Riseborough, 1996).

Therefore, the TTOP model predicts the mean annual ground temperature at the depth of the top of the permafrost, or the base of seasonal freezing and thawing layer if permafrost is absent, using parameters representing climate, surface and lithological factors that have influence in the ground thermal regime (Smith and Riseborough 1996, Way & Lewkowicz, 2016).

These parameters include the air freezing and thawing indexes, air-ground temperature functions *(n-factors)* and the ratio of freezing to thawing thermal conductivities that account for the ground thermal offset (Burn & Smith 1988; Smith & Riseborough 1996, 2002; Karunaratne & Burn, 2003; Bevington & Lewkowicz 2015). N-factors provide a simplified representation of the influence of the surface buffer layer in modulating heat exchange between the atmosphere and the ground surface (Way et al., 2016).

The standard formulation of the TTOP model as a function of all these parameters is expressed below in Equation 1a (Smith & Riseborough, 1996).

Secondary relations between the model's parameters shown in Equation1b were applied to the main TTOP formula in order to give a simplified expression for the model (Equation 2) that was later used on in this work.

a)

$$TTOP = \frac{(\frac{k_t}{k_f}\, n_T I_{Ta} - n_F I_{Fa})}{P}$$

(Smith & Riseborough, 1996)

b)

$$n_T = \frac{I_{Ts}}{I_{Ta}}$$

(Smith & Riseborough, 1996)

$$n_F = \frac{I_{Fs}}{I_{Fa}}$$

(Smith & Riseborough, 1996)

$$\frac{k_t}{k_f} = T_{offset}\frac{P}{I_{Ts}} + 1$$

(Romanovsky & Osterkamp, 1995)

Equation 1. a) TTOP model equation as a function of air freezing and thawing indexes, n-factors and the ratio of thawed to frozen conductivities. b) TTOP parameters as a function of secondary parameters.

$$TTOP = \frac{(n_T I_{Ta} - n_F I_{Fa})}{P} + T_{offset}$$

Equation 2. a) TTOP model equation as a function of air freezing and thawing indexes, n-factors and the seasonal thawing layer's thermal offset (Way et al., 2016).

Where:

Ttop= Temperature at the top of permafrost (ºC)

Kt= Thermal condictivity of thawed ground (W/mK)

Kf= Thermal conductivity of frozen ground (W/mK)

Ita=Cumulative air thawing degree days (ºCdia)

Ifa=Cumulative air freezing degree days (ºCdia)

Its=Cumulative surface thawing degree days (ºCdia)

Ifs=Cumulative air surface degree days (ºCdia)

Nt= Scaling factor between air and surface thawing index

Nf= Scaling factor between air and Surface freezing index

Toffset= Temperature difference between the TTOP and the ground surface (ºC) (Burn & Smith, 1988)

P= Complete period for a whole thawing-freezing cycle (typically around 365 days)

Note that, considering the relation of *n-factors* with *Its* and *Ifs* exposed above (*nt=Its/Ita; nf=IfsIifa*), the expression *(ntIta-nfIfa)/36*5 represents the mean annual ground surface temperature (Smith & Riseborough, 1996) and Equation 2 could also be expressed as the following Equation 3:

$$TTOP = \frac{(I_{Ts} - I_{Fs})}{P} + T_{offset} = MAGST + T_{offset}$$

Equation 3. TTOP as a function of mean annual ground temperature and the thermal offset.

3.3.2 LOCAL COMPUTATION OF THE TTOP MODEL

First, the TTOP model and its parameters were computed for the 9 monitoring sites where empirical data is available. Then, we evaluated the adjustment of the results given by the TTOP model formula to the TTOP values previously estimated or observed in each location using the results given by the *trumpet profile's* analysis in Section 3.2.

3.3.2.1 Freezing and thawing air degree days

Air freezing degree-days *(If)* or air thawing degree-days *(It)* are defined as departures of air temperature from 0 ºC. This index, also known as *freezing* or *thawing* index, is a measure of both duration and magnitude of below-freezing (or above-thawing) temperatures during a specified period. Therefore, the cumulative values of *If* or *It* for a given whole freezing-thawing cycle gives insights about how cold or warm it has been the winter *(freezing)* or summer *(thawing)* season and for how long (Maslanik & Yu, 2010).

As summarized in Frauenfeld et al. (2007), there are different ways to calculate the air freezing and thawing indexes in the literature. Huschke (1959) proposed the concept of a *seasonal freezing and thawing index*, which stayed as the present definition of *freezing/thawing indexes* given by the *American Meteorological Society's* (AMS). The seasonal freezing index is computed in a particular site as the sum of all negative and positive daily air temperatures between the highest point, in autumn, and the lowest point, the next spring, on the cumulative degree-day time curve. In the same way, the seasonal thawing index is calculated as the arithmetic summation of all positive and negative mean daily air temperature at a specific site along the period from the spring until the next autumn.

Harris (1981) determined the *total annual freezing and thawing index*, which is estimated as the respective sum of all negative or positive mean daily air temperatures during a calendar year. Nonetheless, this definition is debatable since the freezing index computed over a calendar year does not include a complete cold season.

For this investigation, we computed the *annual freezing and thawing indexes* as the area falling behead the sinusoidal curve (or integrated mean daily temperatures), for all days with temperatures below or above 0 °C, respectively, during a complete freezing/thawing natural cycle period (equation 4a). Empirically, this freezing and thawing indexes can be simplified as the absolute summation of the mean daily air temperatures for all days with temperatures below freezing *(If)* or above thawing *(It)* during a complete freezing/thawing cycle (Equation 4b) (Frauenfeld et al., 2007).

The annual freezing and thawing complete cycles over our dataset were defined in the PERIOD column of Table 2 (in Section 3.1.2) and go from the beginning of one year's autumn (around March) to the end of the next year's summer (around March next year), including both complete freezing and thawing periods. However, only the air temperatures of year 1 and 2, which have continuous air and ground temperature records during the total cycle (green tick, grey coloured), were used for the estimation of the *Ita* and *Ifa* parameters in this work.

a) b)

$$Ifa = \int_{T0}^{T2} |Ta|\, dt,\ \ Ta < 0ºC \quad \Longrightarrow \quad Ifa = \sum_{i}^{Nf} |Tai|\,, Tai < 0ºC$$

$$Ita = \int_{T0}^{T2} |Ta|\, dt,\ \ Ta > 0ºC \quad \Longrightarrow \quad Ita = \sum_{i}^{Nt} |Tai|\,, Tai > 0ºC$$

Equation 4. Equations for the computation of freezing and thawing air indexes (Frauenfeld et al, 2007).

Where:

Ifa =air freezing index

Ita= air thawing index

Ta= mean daily air temperature, integrated from the beginning of the autumn (t0) to the end of the next summer (t2) in the freezing/thawing cycle.

Nf= Number of days with temperatures below 0 ºC over the whole freezing-thawing period.

Nt= Number of days with temperatures above 0 ºC over the whole freezing-thawing period.

Note that *If* is assigned a positive value when the temperature is below 0 ºC, so that (Ita-Ifa)/P in fact accounts for the mean annual air temperature (Smith & Riseborough, 1996).

3.3.2.2 Surface Freezing/Thawing degree days

Annual surface freezing degree-days *(Ifs)* or surface thawing degree-days *(Its)* are defined as departures of ground surface temperature from 0 ºC, during a complete freezing-thawing cycle (Maslanik & Yu, 2010).

Following the same concept as the air degree days explained in the previous section, the annual surface freezing and thawing indexes are computed as the area falling behead the sinusoidal curve (or integral) of daily ground surface temperatures for all days with daily ground surface temperature below or above 0 °C during a whole freezing-thawing period respectively.

Empirically, the freezing and thawing indexes can be simplified as the absolute summation of the mean daily surface temperatures over those days in the whole period when temperature is below freezing or above thawing (Frauenfeld et al., 2007). The annual freezing-thawing periods considered for the computation of these indexes is the same as the one used for the determination of the thawing and freezing air degree days. The general freezing and thawing indexes are calculated as per Equation 5:

$$Ifs = \int_{T0}^{T2} |Ts|\, dt,\ \ Ts < 0ºC \quad \Longrightarrow \quad Ifs = \sum_{i}^{Nf} |Tsi|\,, Tsi < 0ºC$$

$$Its = \int_{T0}^{T2} |Ts|\, dt,\ \ Ts > 0ºC \quad \Longrightarrow \quad Its = \sum_{i}^{Nt} |Tsi|\,, Tsi > 0ºC$$

Equation 5. Equations for the computation of freezing and thawing ground surface indexes.

As previously mentioned in Section 3.2, as no data was available on temperature at the surface in this work, corresponding values are based on data measured at 5 cm depth under the ground surface. The final expression for *It* and *If* considering the surface at 5cm depth are expressed in Equation 6:

$$Ifs \approx If_{5cm} = \int_{T0}^{T2} |T_{5cm}|\, dt,\ \ T_{5cm} < 0ºC \quad \Longrightarrow \quad Ifs \approx If_{5cm} = \sum_{i}^{Nf} |T_{5cm}i|\,, Tsi < 0ºC$$

$$Its \approx If_{5cm} = \int_{T0}^{T2} |T_{5cm}|\, dt,\ \ T_{5cm} > 0ºC \quad \Longrightarrow \quad Its \approx If_{5cm} = \sum_{i}^{Nt} |T_{5cm}i|\,, Tsi > 0ºC$$

Equation 6. Equations for the computation of freezing and thawing ground indexes at 5cm depth.

Ifs =ground freezing index at 5cm depth

Ita= ground thawing index at 5cm depth

$\boldsymbol{T_{5cm}}$= mean daily ground temperature at 5cm depth, integrated from the beginning of the autumn (t0) to the end of the next summer (t2) in the freezing/thawing cycle.

Nf= Number of days with ground temperatures below 0 ºC over the whole freezing-thawing period.

Nt= Number of days with ground temperatures above 0 ºC over the whole freezing-thawing period.

Note that *If*s is assigned a positive value when the temperature is below 0 ºC, so that *(Its-Ifs)/P* actually accounts for the mean annual ground surface temperature (Smith & Riseborough, 1996).

3.3.2.3 nt, nf

N factors relate seasonal air temperature to ground surface temperatures separated into two seasonal regimes, freezing and thawing (Lunardini, 1978). These affords a highly simplified expression to account for the local influence of vegetation (moss bed in this work) and snow cover in a variety of heat transfer processes (e.g. conduction, convection, transpiration) occurring within the buffer layer constituted by different surface land-covers (Lunardini, 1981). As the snow cover is reduced to the minimum in summer, the summer thawing n-factor incorporates all microclimatic effects (radiation, convection, evapotranspiration, etc.) due mainly to the moss cover while the winter freezing n-factor is mainly dominated by the influence of snow cover. (Smith & Riseborough, 1996)

The n-factors are generally greater in the thawing season (*nt*) than the freezing season (*nf*) (Taylor, 1995; Smith et al., 1998), while the freezing season n-factor has been proved to be lowered at sites without permafrost, or with a very deep active layer, because of the continuing contribution of latent heat released during frost penetration (Burn, 1998).

In general, the n-factors are determined empirically, by collecting air and surface ground temperatures simultaneously at sites representative of ecological units. Then, the n-factors are calculated as the ratio of the ground surface freezing or thawing indexes to the freezing or thawing air temperature indexes for the same season (Lunardini, 1978 in Burn, 1998), as per the Equations 7a and 7b.

a) $$n_T = \frac{I_{Ts}}{I_{Ta}}$$ b) $$n_F = \frac{I_{Fs}}{I_{Fa}}$$

Equation 7. Expressions for the computation of n-thawing (a) and n-freezing (b) factors (Smith & Riseborough, 1996).

Ita = Cumulative air thawing degree days (ºCdia)
Ifa = Cumulative air freezing degree days (ºCdia)
Its = Cumulative surface thawing degree days (ºCdia)
Ifs = Cumulative air surface degree days (ºCdia)
nt = Scaling factor between air and surface thawing index
nf = Scaling factor between air and surface freezing index

Due to the scarce of experimental ground surface temperatures mentioned before in section 3.2, n-factors in this work were computed as the ratio of the ground freezing or thawing indexes at 5cm depth to the freezing or thawing air temperature indexes (Equation 8). Therefore, by considering $Ts \approx T5cm$, the n-factors in this work not only accounts for the moss and snow cover, but for the thermal offset occurring in the top 5cm surface layer as well.

$$n_T = \frac{I_{Ts}}{I_{Ta}} \approx \frac{IT_{5cm}}{I_{Ta}} \qquad n_F = \frac{I_{Fs}}{I_{Fa}} \approx \frac{IF_{5cm}}{I_{Fa}}$$

Equation 8. n-factors as expressed as the ratio between thawing and freezing indexes at 5cm depth and air thawing and freezing indexes.

Following the expressions represented above, in sites 1, 2, 3, 6, 7 and 9 (characterized by a bedrock substrate), the n-factors account for the top 5 cm rock surface layer plus the potential snow cover thermal buffer effect through the year. For sites 4 and 5 (characterized by a unconsolidated substrate), the n-factors account for the top 5 cm soil layer plus the potential snow cover thermal buffer effect through the year. Finally, in site 8 (characterized by 40 cm of moss cover over a peat substrate), the n-factors account for the top 5 cm moss layer plus the potential snow cover thermal buffer effect through the year.

3.3.2.4 Kt/Kf

Kt/Kf stands for the ratio between the thermal conductivity of a thawed soil and the thermal conductivity of the same soil when frozen.

Considering that the soils are composed by multiple phase materials with different physical properties such as solid particles, gas and/or liquid, the thermal properties of the soils are affected by the variation of each phase too. As mentioned in Dong et al. (2015), the thermal conductivity *k* varies depending on the soil phase. As an example, values of k of different materials are given: thermal conductivity of mineral particles *kmineral = 3 W/m K*, thermal conductivity of dry soil *kdry_soil=0.5 W/m K* , thermal conductivity of water *kwater = 0.56 W/m K (at 0 ºC)*, and thermal conductivity of air *kair = 0.026 W/m K*) (Mitchell & Soga 2005; Yun & Santamarina 2008).

In dry soils, which account with a lower packing density of particles and more porosity, the air obstructs the heat conduction occurring through the particle contacts. This fact, together with the mineral composition, explains the significant difference between k values of pure mineral soils and dry soils (Farouki, 1981). At the other end, in water saturated soils, the replacement of air with water provides a significant improvement in the heat conduction through the soil mixture. Consequently, the magnitude of the thermal conductivity of water-saturated soil is between that of the pure mineral and that of water. The ordered sequence of typical thermal conductivity values is: *kair<kdry_soil<kwater<ksaturated_soil<kmineral*.

Therefore, the thermal properties of soils, considering isothermal conditions, mainly depend on different factors as: mineralogy, particle size, particle shape, porosity and moisture content (Dong et al., 2015). These factors can be sum up in two main groups: soil type and ground water content.

- *Soil type:* Mineralogy, porosity particle size and shape are the characteristics defining de different types of soil. Pure mineral soils are the ones characterized by the highest thermal conductivity in the air–water–solid soil system.
  Considering that a larger particle's diameter promotes a higher rate of heat flux between particles, larger particles with less contacts in a given volume result in higher thermal conductivity (Aduda, 1996).
- *Water content:* Moisture content in the soil is a dominant factor to the thermal conductivity. The higher the water content in the soil, the higher heat transfer rate through the substrate, especially in unconsolidated and high porosity soils.

3.3.2.5 Thermal Offset

The thermal offset is defined as the difference between the TTOP and at the MAGST (Wu & Shi, 2003) (see Equation 9). This equation comes from the relation previously represented in Equation 3.

$$Toffset = TTOP - MAGST$$

Equation 9. Thermal offset as a function of TTOP and MAGST (Burn & Smith, 1988)

In Equation 9, TTOP stands for the temperature at the top of permafrost and MAGST for the mean annual ground surface temperature, which in this work, is considered 5 cm below the surface.

The thermal offset arises because the thermal conductivity of a soil is higher when frozen than when thawed. This effect can be explained by the seasonal variations in soil moisture near the ground surface, with drier surface conditions in the thawing period and wetter conditions in the freezing period increasing the effect (Smith & Riseborough, 1996).

A theoretical expression to link thermal offsets with the thermal regime and characteristics of the active layer near-surface permafrost (Equation 10) was put forward by Romanovsky & Osterkamp (1995):

$$Toffset = \frac{Its}{P}\left(\frac{Kt}{Kf} - 1\right)$$

Equation 10. Active layer thermal offset related with its thermal regime and characteristics (Romanovsky & Osterkamp,1995).

In Equation 10, *kf* and *kt* are the thermal conductivities of the active layer in frozen and thawed states, *Its* is the annual total thawing degree-days at the ground surface and P is the period of the thawing and freezing cycle.

As ground thermal fluxes were not measured in this investigation, the values of *Kt* and *Kf* could not be compute for our locals and its uncertainty cannot be discussed. However, the thermal offset values for each monitoring site was determined with the application of Equation 9 when analysing the ground temperature to depth "*trumpet profile"* graphs. Therefore, Equation 2 was the general expression chosen for the computation of the TTOP model in this work.

3.3.2.6 TTOP local implementation and validation

Once the TTOP model parameters were determined for the 9 monitoring sites, we used the results to implement the general TTOP model formula (Equation 2) in these locations to determine the Temperature at the Top of Permafrost. Then, we evaluated the adjustment of the results given by the TTOP model formula to the TTOP values previously estimated or observed in each location using the analysis of the *trumpet profile*.

To validate the TTOP model at a local scale, we plotted the TTOP formula results with the values observed or estimated values by graphical analysis of the trumpet profile. The better the adjustment of the scatter dots to the *y=x* line, the better is considered the estimation of the TTOP model.

After evaluating this adjustment, the TTOP model was found to be a good estimator for the temperature at the top of permafrost, suitable to be spatially extrapolated for the whole area extent.

3.3.3 SPATIAL COMPUTATION OF THE MODEL

Once calculated the values of all the parameters of the TTOP model for the 9 sites, we aimed to spatialize these parameters, in order to extend the local TTOP model results to the study area. Each parameter of the model was spatialized following its statistical relations with different terrain features.

In order to identify the spatial controls on the TTOP parameters, literature was reviewed to identify which features were expected to show a higher influence in each TTOP parameter using the literature.

Secondly, the spatial distribution of these terrain features was modelled using the software ArcMap10.4.

Later on, the correlations between each terrain feature and the TTOP parameters, were calculated, in order to identify their statistical significance in our particular area of interest.

Finally, statistical relations were established between TTOP parameters and its most influencing terrain features. The workflow for this process is explained below.

3.3.3.1 Potential influence of terrain features in the TTOP parameters

A) <u>Air thawing and freezing indexes</u>

The air thawing and freezing indexes *(It, If)* are directly related with the air temperature. However, the atmosphere is not isothermal but air temperature generally falls quite noticeably with increasing altitude following the *adiabatic lapse rate* of the atmosphere, defined as "the change of temperature with a change in altitude of an air parcel that decreases in pressure and temperature and increases in volume without gaining or losing any heat to the environment surrounding the parcel" (Muralikrishna & Manickam, 2017).

As a function of air temperature, the air thawing and freezing indexes are also expected to be linearly related with height.

B) <u>N-factors</u>

In section 3.3.2.3, we introduced that n-factors mainly account for the local influence of moss cover, snow cover and the 5 cm surface layer thermal offset, which variates depending on surface characteristics (soil type and moss bed).

The primary influence of moss cover in *n-factors* is due to the great insulation effect, as the moss both shades and insulates the ground resulting in a reduction of solar radiation reaching

the ground surface and summer heat flux (Guglielmin et al., 2012). In addition, the interception of precipitation and the transpiration by the moss influences the ground thermal regime through the water balance (Smith & Risebourgh, 1996). Consequently, sites covered by moss are expected to be characterized by lower values of *n-factor*, representing a greater ground insulating buffer layer, while bare ground sites show higher *n-factors* with values closer to the unity (air temperature equals the ground surface temperatures).

On the other hand, considering that our study area consists only of the snow-free areas in the end of summer, a buffer layer of snow will form over most places, mainly during the winter. Snow cover of any depth acts as a physical barrier, preventing solar radiation and wind variations from influencing temperature fluctuations on the ground surface (Humlum, 1997). In addition, the low thermal conductivity of snow restricts the loss of heat from the ground during the coldest part of the year. As a result, local spatial variability in snow cover is the largest single factor accounting for variations in the ground surface temperature mainly during the winter months (Desrochers & Granberg, 1988), but also in spring and autumn, although at a lower rate as these seasons are generally characterized by thinner snow cover (Guglielmin et al., 2012). Therefore, snow cover has a strong influence mostly in the *freezing* n-factor values. This relationship between snow cover and *nf* is expected to be negative, thus the thicker the snow cover, the higher the insulation and the lowest the freezing *n-factor* (Lanouette et al., 2015).

The spatial distribution of snow cover usually depends on topographic features and characteristics of the ground. Elevation, aspect and curvature are topographic features that have been found to be statistically significant in the variability of winter snow accumulation and spring melt according to results obtained by Erickson & Williams (2005) and Jost et al. (2007). These studies showed that elevation had a strong positive relationship mainly in the periods of peak snow accumulation and during snow-melt. Regarding to aspect, south-facing slopes would have the highest correlation with snow accumulation in the southern hemisphere.

The curvature affects the acceleration, deceleration, convergence and divergence of flow across the surface and, therefore, influences snow deposition. Concave curvatures are expected to have a higher potential accumulation of snow than convex sites.

The last factor influencing in the *n-factors* would be the thermal offset present in the 5 cm top surface layer, this mainly depending on the thermal characteristics of the top 5 cm soil layer,

being the substrate type and water content the main factors with potential influence on its thermal characteristics.

Therefore, elevation, aspect, curvature, moss cover, substrate type and water content might be somehow correlated with *n-factors* and were assumed as possible candidates explaining a large proportion of the spatial variability of *n-factors*.

B) Thermal Offset

In section 3.3.2.5, we introduced that the active layer thermal offset, as a function of the thawed and frozen thermal conductivity ratio *kt/kf*, accounts for the thermal properties of the substrate, which mainly depend on the type and water content of the substrate at different depths and locations (Wu & Shi, 2003). Equation 9 defines the thermal offset of the seasonally thawing layer as the difference of the temperature in the TOP and the ground surface.

Figure 28 suggests that the substrates with higher conductivity show steepest temperature gradients than the ones with lower conductivities (Williams & Smith, 1989). The steeper the thermal gradient (and thus the higher conductivity), the lower the result of the absolute value of the thermal offset (TTOP-MAGST) and vice-versa.

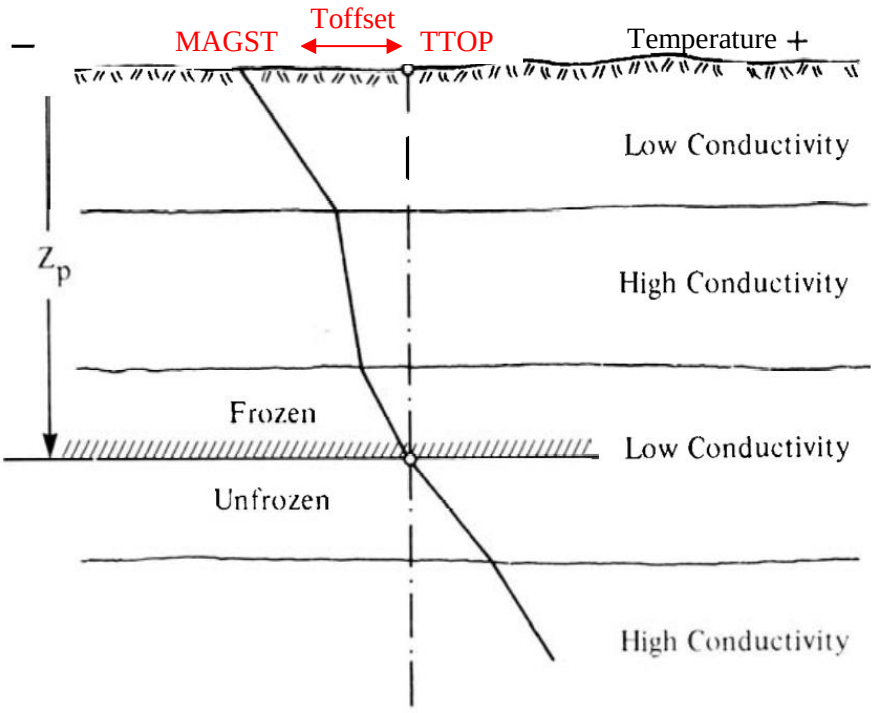

Figure 28. Influence of thermal conductivity on the ground thermal offset (modified from Williams & Smith, 1989).

Considering the aforementioned relation in section 3.3.2.4 (*kair* < *kdry_soil* < *kwater* < *ksaturated_soil* < *kmineral)*, the mineral soils and bedrock (with low porosity) have the highest thermal conductivity when they are dry, however, for peat and uncosolidated substrates (with higher porosity), a higher soil moisture content increases the soil's conductivity (Wu & Shi, 2003). Therefore, the water content of the substrate is expected to have a large influence in the thermal offset. However, the statistical relationships between thermal offset and water content must be determined separately for bedrock areas in one side and for peats and unconsolidated materials on the other.

3.3.3.2 Spatial distribution of TTOP controlling factors

Elevation, aspect, curvature, moss cover, substrate type and water content have been considered to have potential influence in TTOP parameters and are assumed to explain a large proportion of the spatial variability these parameters. The spatial distribution of these terrain features over the area of interest was implemented with a resolution of 1 m using the GIS based software ArcMap10.4 as follows:

- **Moss cover:** The areas covered by moss were determined by analysis of the high-resolution orthomosaic presented in Section 3.1.3. Feature polygons were manually created over the most noticeable moss patches using the software ArcMap 10.4. This feature layer was later converted to raster format (Figure 29).

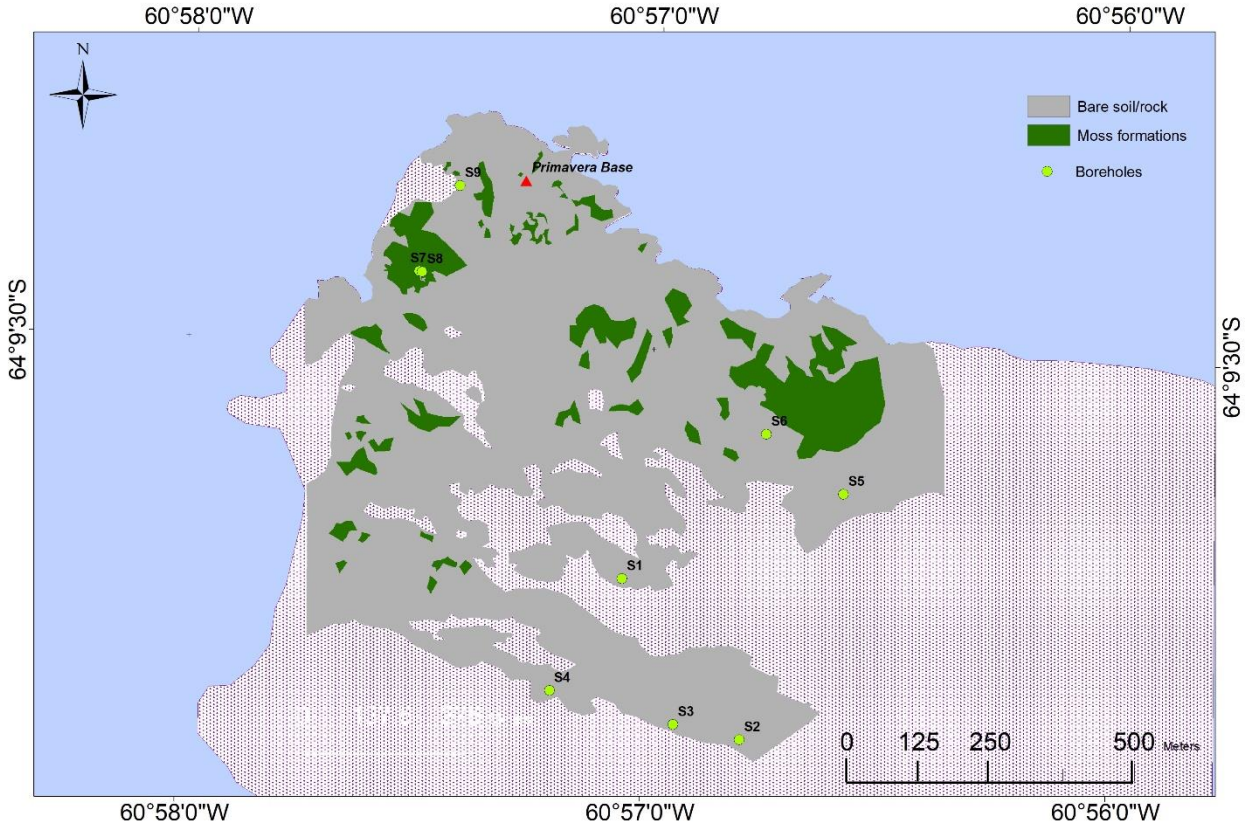

Figure 29. Moss-cover distribution in the modelled sectors of Cierva Point.

White dotted region represents areas of permanent snow, ponds or topographic errors standing out of the model. Spatial resolution: 1m.

- **Snow cover:** The seasonal snow cover cannot be determined by simple observation of the mosaic, as it represents an end of summer scenario and the distribution and thickness of the snow vary spatially and temporarily. As mentioned in section 3.3.3.1B, the surface snow accumulation depends on different landforms and terrain features, as elevation, aspect, terrain curvature or solar radiation.

  These parameters were derived from the 1 m resolution's digital surface model (DSM) described in Section 3.1.3 using the ArcGIS's Spatial Analyst tools:

- **Elevation:** Implicit in the DSM. Expressed in meters above the ellipsoid WSG84, being that the measure reference of the D-GPS devices used to cartograph the area (Figure 30).
- **Aspect:** Extracted from the DSM. Expressed in 5 classes, north (N), east (E), south (S), west (W) and flat (F) (Figure 31).
- **Curvature:** Profile curvature parallel to the direction of maximum slope. Extracted from the DSM as the second derivative of the surface. A positive curvature indicates the surface is concave at that cell. A negative curvature indicates the surface is convex at that cell. A value of 0 indicates the surface is rectilinear (Figure 32).

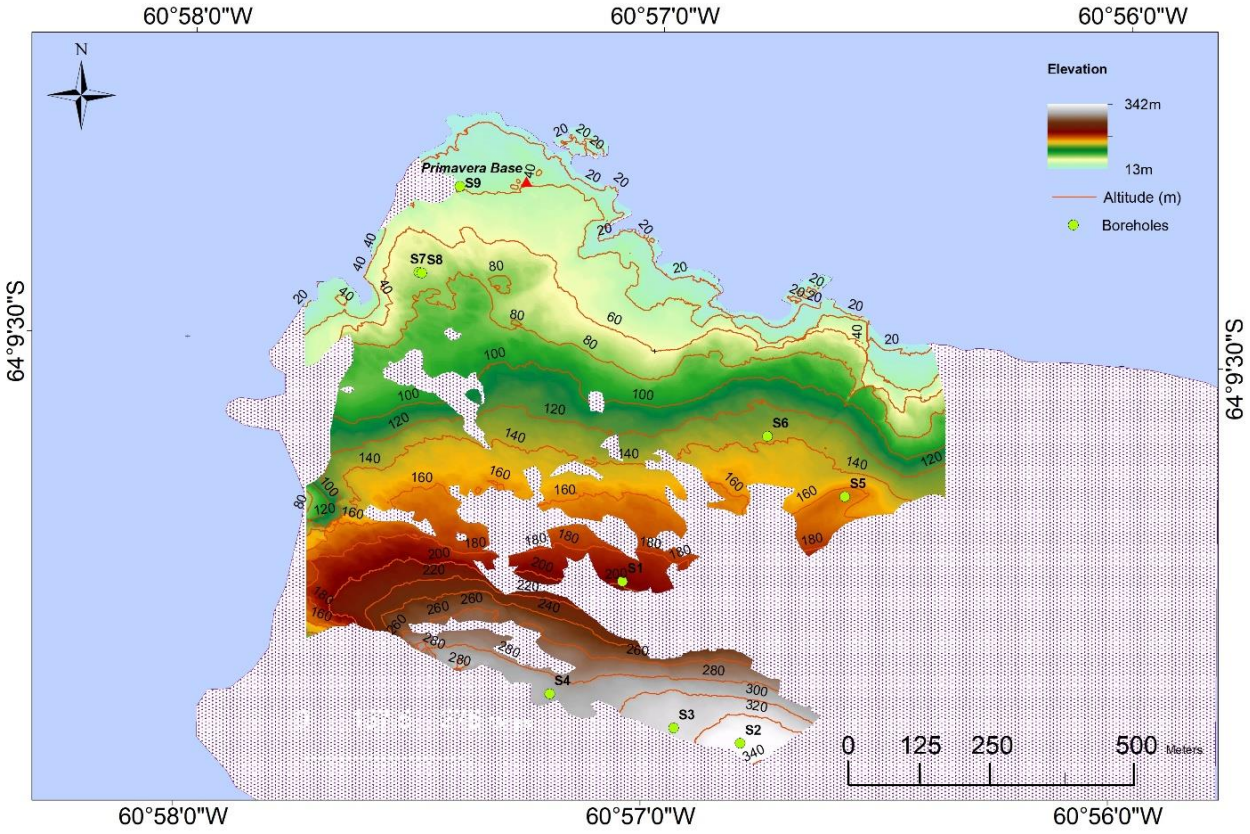

Figure 30. Altitude distribution in the modelled sectors of Cierva Point, expressed in meters above the ellipsoid WSG84. White dotted region include areas of permanent snow, ponds or topographic errors standing out of the model. Spatial resolution: 1m.

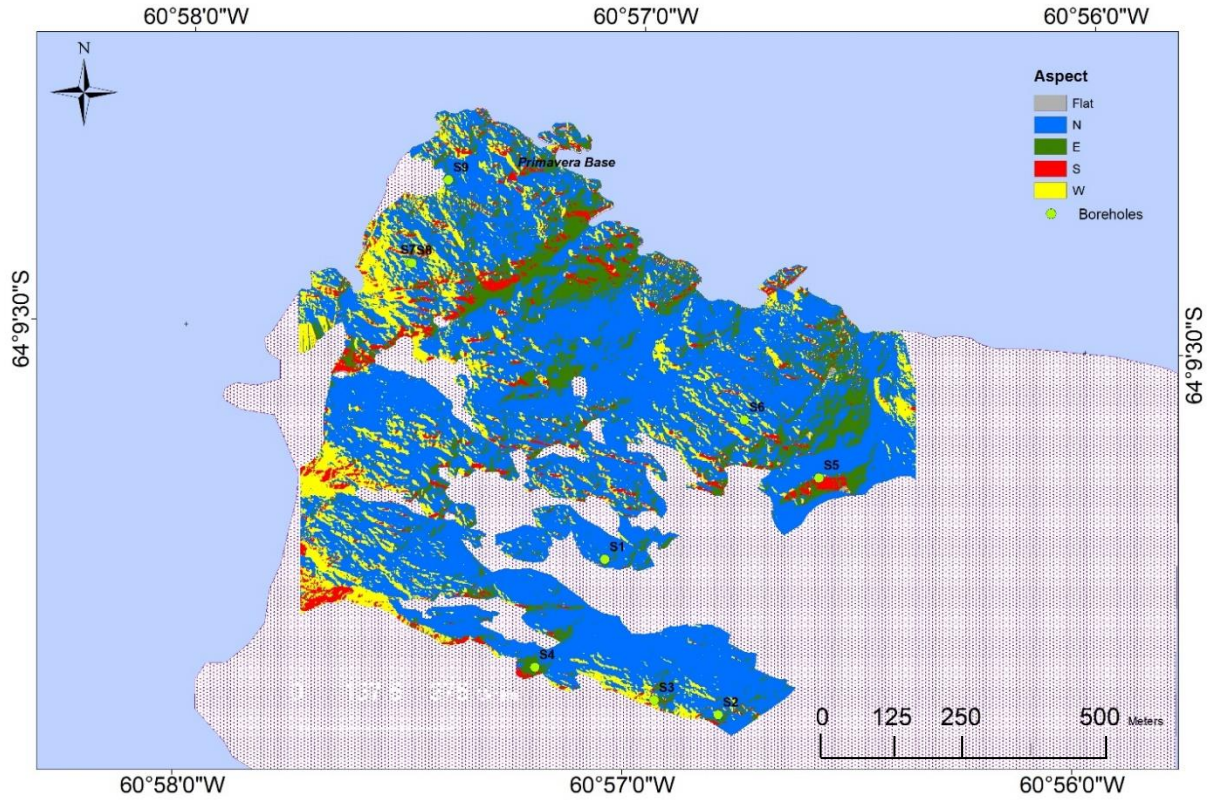

Figure 31. Aspect distribution in the modelled sectors of Cierva Point.

White dotted region include areas of permanent snow, ponds or topographic errors standing out of the model.

Spatial resolution: 1m.

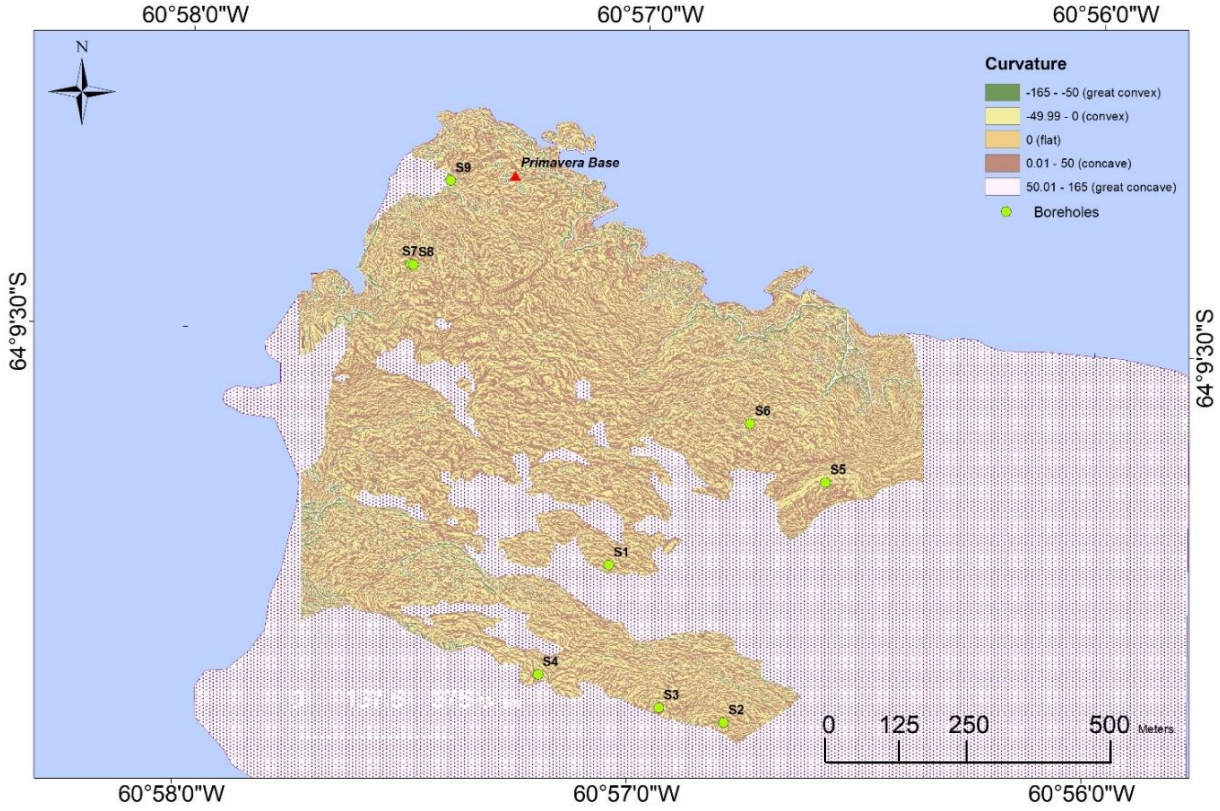

Figure 32. Distribution of the profile curvature in the modelled sectors of Cierva Point.

White dotted region include areas of permanent snow, ponds or topographic errors standing out of the model.

Spatial resolution: 1m.

- **Ground thermal offset:** The ground thermal offset is related with the soil's active layer ratio of thawed and frozen thermal conductivity (Equation 10). Therefore, the main influencing factors in the thermal offset are expected to be the same ones influencing the soil's thermal conductivity, such as the substrate type and water content (see Section 3.3.2.5).

  These two factors were determined as follows:

  - **Substrate type:** A soil type map was implemented through aerial photo interpretation in ArcMap 10.4 based on the high resolution ortophotomap. The substrate was classified in bedrock, unconsolidated soil and peat. Feature polygons were shaped over the different soil type's areas to be later converted to raster format (Figure 33).
  - **Topographic wetness index (TWI)**: The TWI is a steady-state wetness index that describes a form of potential wetness due to topographic and not subsurface conditions. The index is widely employed as a soil moisture substitute, and several studies exist relating it to measured soil moisture (e.g. Etzelmüller, 2006; Sulebak et al., 2000; Hugget and Cheesman, 2002).

    TWI index involves the upslope contributing area (*a*), a slope raster (B), in the following relation (Cooley, 2016a):

    $$TWI = \ln(a/\tan B)$$

    Equation 11. Equation for the calculation of the Topographic Wetness Index (TWI).

    The value of *a* for each cell in the output raster is the value of the flow accumulation for the corresponding DEM raster. It was extracted from the filled DSM following the method explained in Cooley (2016b).

    Higher TWI values represent drainage lines, with low gradient areas showing greater potential to gather water and increase potential soil water saturation. Lower values represent crests and ridges with steep and convex characteristics, tending to disperse water and showing lower potential soil moisture. The computed TWI spatial distribution is shown in Figure 34.

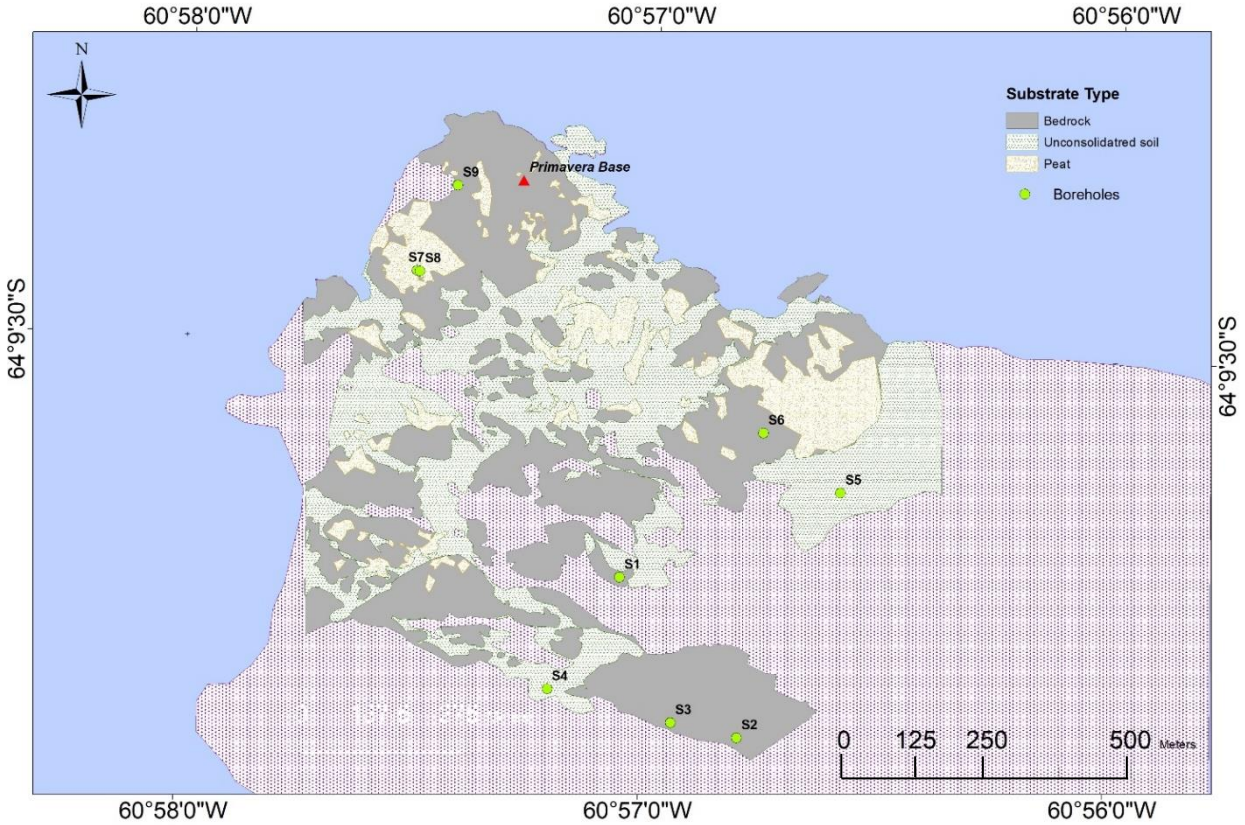

Figure 33. Distribution of the Type of substrate in the modelled sectors of Cierva Point.

White dotted region represents areas of permanent snow, ponds or topographic errors standing out of the model.

Spatial resolution: 1m.

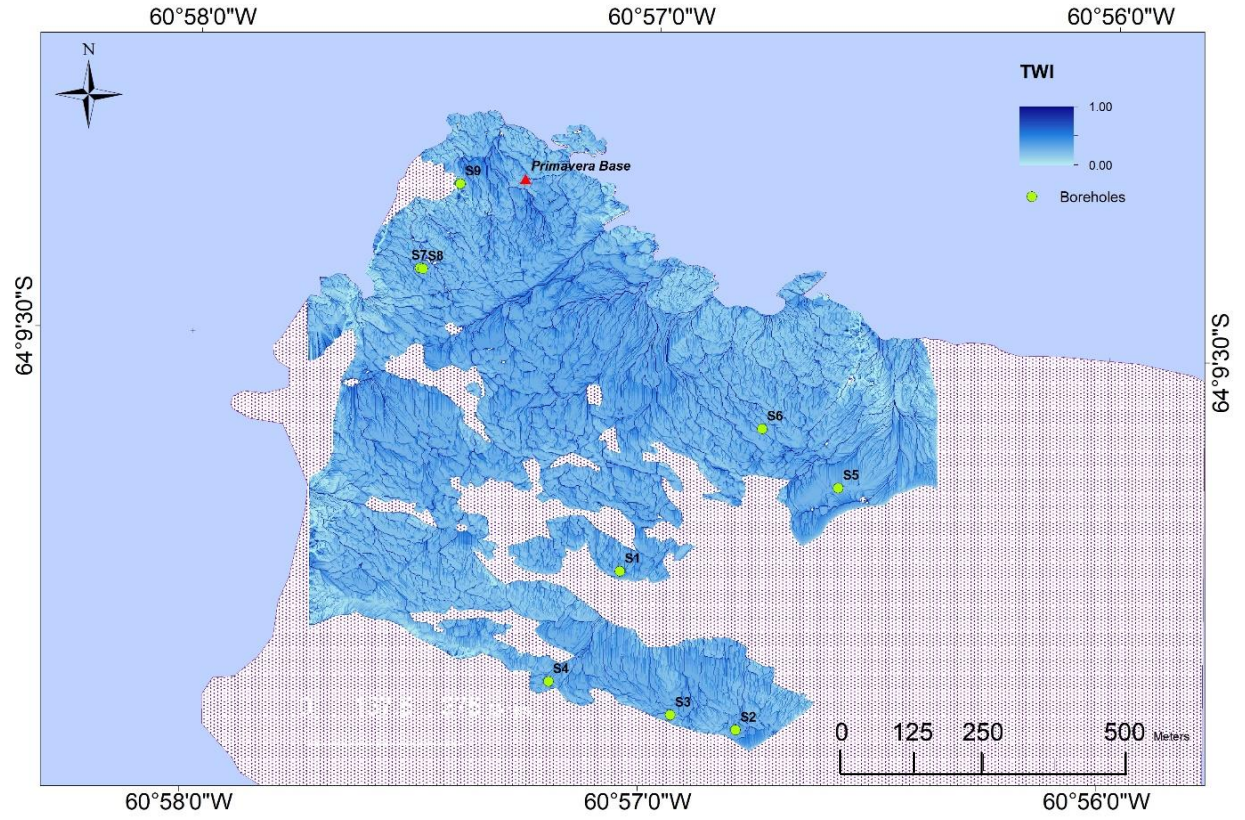

Figure 34. Distribution of the Topographic Wetness Index in the modelled sectors of Cierva Point.

White dotted region represents areas of permanent snow, ponds or topographic errors standing out of the model.

Spatial resolution: 1m.

3.3.3.3 Correlation between TTOP parameters and controlling factors

Once determined the spatial distribution of terrain features over the area, we analysed the statistical correlation between each feature and the previously computed local TTOP parameters for each monitoring site. This allows determining the statistical significance of the control of each terrain feature for the TTOP parameters.

To determine the correlations of these features, we computed non-parametric (Spearman) correlations and regression parameters using the statistical package IBM SPSS Statistics 25.

Spearman rank correlation is a non-parametric test that is used to measure the degree of relation between two variables. It assesses how well the relationship between two variables can be described using a monotonic function. The Spearman rank correlation test does not carry any assumption about the distribution of the data and is the appropriate correlation analysis when the variables are measured on a scale that is at least ordinal (Statistical Solutions, 2018).

The following formula was used to calculate the Spearman rank correlation:

$$\rho = 1 - \frac{6 \sum {d^2}_i}{n(n^2 - 1)}$$

Equation 12. Spearman Rank correlation formula (Statistical Solutions, 2018)

Where:

ρ= Spearman rank correlation

di= the difference between the ranks of corresponding variables

n= number of observations

A perfect Spearman correlation of +1 or −1 occurs when each of the variables is a perfect monotone function of the other. A positive correlation coefficient indicates a direct relationship between the two variables (as one variable increases, the other variable also increases), while a negative correlation coefficient expresses an inverse relationship (as one variable increases, the other variable decreases). A correlation coefficient of 0 indicates that no relationship exists between the variables and a coefficient of 1 indicates a perfect relationship (Statistical Solutions, 2018).

In order to determine the strength of the relationship, the conventions proposed by Cohen (1988) may be considered. He proposed that correlation coefficients between .10 and .29 represent a weak association, coefficients between .30 and .49 represent a medium association, and coefficients of .50 and above represent a large association or relationship.

3.3.3.4 Relationship functions and parameter spatialization

In order to identify the relationships between the TTOP parameters (dependent variables) and its most influencing factors (independent variables or predictors), we computed multivariate linear regressions using the SPSS software tool.

Following the Peter's rule of thumb, in order to estimate a dependant variable using multivariate linear regressions, ideally a minimum sample size of 10 sample points is needed per each independent variable used as a predictor (Peduzzi et al., 1996). The available sample size in this investigation is just 9 sample points, however this sample size was considered close enough to the minimum to apply this estimation method using only one estimator per each dependent variable. It is important to take in consideration that the scarce number of sample points might create a higher probability of relation due to randomness in the results.

For the estimation of functions using multivariable regression, it is first necessary to check some assumptions regarding to the input data. These assumptions are described below as per Statistical Solutions (2018b):

- Linearity: The outcome variable and the independent variables must follow a linear relationship. Scatterplots are a good tool to evaluate if there is a linear or curvilinear relationship.
- Multivariate Normality: Multiple regression consider that the residuals (differences between the observed value of the dependent variable and the predicted value) present a normal distribution. The normality of residuals can be evaluated with a normal Predicted Probability (P-P) plot. If they are, they will adjust to the diagonal normality line indicated in the plot.

- Homoscedasticity: Multiple regression assumes that the variance of residuals is similar across the values of the independent variables. When exanimating a plot of standardized residuals versus predicted values, we can evaluate weather points are equally distributed across all values of the independent variables. There should be no defined pattern in the distribution, the data should look like randomly speared over the plot; if there is a cone-shaped pattern, the data is heteroscedastic.
- No Multicollinearity: The independent variables must not be highly correlated with each other. This assumption can be tested using the Spearman correlation matrix (correlations among all predictor variables should be less than .80) or the Variance Inflation Factor (VIF) values should be lower than 10.

  However, as we just used one independent variable as a predictor for each model parameter (following the Peter's rule of thumb), it was not necessary to check this assumption conscientiously.

Following these considerations, each TTOP parameter was expressed as a function of the terrain feature with the highest Spearman correlation, besides a logic physical relationship as explained in section 3.3.3.1. Thus, *It* and *If* were expressed as a function of the elevation, *Nt* and *Nf* were to be expressed as a function of the moss cover and curvature respectively and, *toffset* as a function of TWI depending on the different soil types.

The rules compliance of the assumptions mentioned above was tested for each parameter of the linear regression. Exceptionally, a different method was used for the computation of the relationship between *nt* and moss cover. Simple linear regression cannot be applied to this parameter due to the availability of a single borehole with the moss cover attribute. This fact limited the statistical analysis of these data to correlations and created a high probability of relation due to randomness. However, the moss cover was shown to have a noticeable influence in the *nt* parameter in the correlation matrix and a difference of 1.01 in the *nt* values was observed between analogue monitoring sites 7-MossRock (*nt=2.00)* and 8-MossMoss (*nt=0.99)* only differenced by the presence of absence of moss cover. Thus, a different relation between *nt* factor and moss cover was applied for the spatialization of the parameter. The mean of *nf* values obtained in the moss-free monitoring sites (*nt=2.08)* was given to the moss-free areas, whereas this mean value minus 1.01, was given to all the areas covered by mosses.

3.3.4 SPATIAL MODEL IMPLEMENTATION

Once the relationship functions were established for each TTOP parameter, these expressions were computed in ArcMap 10.4 over the study area. The spatial distribution of the different parameters of the model resulted in five 1 m resolution rasters. Then, the TTOP model expression (Equation 2) was computed introducing as inputs the previously spatialized parameters. The resulting map for the spatial distribution of the TTOP model all over the study area had a resolution of 1 m as well and are presented in the results section 4.

3.4 Spatial model validation

Once a spatial model was created for each parameter, we checked how close the results of the parameters' spatial estimation were to the parameters determined locally for each monitoring site using observed data. Then, we validated the final TTOP spatial model by comparing the results to the observed data about the Temperature in the Top Of Permafrost previously determined in section 3.2.

3.5 TTOP spatial model considering a 1 ºC air temperature increase scenario

Once the TTOP spatial model was created, the resulting model was used to identify and evaluate the potential sensitivity of permafrost and the seasonal thawing layer in case of a hypothetical scenario, showing a 1 ºC increase in the long term mean annual temperatures. For this purpose, we computed the air thawing and freezing indexes with a 1 ºC increment over the recorded air temperatures during years 1 and 2. As a generalization, n-factors and thermal offset values were considered to remain constant in this hypothetical scenario, disregarding changes in any other topo-climatic factor such as seasonal snow pack, moss distribution or soil moisture content.

The TTOP spatial model was ran using the new input values of *Ita* and *Ifa*, considering the mean daily temperature increase of 1 ºC in a long-term scenario.

When the air temperatures increase considering these assumptions, the ground temperatures are expected to also increase, at higher or smaller rates, until the thermal regime reaches a stationary state. When this happens, the three curves (MinAGT, MAGT and MaxAGT) in the

ground thermal “trumpet profile” (Figure 2) will slightly shift over the x-axis to warmer temperatures maintaining the original profile (once reached the stationary state).
When the new TTOP point reaches 0 ºC in the MAGT curve as a consequence of a general ground warming, it means that below the depth at that point, the mean annual ground temperature will keep positive values until reaching the ZAA point. Therefore, positive TTOP values below that depth, whichever it is, correspond to the mean annual temperature at the top of the seasonal freezing and thawing layer, where permafrost is not present anymore.

Considering these properties of the ground’s thermal regime, the spatial distribution of the Temperature of the Top of Permafrost after the hypothetical MAAT increment was computed over the study area. This allowed for the determination of the most sensitive permafrost areas to warming.

4. Results and discussion

4.1 Characteristics of the local ground temperature regimes

Site 1 borehole provided the most complete ground and air temperature graph, with continuous records from 2012 to 2018 (Figures 20 and 35) and shows the best data to evaluate how the ground temperature regime evolved during this period in Cierva Point and its relations with air temperature fluctuations. Permafrost was found in this borehole within the thermistors' depth extent with the top of permafrost occurring at approximately 5 m depth.

Figure 37 shows the difference on the inter annual fluctuations of the temperatures at 3 different levels: air (at 150 cm above the surface), the surface (at 5cm depth) and the mean depth of the top of permafrost (5 m). This graph is a useful tool for the interpretation of the climate characteristics of this site and its linkages with ground temperature fluctuations over the period from 2012 to 2018 (even though a gap exists in the air temperature records from 2014 to 2016). The analysis of this graph gives some insights about the thermal impact of the snowpack on the ground surface temperature. Through its buffer effect as an insulator layer, the snowpack influences the thermal offset existing between air and surface temperature. The thermal offset between air and surface (ΔT) is defined as the difference between the ground surface temperature (GST) and air temperature (Tair).

$$\Delta T\ (°C) = GST - Tair$$

Winter and summer air temperatures over the period did not show significant differences, despite an outlier minimum peak of -20°C in the winter of 2013. The maximum air temperature reached over the period was 4.25°C in the last summer season (2017).

However, some differences were found in the thermal offset (ΔT) values during the periods from 2012-2014 and 2016-2018. In the first period, the winter ground surface thermal regime shows a stronger decoupling from the cold air temperatures than in the period of 2016-2018, resulting in a strong positive surface thermal offset and a warmer value of the MAGST. In contrast, the surface thermal regime at the second period is strongly coupled with the atmospheric conditions involving a lower surface thermal offset and lower values of MAGST, indicating that the snowpack provided a weak insulation to the surface. These observations may reflect a longer lasting and thicker snowpack accumulation during the winter seasons of 2012 and 2013, which would have provided a higher insulation to the surface for longer than

the thinner snowpack in 2016-2018. A reduction of the active layer thickness during the first two years of the dataset in Figure 36a may also be explained by this fact.

This phenomenon was observed as well in nearby Western Antarctic regions such as Deception Island (WAP). Here, between 2006 and 2014, a reduction of the active layer thickness at a rate of about 1.5– 2cm a^{-1} linked with episodes of longer lasting and thicker snow accumulation over the surface, was reported (Goyanes et al., 2014; Ramos et al., 2017).

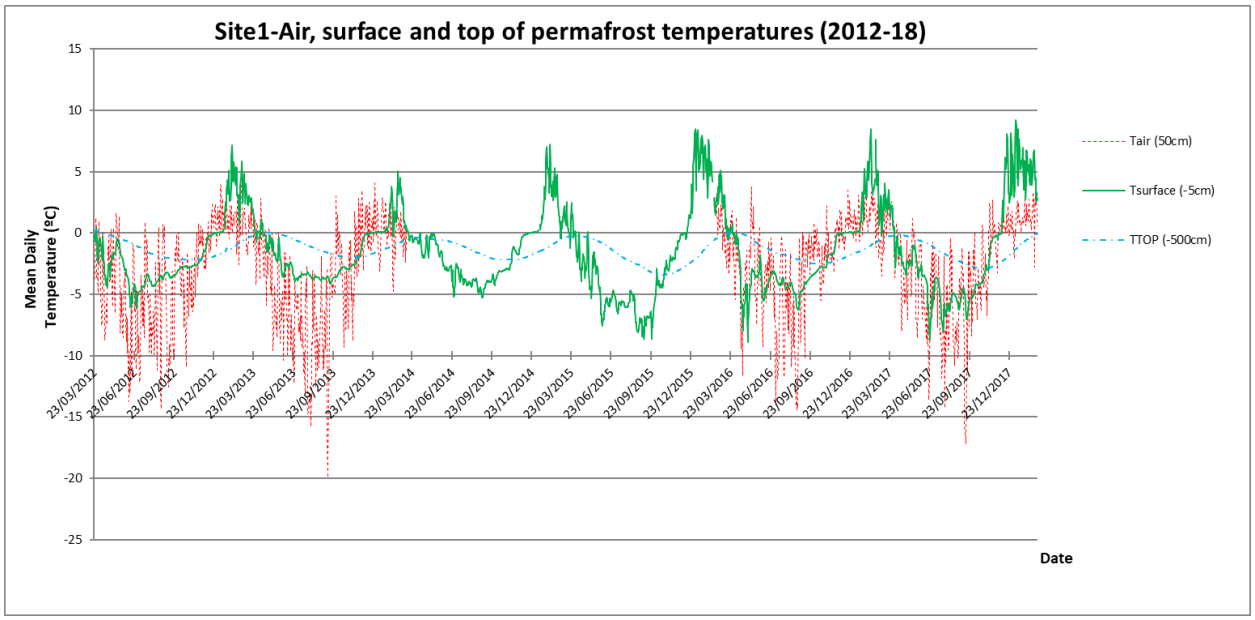

Figure 35. Air, ground surface and top of permafrost temperatures over the period from 2012 to 2018. Records of air temperature from 2014 to 2016 were not available.

However, not only the snow cover thickness can influence the MAGST fluctuations but also the snow properties, the near-surface material properties, and especially the snowpack timing and duration (Ling & Zhang, 2003).

The timing of the snowpack disappearance in spring coincides with the time when the GST rises above 0 ºC, normally after a brief *zero curtain effect* period. This effect maintains the GST close to 0 ºC due to the influence of the latent heat consumption in spring during snowmelt (Davense et al., 2017). During the spring of 2015 and 2017, the zero curtain effect was observed to be very short (only a few days starting at the end of November and ending in early December), in comparison with the previous years (when the zero curtain effect lasted for more than a month from the end of November to early January), which suggests the thinner snowpack accumulation during these years.

The early and brief snowmelt in spring is favourable to quick surface warming and higher temperatures at the top of permafrost after the warm season because of the direct exposure of

the ground to solar radiation, positive air temperature, and the low amount of heat required to melt the thin snowpack (Ling & Zhang, 2003).

Nevertheless, significant variations on the top of permafrost thermal wave have not been found. Only a slightly decrement of the TTOP below 0 ºC during the warm season was spotted after the winters showing longer zero curtain effects and therefore, a possible thicker snowpack accumulation.

Figure 36b shows the inter-annual oscillations observed in the depth of the top of permafrost. The active layer thickness slightly decreased along the first two years of monitoring (2012-2014), from almost 6 m the first year and reaching its minimum depth in 2014 (ci. 4 m). During the following years, from 2015 to the beginning of 2018, the top of permafrost ranged between 4.5 and 5 m.

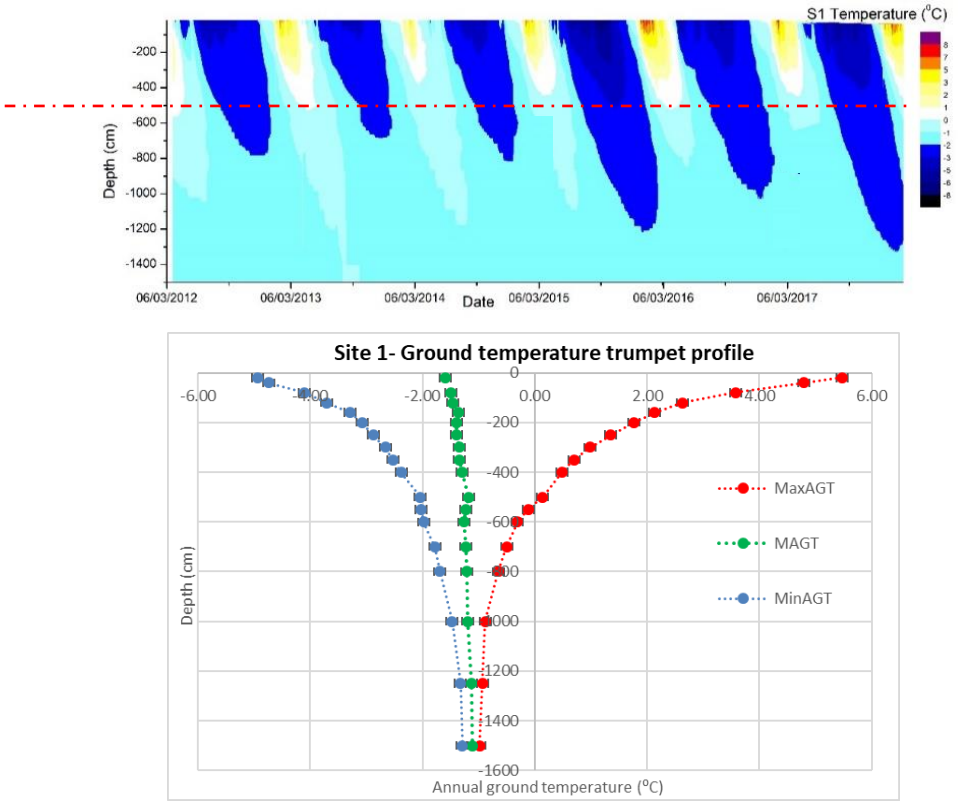

Figure 36. a) Observed ground temperature profile in Site 1 (Permafrost) between 2012 and 2018. Grey patches represent gaps in the observed dataset. The red dotted line indicates the mean depth at the top of permafrost (5m) b) Trumpet profile built up using mean temperature values from 2012 to 2014. Black segments represent a 0.1 ºC thermistors' measurement uncertainty.

The dataset of ground temperatures for the other sites is not continuous, thus the ground thermal profile graphs (Figures 37a-44a) show several gaps. Consequently, for the implementation of the "trumpet profile" graphs (Figures 37b-44b) in each borehole, only the average temperatures of years 1 and 2, from March 2012 to March 2014 (with complete records for a thawing/freezing cycle), were used to estimate the MaxAGT, MAGT and MinAGT. The best-fit functions, approximated by least squares regression to the MaxAGT, MAGT and MinAGT are presented in Table 4.

	Curve function			R2		
	MinGAT	MGAT	MaxGAT	MinGAT	MGAT	MaxGAT
S1-Permafrost	-	-	-	-	-	-
S2-Summit	$d(cm) = -8.2672(T)^2 - 162.21(T) - 801.42$	$d(cm) = 499.94(T) + 846.16$	$d(cm) = 0.1032(T)^3 - 3.2833(T)^2 + 46.038(T) - 277.33$	0.997	0.542	0.997
S3-Belowsummit	$d(cm) = -23.951(T)^2 - 362.75(T) - 1378$	$d(cm) = 574.3(T) + 1171$	$y = 0.5227(T)^3 - 9.4711(T)^2 + 68.871(T) - 221.84$	0.999	0.594	0.999
S4-Saddle	$d(cm) = -19.568(T)^2 - 243.48(T) - 766.37$	$0< d(cm) <-400; T=-1.61$	$d(cm) = 0.5857x^3 - 10.198x^2 + 68.249(T) - 188.4$	0.982	0.101	0.999
S5-Moraine	-	-	-	-	-	-
S6-Midslope	$d(cm) = -3.9422(T)^3 - 65.48(T)^2 - 375.44(T) - 763.55$	$0< d(cm) <-550; T=-0.69$	$d(cm) = 0.5005x^3 - 12.776x^2 + 120.7x - 424.38$	0.987	-	0.998
S7-MossRock	$d(cm) = 4195.2(T)^3 + 6377.5(T)^2 + 3291.7(T) + 540.39$	$d(cm) = -5.0334(T)^2 - 92.149(T) - 431.31$	$d(cm) = 0.3437(T)^3 - 8.8005(T)^2 + 81.588(T) - 295.45$	0.941	0.989	0.999
S8-MossMoss	-	-	-	-	-	-
S9-LowDeep	$d(cm) = -0.6747(T)^3 - 18.984(T)^2 - 192.25(T) - 744.21$	$d(cm) = -937.03(T)^2 - 1669.4(T) - 773.29$	$d(cm) = 0.7322(T)^3 - 19.474(T)^2 + 195.54(T) - 814.14$	0.996	0.69	0.997

Table 4. Functions for the estimation of the minimum, mean and maximum annual ground temperature for each boreholes's *trumpet profile*. The adjustment of the estimation to the observed data is represented in the R^2 column.

In the "trumpet profiles" for Sites 5-Moraine and site 8-MossMoss (Figures 40b and 43b), the MaxAGT was observed to stay invariable close to 0 ºC below 1 m and 0.4 m, respectively. This reflects the high moisture content at these depths, as no temperature change occurs from heat transfer during the phase change from ice to liquid water due to its latent heat of fusion, so that during the summer the temperature remains constant at 0 ºC.

Considering that the thermistors provide measurements with an uncertainty of 0.5 ºC, and the ice-water mixture stability, 0 ºC was considered to be the actual temperature existing in the ground during the warm season and matching with continuous ice-thawing below 1 m depth in Site5 and 0.4 m in Site8. Therefore, the mean difference between the measured MaxAGT and 0 ºC during the phase change for each borehole (0.15 ºC and 0.3 ºC respectively) were subtracted from the observed ground temperature for 0 ºC calibration.

The thermal trumpet profile, after rectification, is shown in figures 40c and 43c. These figures show that below 1 m and 0.4 m respectively in boreholes 5 and 8, the ground never thaws completely and therefore these depths were considered the upper limit of the permafrost table. Permafrost was not clearly observed in the rest of the boreholes, which are not deep enough to reach the permafrost table, or even because permafrost may be absent.

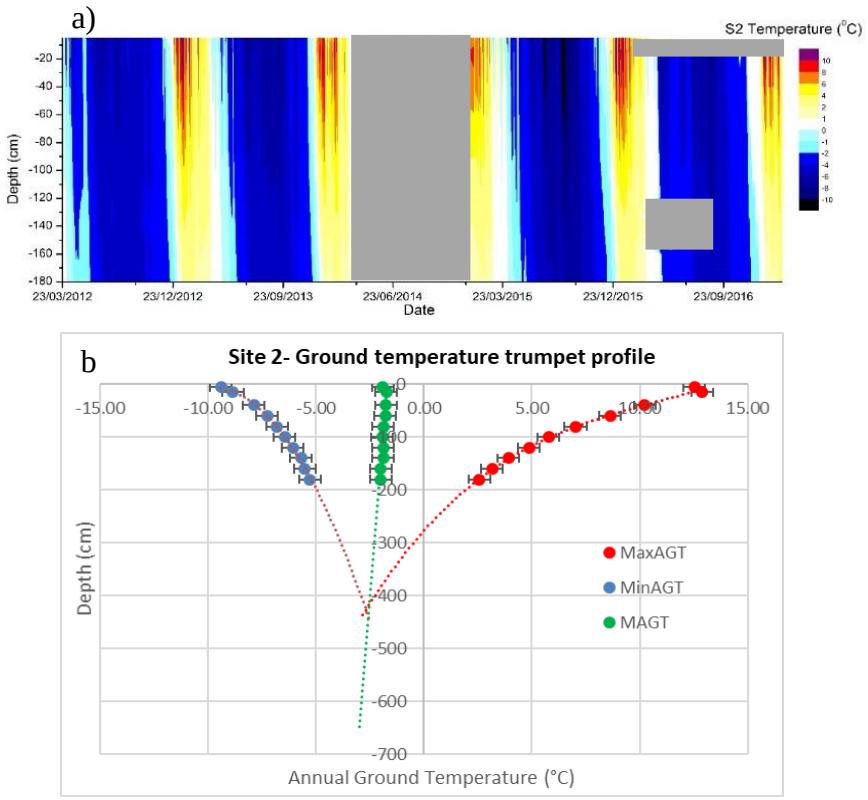

Figure 37. a) Observed ground temperature profile in Site 2 (Summit) between 2012 and 2017. Grey patches represent gaps in the observed dataset. b) Trumpet profile built up using mean temperature values from 2012 to 2014. Black segments represent a 0.5 ºC thermistors' measurement uncertainty.

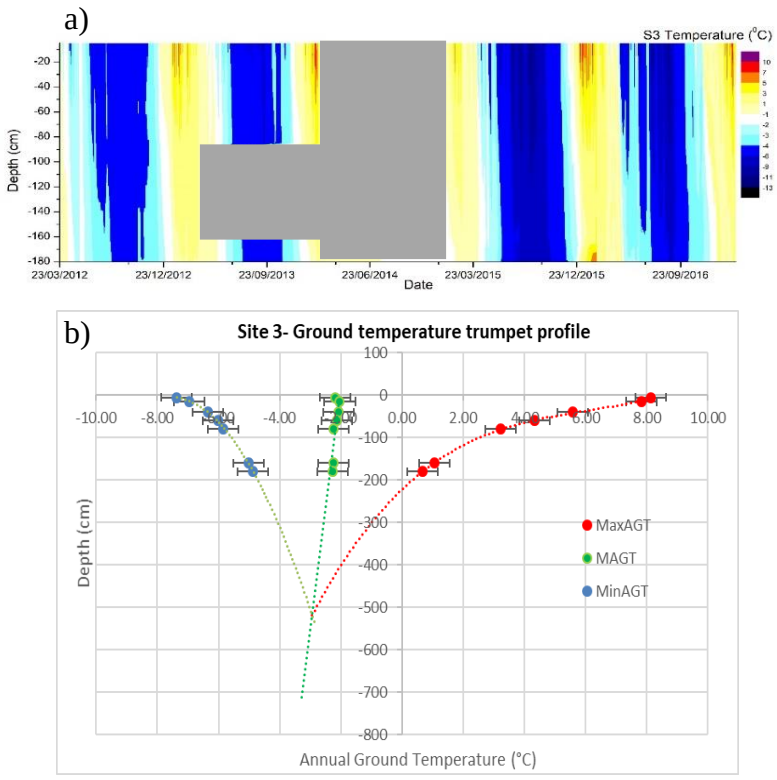

Figure 38. a) Observed ground temperature profile in Site 3 (BelowSummit) between 2012 and 2017. Grey patches represent gaps in the observed dataset. b) Trumpet profile built up using mean temperature values from 2012 to 2014. Black segments represent a 0.5 ºC thermistors' measurement uncertainty.

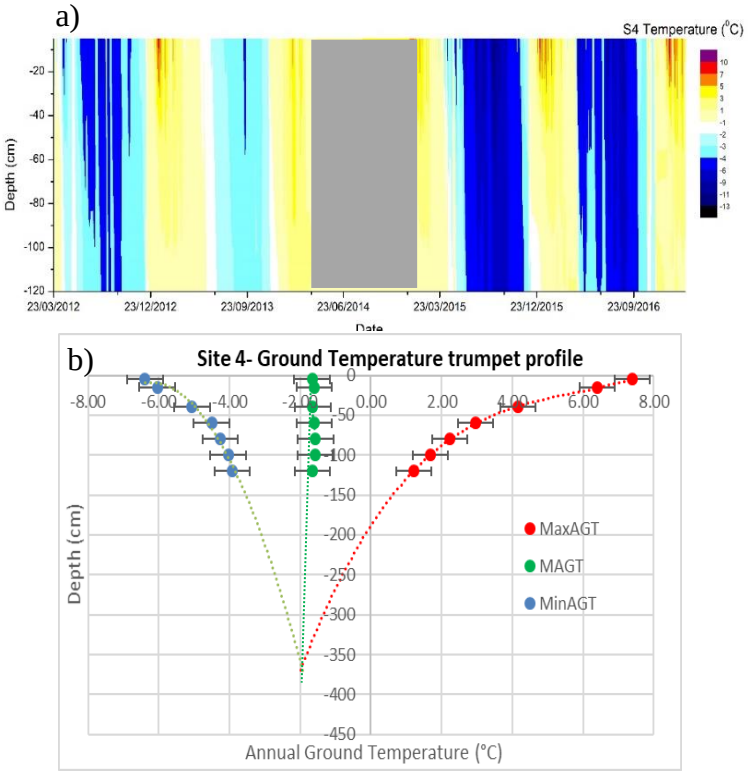

Figure 39. a) Observed ground temperature profile in Site 4 (Saddle) between 2012 and 2017. Grey patches represent gaps in the observed dataset. b) Trumpet profile built up using mean temperature values from 2012 to 2014. Black segments represent a 0.5 ºC thermistors' measurement uncertainty.

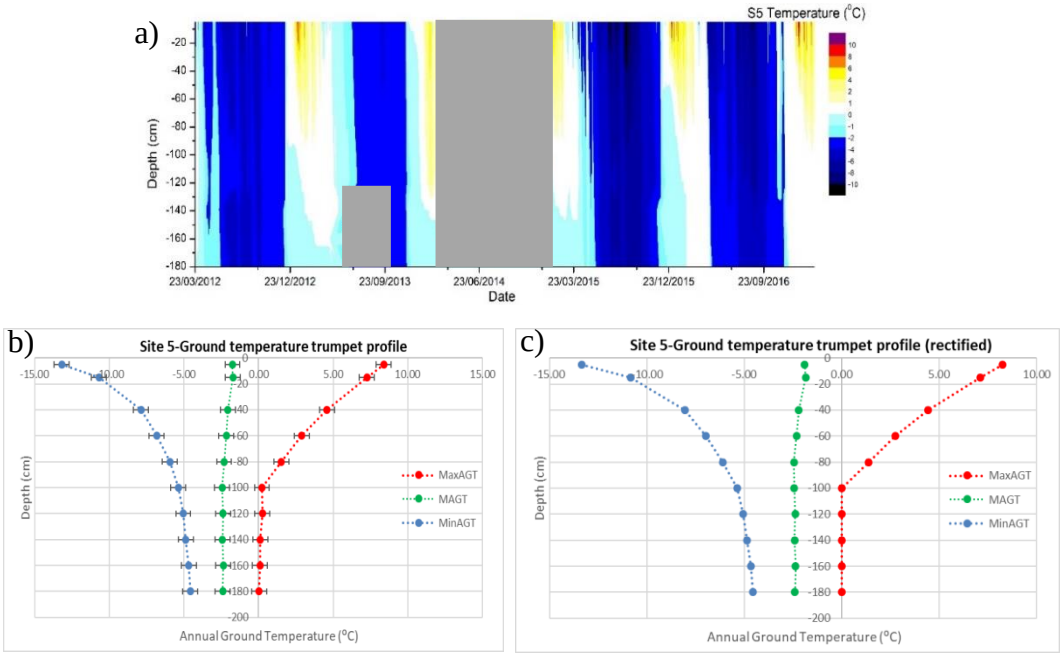

Figure 40. a) Observed ground temperature profile in Site 5 (Moraine) between 2012 and 2017. Grey patches represent gaps in the observed dataset. b) Trumpet profile built up using mean temperature values from 2012 to 2014. Black segments represent a 0.5 ºC thermistors' measurement uncertainty. c) Trumpet profile after measurement uncertainty rectification down to 0.09°C.

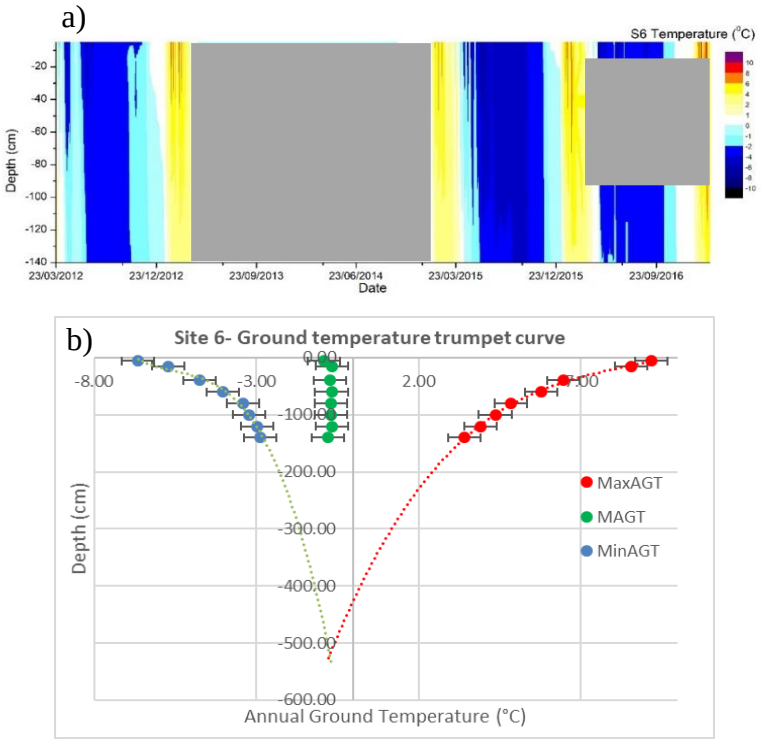

Figure 41. a) Observed ground temperature profile in Site 6 (MidSlope) between 2012 and 2017. Grey patches represent gaps in the observed dataset. b) Trumpet profile built up using mean temperature values from 2012 to 2014. Black segments represent a 0.5 ºC thermistor's measurement uncertainty.

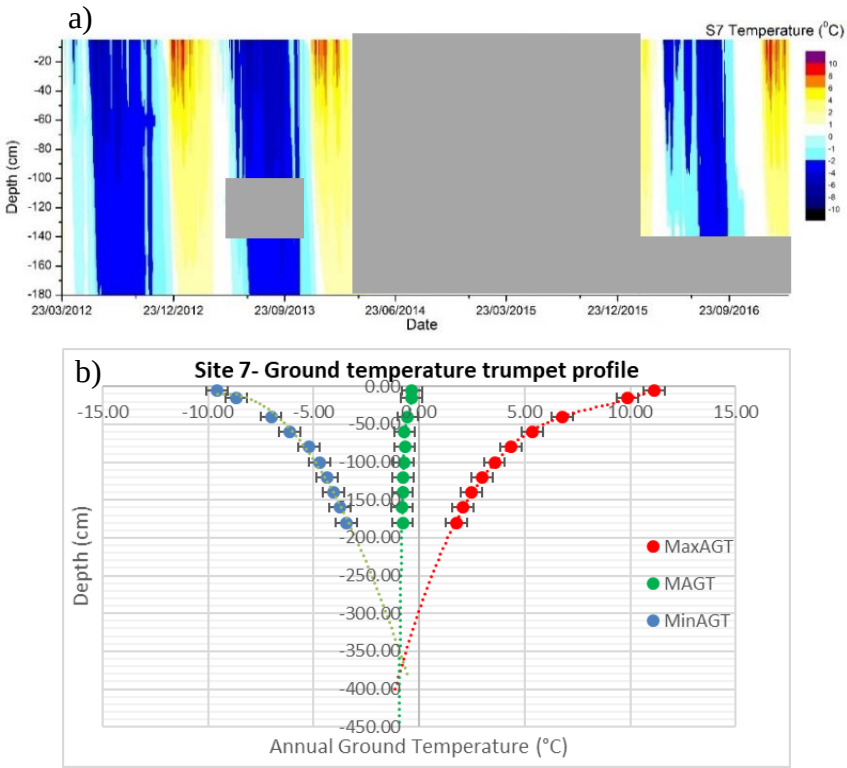

Figure 42. a) Observed ground temperature profile in Site 7 (MossRock) between 2012 and 2017. Grey patches represent gaps in the observed dataset. b) Trumpet profile built up using mean temperature values from 2012 to 2014. Black segments represent a 0.5 ºC thermistors' measurement uncertainty.

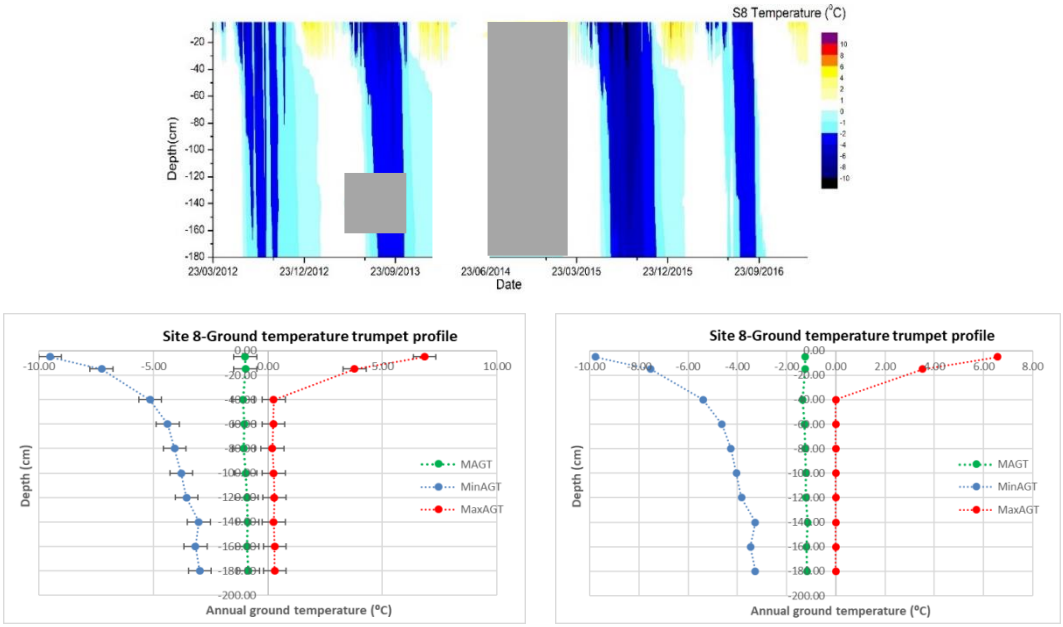

Figure 43. a) Observed ground temperature profile in Site 8 (MossMoss) between 2012 and 2017. Grey patches represent gaps in the observed dataset. b) Trumpet profile built up using mean temperature values from 2012 to 2014. Black segments represent a 0.5 ºC thermistors' measurement uncertainty. c) Trumpet profile after measurement uncertainty rectification down to 0.04°C.

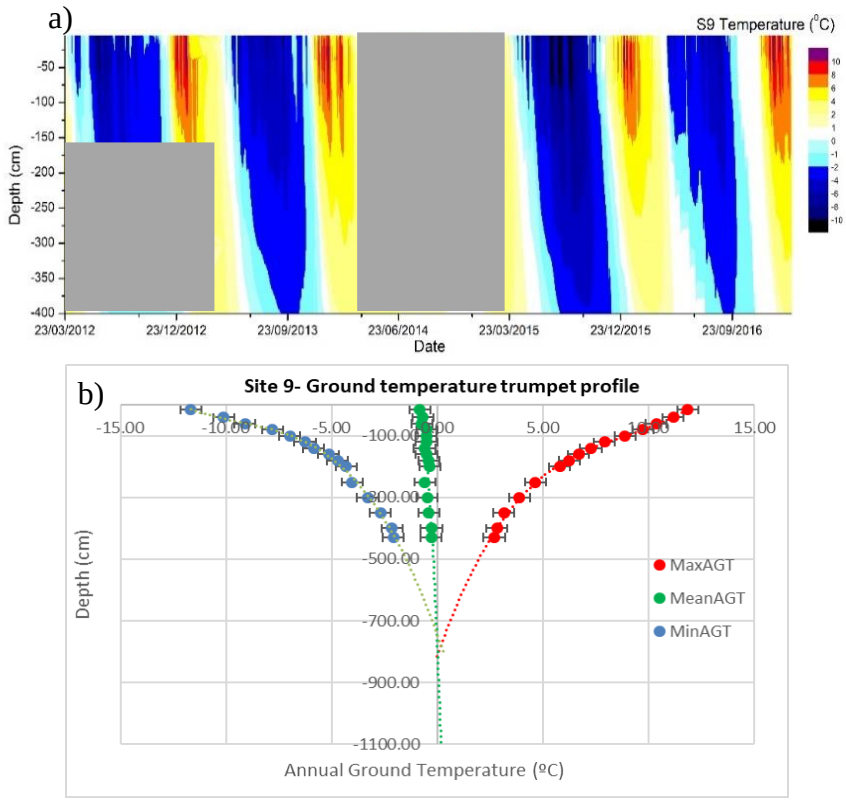

Figure 44. a) Observed ground temperature profile in Site 9 (LowDeep) between 2012 and 2017. Grey patches represent gaps in the observed dataset. b) Trumpet profile built up using mean temperature values from 2012 to 2014. Black segments represent a 0.5 ºC thermistors' measurement uncertainty.

After the analysis of the thermal regimes, observed or estimated values for the mean annual ground surface temperature (MAGST), the depth at the Top of Permafrost (TOP), the temperature at the Top of Permafrost (TTOP), the thermal offset and the depth and temperature at the point of Zero Annual Amplitude (ZAA) were calculated and are presented in Table 5.

	S1-Permafrost	S2-Summit	S3-Belowsummit	S4-Saddle	S5-Moraine	S6-Midslope	S7-MossRock	S8-MossMoss	S9-LowDeep
Ovserved MAGST-5cm (°C)	-1.59±0.10	-1.90±0.50	-2.18±0.50	-1.67±0.50	-1.89±0.50	-0.92±0.50	-0.33±0.50	-1.25±0.50	-0.78±0.50
Observed/estimated TOP (m)	-5.00	-2.78	-2.20	-1.90	-1.00	-4.26	-2.95	-0.40	No permafrost presence estimated
Observed/estimated TTOP (°C)	-1.21±0.10	-2.25±0.50	-2.42±0.50	-1.61±0.50	-2.59±0.50	-0.69±0.50	-0.18±0.50	-1.35±0.50	0.32±0.50
Observed/estimated Toffset (°C)	0.38±0.20	-0.35±1.00	-0.24±1.00	0.06±1.00	-0.70±1.00	0.23±1.00	0.15±1.00	-0.10±1.00	1.10±1.00
Observed/estimated ZAA depth(m)	-15.00	-4.30	-5.10	-3.50	-	-5.15	-3.60	-	-7.80
Observed/estimated ZAA temperature (°C)	-1.11±0.10	-2.60±0.50	-2.93±0.50	-1.61±0.50	-	-0.69±0.50	-0.30±0.50	-	0.00±0.50

Table 5. Local ground thermal profile parameters derived from each borehole's trumpet profile. Green coloured values were directly obtained from observed data. Orange values were estimated by extrapolation of observed data to the ZAA depth extent. results are shown with the uncertainty of the measurement.

4.2 TTOP model results in the different monitoring sites

4.2.1 LOCAL RESULTS OF TTOP PARAMETERS

4.2.1.1 Ita/Ifa

The air thawing and freezing indexes for the 9 monitoring Sites in Cierva point are shown in Table 6. These were computed as explained in Section 3.3.2.1 using empirical data from natural years 1 and 2 with continuous dataset in the complete freezing/thawing cycle (see Table 2. Section 3.1.2).

Period			Days	S1-Permafrost	S2-Summit	S3-Belowsummit	S4-Saddle	S5-Moraine	S6-MidSlope	S7-MossRock	S8-MossMoss	S9-LowDeep
Year 1: 2012/13	Freezing season	23-Mar-12	364	1269.85	1416.10	1399.75	1355.85	1208.56	1049.60	953.24	953.24	1027.17
		03-Dec-12										
	Thawing season	04-Dec-12		123.16	153.56	157.71	181.34	192.54	334.90	344.69	344.69	268.46
		22-Mar-13										
Year 2: 2013/14	Freezing season	23-Mar-13	352	1396.95	1428.13	1339.36	1381.12	1189.19	905.98	1023.16	1023.16	978.36
		21-Nov-13										
	Thawing season	22-Nov-13		113.63	71.44	85.22	86.29	103.10	257.22	264.72	264.72	192.83
		10-Mar-14										
Average If			358	1333.40	1422.11	1369.56	1368.48	1198.87	1049.60	988.20	988.20	1002.76
Average It				118.40	112.50	121.47	133.81	147.82	334.90	304.71	304.71	230.64

Table 6. Air thawing and freezing indexes for years 1 and 2, and average values for both years. Values expressed in °Cdays.

The average value of each borehole's thawing and freezing indexes were considered for the determination of the TTOP model. Generally, and accordingly to the adiabatic lapse rate mentioned in section 3.3.3.1, sites located at higher elevation resulted to have higher values of Ifa and lower values of Ita occurred at elevations (ex. Site 2, the highest altitude site at 336 m shows Ifa = 1422.11 °Cdays and Ita = 112.5 °Cdays.). Low altitude sites were characterized by lower values of Ifa and higher values of Ita (ex. Site 7 and 8, at 70 m show an Ifa = 988.2 °Cdays and an Ita = 304.7 °Cdays).

4.2.1.2 Its/Ifs

The ground thawing and freezing indexes for the 9 monitoring sites in Cierva Point are shown in Table 7. These were computed as explained in Section 3.3.2.2 using empirical data from natural years 1 and 2, which had a continuous dataset for the complete freezing/thawing cycles (see Table 2. Section 3.1.2). The average value of each borehole's thawing and freezing indexes were used for the determination of the TTOP model.

Period			Days	S1-Permafrost	S2-Summit	S3-Belowsummit	S4-Saddle	S5-Moraine	S6-MidSlope	S7-MossRock	S8-MossMoss	S9-LowDeep
Year 1: 2012/13	Freezing season	23-Mar-12 / 03-Dec-12	364	786.14	1141.58	1013.85	1042.19	1092.07	630.97	712.87	631.99	827.08
	Thawing season	04-Dec-12 / 22-Mar-13		233.27	520.26	250.09	266.54	377.76	292.16	611.29	294.28	540.14
Year 2: 2013/14	Freezing season	23-Mar-13 / 21-Nov-13	352	643.18	1182.70	1003.48	560.63	1088.82	351.77	745.55	863.84	873.98
	Thawing season	22-Nov-13 / 10-Mar-14		104.76	451.36	209.04	139.44	270.24	66.11	610.14	309.30	557.15
Average If			358	**714.66**	**1162.14**	**1008.66**	**801.41**	**1090.45**	**630.97**	**729.21**	**747.91**	**850.53**
Average It				**169.01**	**485.81**	**229.57**	**202.99**	**324.00**	**292.16**	**610.71**	**301.79**	**548.65**

Table 7. Thawing and freezing ground surface indexes (at 5cm depth) for years 1 and 2, and average values for both years. Values expressed in °Cdays.

Exceptionally, due to the scarce of experimental data for year 2 in Site 6, only the values of Its-Ifs of year 1 were taken in consideration for this borehole.

Site 2 (Summit) was characterized by the highest value of surface freezing index (Ifs = 1162.14 °Cdays) and Site 6 (Midslope) by the lowest (Ifs = 630.97 and Ifs = 1162.14 °Cdays). On the other hand, the maximum surface thawing index obtained was in Site 9 (Its = 548.65 °Cdays) and the minimum in Site 1 (Permafrost) with a value of Its = 169.01 °Cdays. These values are influenced by the topo-climatic characteristics of each site and by other attributes, such as the substrate thermal properties and the insulation effect of moss or snow cover.

4.2.1.3 Nt/Nf

The local results of the thawing and freezing n-factors for the 9 monitoring Sites in Cierva point are shown in Table 8. These were computed as explained in Section 3.3.2.3 as the ratio of average ground and air thawing and freezing indexes previously computed.

	S1-Permafrost	S2-Summit	S3-Belowsummit	S4-Saddle	S5-Moraine	S6-Midslope	S7-MossRock	S8-MossMoss	S9-LowDeep
Nf	0.54	0.82	0.74	0.59	0.91	0.60	0.74	0.76	0.85
Nt	1.43	4.32	1.89	1.52	2.19	0.87	2.00	0.99	2.38

Table 8. Resulting *nt* and *nf* for computed using the average thawing and freezing air and surface indexes for years 1 and 2.

As previously introduced in section 3.3.3.1.B, n-factors mainly account for the local influence of moss cover, snow cover and the 5 cm surface layer thermal offset, which varie depending on surface characteristics (soil type and moss bed).

The highest value of freezing N-factor (0.91) was found in Site 5 (Moraine) and in Site 2 (summit), the maximum thawing n-factor was found (4.32).

The lowest value of freezing n-factor (1.43) was found in Site 1 (Permafrost), being Site 8 (MossMoss) characterized by the lowest thawing factor (0.99). Here, the lower value of Nt for Site 8 (0.99) against the value in the analogue Site 7 (2.00) is explained by the presence of a thick moss cover in the first site, which acts as a thermal insulator layer.

The linkages between the potential snow cover and the top layer thermal offset with the magnitude of n-factors in the rest of the boreholes are further discussed in Section 4.3, after the analysis of the curvature and thermal offset characterizing these sites.

4.2.1.4 Toffset

The local results of the active layer thermal offset for the 9 monitoring Sites in Cierva Point are shown in Table 9. These were computed as explained in Section 3.3.2.5 as the difference of the Temperature at the Top of Permafrost *(TTOP)* and the Mean Annual Ground Surface Temperature *(MAGST).*

	S1-Permafrost	S2-Summit	S3-Belowsummit	S4-Saddle	S5-Moraine	S6-Midslope	S7-MossRock	S8-MossMoss	S9-LowDeep
Observed/estimated Toffset (°C)	0.38	-0.35	-0.24	0.06	-0.70	0.23	0.15	-0.10	1.10

Table 9. Resulting values of seasonal thawing layer's thermal offset computed using the average of year's 1 and 2 ground temperature data.

The highest value of thermal offset between the permafrost table and the surface was observed in Site 9 with 1.19 °C, being Site 5 characterized by the lowest value, with -0.70 °C. The differences in these values arise mainly due to the differences on the thermal properties of the substrate, which mainly depend on the type of substrate and water content at different depths and locations (Wu & Shi, 2003). The linkages between the resulting thermal offset values with the substrate characteristics and moisture content are further discussed in Section 4.3, after the analysis of the substrate type and topographic wetness indexes characterizing these sites.

4.2.2 LOCAL RESULTS OF TTOP AND MODEL VALIDATION

Table 10 summarizes the results for all the TTOP model parameters *(Is, Ia, n-factors, toffset)* previously computed using the observed data together with the local results for the depth at the TOP and the TTOP values estimated or observed using the analysis of the *trumpet profile*. At the bottom of the Table 10, the TTOP results given by the TTOP model equation (Equation 2) are presented.

	S1-Permafrost	S2-Summit	S3-Belowsummit	S4-Saddle	S5-Moraine	S6-Midslope	S7-MossRock	S8-MossMoss	S9-LowDeep
Ifs (5cm) (°C day)	714.7	1162.1	1008.7	801.4	1090.4	631.0	729.2	747.9	850.5
Its (5cm) (°C day)	169.0	485.8	229.6	203.0	324.0	292.2	610.7	301.8	548.6
Ifa (°C day)	1333.4	1422.1	1369.6	1368.5	1198.9	1049.6	988.2	988.2	1002.8
Ita (°C day)	118.4	112.5	121.5	133.8	147.8	334.9	304.7	304.7	230.6
Nf	0.54	0.82	0.74	0.59	0.91	0.60	0.74	0.76	0.85
Nt	1.43	4.32	1.89	1.52	2.19	0.87	2.00	0.99	2.38
Observed/estimated TOP (m)	-5.00	-2.78	-2.20	-1.90	-1.00	-4.26	-2.95	-0.40	No permafrost presence estimated
Observed/estimated Toffset (°C)	0.38	-0.35	-0.24	0.06	-0.70	0.23	0.15	-0.10	1.10
Observed/estimated TTOP (°C)	-1.21	-2.25	-2.42	-1.61	-2.59	-0.69	-0.18	-1.35	0.32
TTOP formula (°C)	**-1.14**	**-2.24**	**-2.42**	**-1.61**	**-2.84**	**-0.72**	**-0.18**	**-1.35**	**0.26**

Table 10. Results for all the TTOP model parameters (Is, Ia, n-factors, toffset), the depth at the Top of Permafrost (TOP) and the Temperature at the Top Of Permafrost (TTOP) values estimated or observed using the analysis of the *trumpet profile* and TTOP results given by the TTOP model equation. All values are given together with the propagated measurement uncertainty.

The deepest permafrost table was found to be in Site 1 (Permafrost), where the permafrost table was observed at 5 m depth with a temperature of -1.21°C. However, a value 0.07°C higher was obtained computing the TTOP formula (equation 2). In Sites 5 (Moraine) and 8 (MossMoss), the temperature at the top of permafrost was found to be -2.59°C and -1.35°C, at 1 m and 0.4 m respectively, coinciding with the depth of isothermal maximum annual surface temperature at 0°C. A slight difference of -0.25°C was found between the observed data in

Site 5 and the value obtained through the TTOP equation (which is the maximum difference found in all the boreholes), while no difference occurs in Site 8.

For the other monitored sites, TOP and TTOP were estimated by graphical analysis of the temperature regression functions in their trumpet profiles. The permafrost table was estimated to exist at depths ranging from 4.26 m (in Site 6) and 1.9 m (in Site 4) below the ground surface and the TTOP values determined range from -2.42°C (in Site 3) and -0.18°C (in Site 7). In Site 9, no permafrost is estimated to occur. Therefore, the value of 0.26°C in this location corresponds to the ground temperature at the base of the seasonal freezing and thawing layer.

Figure 45 shows the degree of adjustment of the TTOP formula (Equation 2) results with the observed or estimated values by graphical analysis. The adjustment is better when observed/estimated values equal the values resulting from the TTOP model equation. Therefore, the adjustment is considered to be better when the distribution of dots and triangles is closer to the $y=x$ line (grey dotted line in the Figure 45). The plot results show a value of adjustment of the data of $R^2=0.98$ to the $y=x$ line and a mean error of 0.05 ºC between modelled and observed data, being the site 1 (Permafrost) the one presenting the highest deviation. With these values, the TTOP model was considered as a good estimator for the temperature at the top of permafrost, suitable to be spatially extrapolated for the whole area extent.

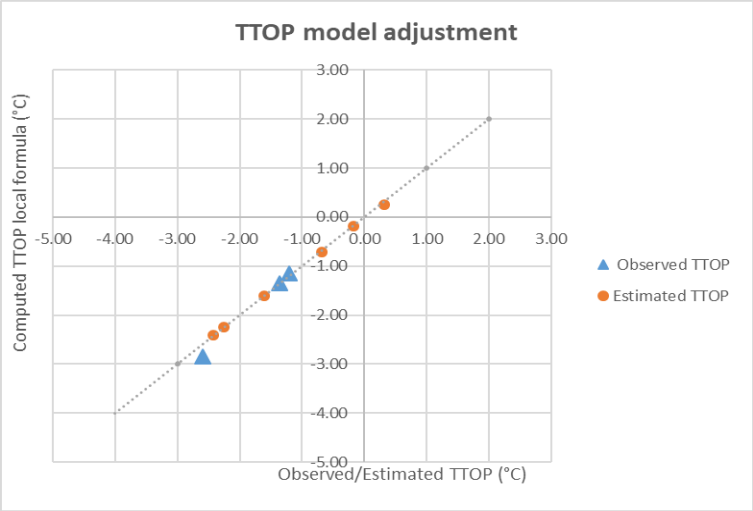

Figure 45. Local TTOP model validation by analysis of adjustment of TTOP model formula results to the observed or estimated values determined first by graphical analysis of the *trumpet profile*.

4.3 Terrain factors and their correlation with TTOP parameters

Table 11 shows the values of terrain factors in each monitoring site determined as explained in section 3.3.3.2.

	S1-Perma	S2-Summit	S3-Belowsummit	S4-Saddle	S5-Moraine	S6-Midslope	S7-mossrock	S8-mossmoss	S9-Lowdeep
Elevation (m)	198.12	335.78	317.82	289.79	165.62	136.53	71.34	71.67	37.53
Aspect	N	E	N	E	N	N	N	N	N
Curvature	8.20	-3.26	3.61	0.75	-11.25	-4.90	11.77	9.67	0.65
Moss Cover	No	No	No	No	No	No	No	Yes	No
TWI	0.22	0.26	0.23	0.30	0.21	0.21	0.30	0.28	0.47
Substrate Type	Bedrock	Bedrock	Bedrock	Unconsolidated soil	Unconsolidated soil	Bedrock	Bedrock	Peat	Bedrock

Table 11. Local values of terrain factors influencing on the different TTOP parameters in each monitoring boreholes. In the *Aspect* row: N=North aspect, E=East aspect. In the *Curvature* row: possitive values represent concave profiles; negative values represent convex profiles.

The results of the Spearman correlation values (ρ) between terrain factors and TTOP parameters are shown in Table 12. Values coloured in red highlight the correlation indexes which absolute value is high enough (ρ>0.5) to consider the influence of that terrain feature statistically significant in the respective TTOP parameter. This threshold was considered following the standards presented by Cohen (1988) and aforementioned in section 3.3.3.3. Moreover, just the statistically significant results with a logic physical relationship are considered later for the spatial modelling of each parameter.

Air thawing and freezing indexes *(Ita* and *Ifa*) were found to be highly correlated with elevation; *Nt* was found to have an inverse correlation with the presence of moss cover; *Nf* is mainly influenced by the terrain curvature; finally, the *thermal offset* showed the greater correlation index with the Topographical Wetness index. These results about the most influencing factors for each TTOP parameter based on the Spearman correlation indexes are close to the previously expected in section 3.3.3.1.

	Ita	Ifa	Nt	Nf	Toffset
Elevation	-0.845	0.845	0.117	-0.204	-0.567
Aspect	0.520	0.620	0.311	-0.127	-0.311
Moss Cover	0.481	-0.344	-0.503	0.000	-0.137
Curvature	0.293	-0.126	-0.267	-0.527	0.283
TWI	0.232	-0.013	0.303	0.006	0.497
Soil Type	0.305	-0.115	-0.249	0.127	-0.428

Table 12. Spearman correlation indexes between terrain factors and TTOP parameters.

Note that the results of correlation between aspect and the TTOP parameters cannot be considered due to the small diversity of aspects in the monitoring sites (i.e all the boreholes are situated in locations with North or East aspects). Hence, there is no knowledge on how South and West aspects influence in the TTOP parameters values.

4.4 Relationship functions between terrain features and TTOP parameters

The sections below include the results of the statistical relationships functions between the terrain factors and model parameters which resulted to be highly correlated in previous section. Included as well in this section is the analysis of results of the compliance test of the assumptions for applicability of single or multilinear relationships functions, previously explained in section 3.3.3.4.

4.4.1 THAWING AND FREEZING INDEXES

To understand how the indexes are correlated with altitude in Cierva Point and check for the first assumption of "linearity", we plotted the resulting values of *Ita* and *Itf* for the 9 different locations as a function of their altitude (Figures 46a and 46b). Similarly to the air temperature decrease with elevation, thawing degree-days decrease with altitude as well. On the contrary,

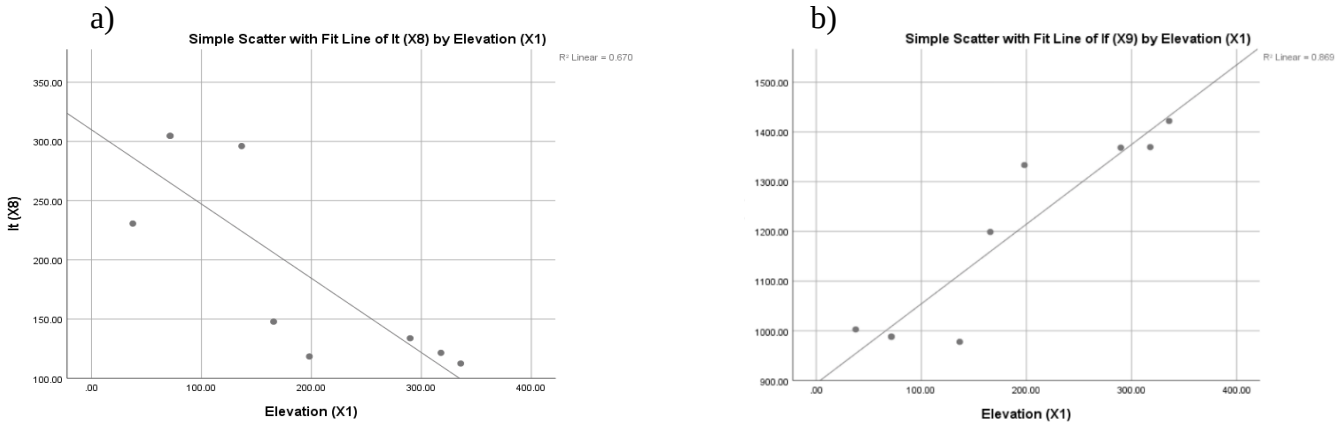

Figure 46. a) Linear relationship between *Ita* and elevation. b) Linear relationship between *Ifa* and elevation.

the freezing degree-days increase with altitude.

Secondly, we checked for normality of residuals in a normal P-P plot (Figures 47a and 47b). The distribution is normal when conforms to the diagonal normality line $y=x$ indicated in the plot (Statistical Solutions, 2018c). Sometimes, small deviations can be assumed as normality, as long as they are not drastic. In the figure below, the distribution of the residuals for both graphs was close to the normality enough to consider the assumption compiled.

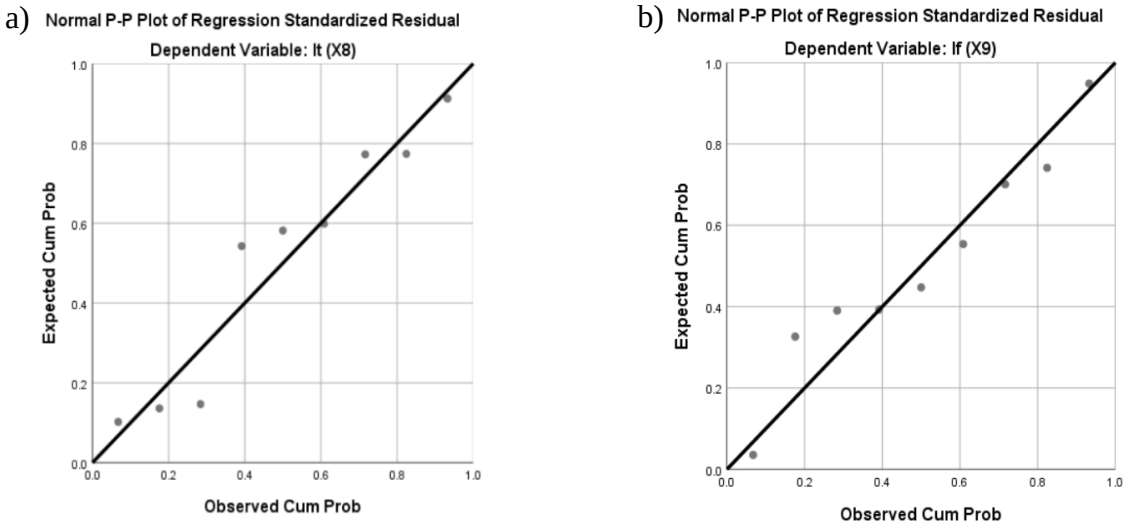

Figure 47. a) Normal Predicted Probability (P-P) plot for *Ita* as a dependent variable of elevation. b) Normal Predicted Probability (P-P) plot for *Ifa* as a dependent variable of elevation.

The next assumption to check was homoscedasticity (figures 48a and 48b). Ideally, in the scatter plot of residuals, the data should be scattered randomly, there are points equally distributed above and below zero on the X axis, and to the left and right of zero on the Y axis. In the scatter plots below, the data is randomly scattered and does not follow any obvious pattern, so the assumption was considered valid.

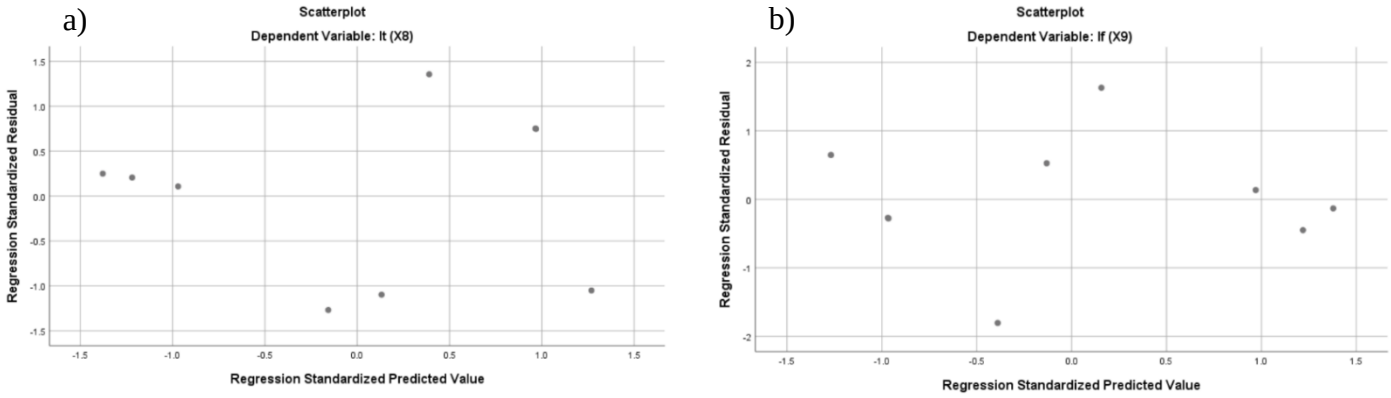

Figure 48. a) Plot of standardized residuals versus predicted values when performing a linear regression between *Ita* and elevation. b) Plot of standardized residuals versus predicted values when performing a linear regression between *Ita* and elevation

Finally, the absence of multicollinearity should be checked using the Spearman correlation matrix (correlations among all predictor variables should be less than 0.80) or the Variance Inflation Factor (VIF), with values needing to be lower than 10. However, as we just used one independent variable as a predictor for each model parameter it was not necessary to check for this assumption to be compiled.

Once all the assumptions were tested, the expressions that relate the thawing and freezing indexes as a function of elevation (Equations 13a and 13b) were determined, based on the observational data collected in our study area. These functions are later used for the spatialization of the indexes in next section.

a) $It = -0.627x(Elevation) + 309.846$ R^2=0.67

b) $If = 1.602x(Elevation) + 894.226$ R^2=0.67

Equation 13. a) Relationship function between *Ita* and elevation with respective estimation adjustment value of R^2. b) Relationship function between *Itf* and elevation with respective estimation adjustment value of R^2.

4.4.2 N-FACTORS

In order to understand how the n factors are correlated with the moss cover and curvature and to check for the first assumption of "linearity", we plotted the resulting values of nt and nf for the 9 different locations as a function of moss-cover and curvature respectively (Figure 49a and 49b).

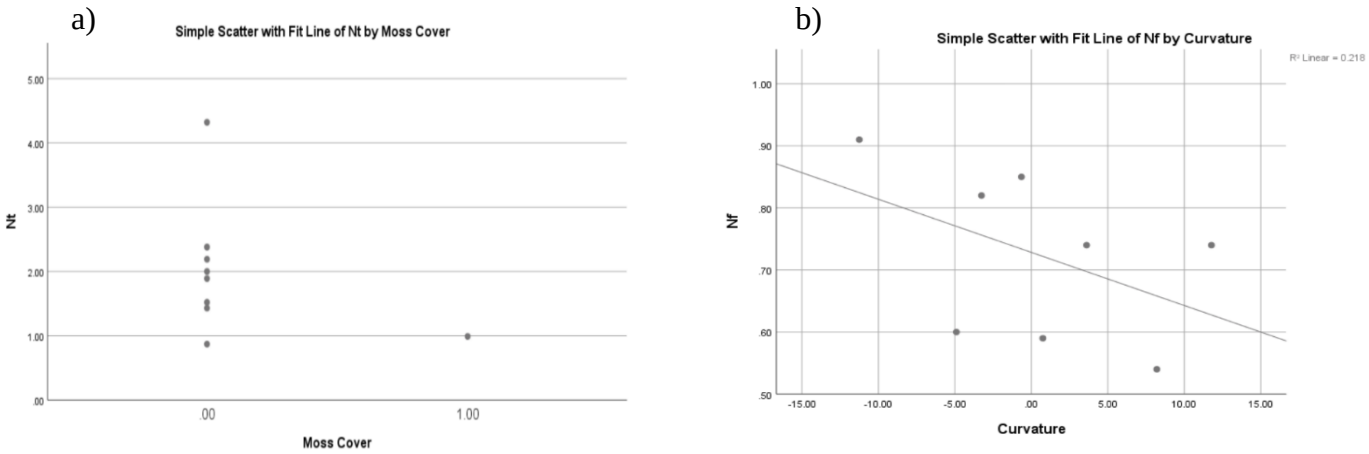

Figure 49. a) Relationship between nt and moss cover. In the x-axis, a value of 0 stands for the absence of a moss cover and a value of 1 for the presence. b) Linear relationship between *nf* and curvature.

In the *nt* plot, the assumption "linearity" is violated, so simple linear regression cannot be applied to this parameter. However, a difference of 1.01 in the *nt* value was observed between adjacent monitoring sites 7-MossRock and 8-MossMoss (see Table 9), only differentiated by the presence or absence of moss cover. Thus, a different method was exceptionally used for the computation of relationship between *nt* and moss cover for the spatialization, as explained in section 3.3.3.4. The mean of *nt* values obtained in the moss-free monitoring sites (*nt*=2.08) was given to the moss-free areas, whereas this mean value minus 1.01 (*nt*=1.07) was given to all the areas covered by mosses.

In the nf to curvature scatterplot (Figure 49b), we observed a poor linear correlation, where the nf values decrease with the increase of the curvature (i.e. the insulation of the top surface layer increases as the concavity of the terrain does). This relation fits to the logics of potential relationships mentioned in section 3.3.3.1, where concave surfaces were expected to have a higher potential for the snowpack accumulation than convex surfaces.

Secondly, we checked for normality of residuals in a normal P-P plot for the *nf-curvature* relation and observed an approximately normal distribution (Figure 50).

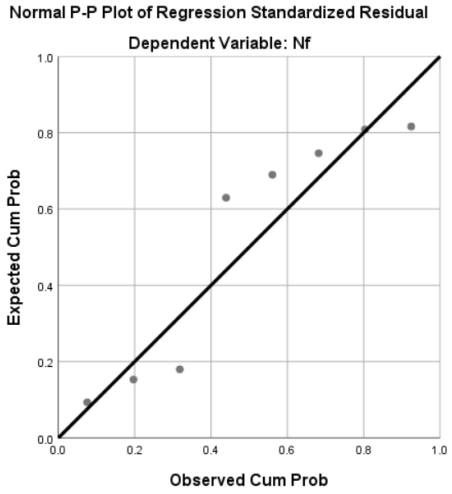

Figure 50. Normal Predicted Probability (P-P) plot for *nf* as a dependent variable of the terrain curvature.

Finally, we checked for homoscedasticity, with the scatter plot in Figure 51 showing a valid distribution .

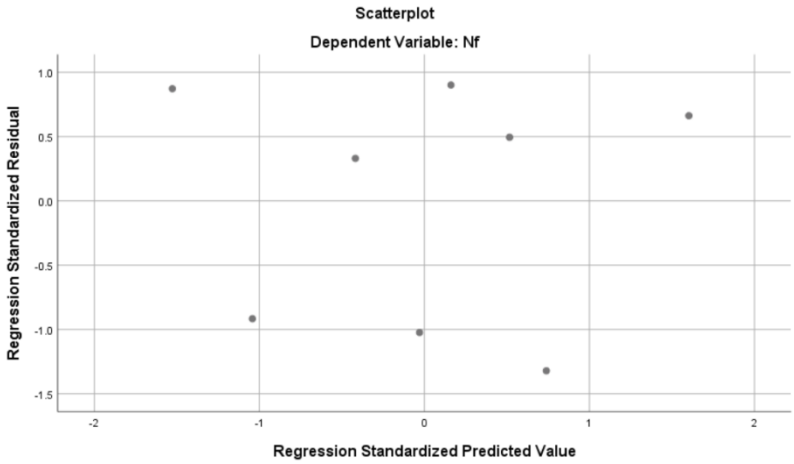

Figure 51. Plot of standardized residuals versus predicted values when performing a linear regression between *nf* and curvature.

Once all the assumptions were tested, the relationship function between the thawing and freezing n-factors and elevation was determined, based on the empirical data gathered in our study area (Equations 14a and 14b). These functions are used for the spatialization of these factors in next section.

a) $nt\ (no\ moss) = 2.08$

$nt\ (moss\ ) = 1.07$

b) $nf = -0.009x(Curvature) + 0.728$

R^2=0.22

Equation 14. a) Values assigned for nt in moss free and moss covered areas respectively. b) Relationship function between nf and curvature with respective estimation adjustment value of R^2.

4.4.3 THERMAL OFFSET

Soil water content does not show the same influence on the ground thermal offset in different substrates. Therefore, the statistical relationships between the thermal offset and water content (represented as the Topographic Wetness Index - TWI) must be determined separately for bedrock and for peat and unconsolidated soils.

First, it was plotted the absolute thermal offset values obtained in the monitoring boreholes in bedrock substrates (sites 1, 2, 3, 6, 7 and 9) as a function of the TWI (Figure 52a). Then the same plot was implemented for thermal offset absolute values obtained in boreholes characterized by unconsolidated soils and peat substrates (4, 5 and 8) (Figure 52b).

a)

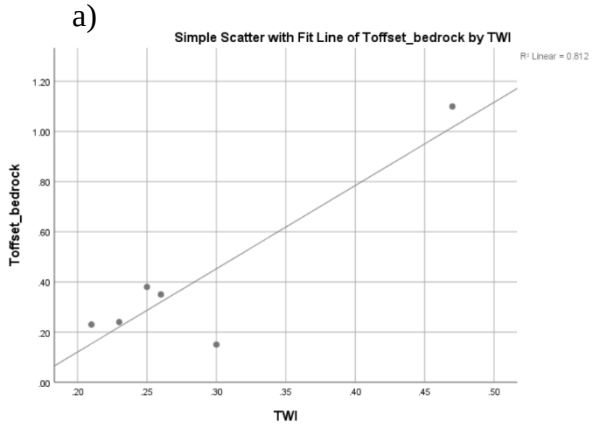

b)

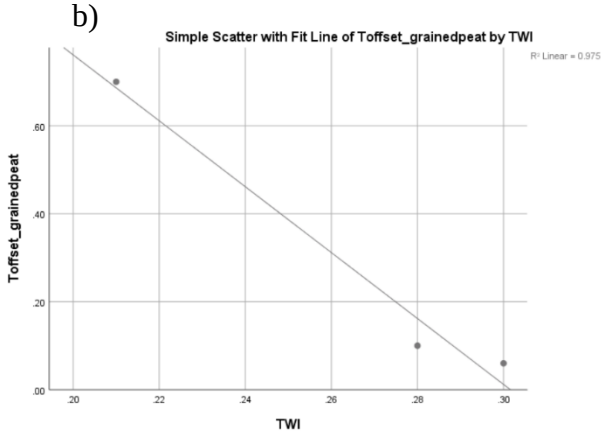

Figure 52. a) Linear relationship between *toffset* and the Topographic Wetness Index (TWI) in bedrock areas. b) Linear relationship between *toffset* and the Topographic Wetness Index (TWI) in unconsolidated soils or peat areas.

In Figure 52a, we observed a direct relationship between the thermal offset in bedrock substrates and the moisture content, fitting the expected results as mentioned in section 3.3.2.1, meaning that dryer bedrock (characterized by higher thermal conductivities) show lower absolute values of thermal offset (see Figure 28). In figure 52b, we observed an inverse relationship between the thermal offset and TWI in unconsolidated soils and peat substrates. These results fit the expected relation mentioned in section 3.3.3.1.C, moister soils and peat (with higher thermal conductivities than drier soils), show lower absolute values of thermal offset.

We checked for normality of residuals in a normal P-P plot as well for both substrate classes (Figures 53a and 53b). These plots showed an approximately normal distribution.

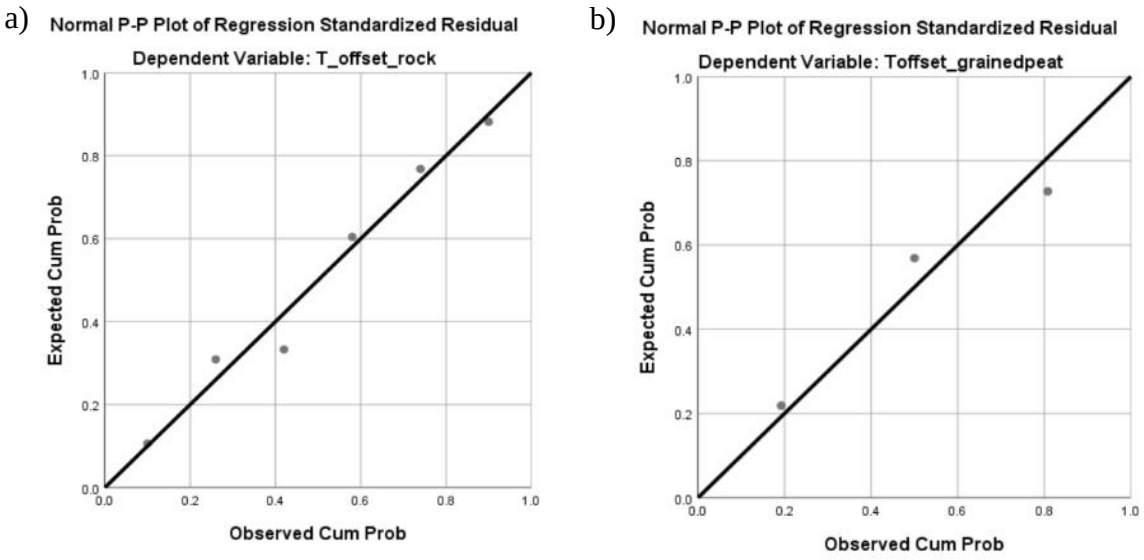

Figure 53. a) Normal Predicted Probability (P-P) plot for *thermal offset* as a dependent variable of the Topographic Wetness Index (TWI) in bedrock areas. b) for *thermal offset* as a dependent variable of the Topographic Wetness Index (TWI) in unconsolidated soils and peat areas.

Finally, we checked for homoscedasticity in Figures 54a and 54b that do not show a clear pattern. Thus, the distribution was considered homoscedastic.

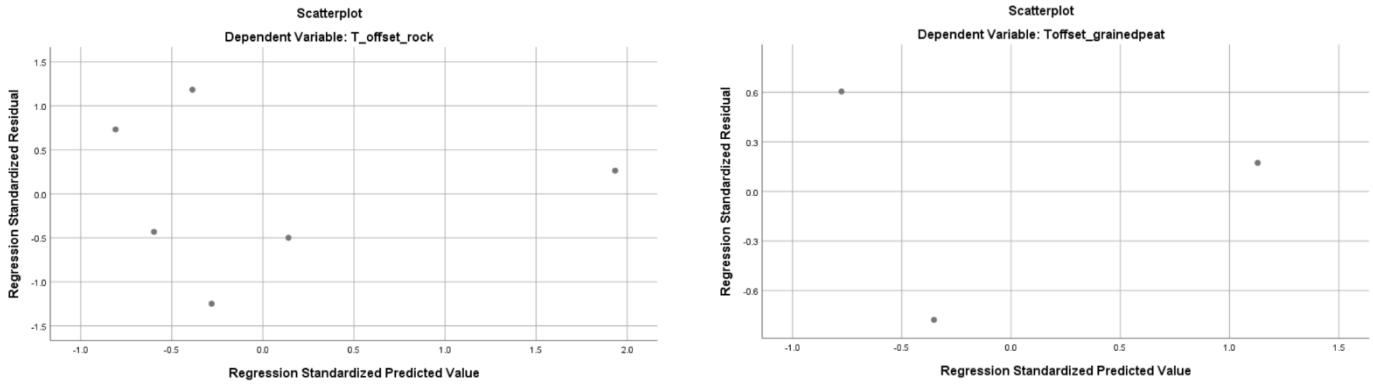

Figure 54. a) Plot of standardized residuals versus predicted values when performing a linear regression between *thermal offset* and TWI in bedrock areas. b) Plot of standardized residuals versus predicted values when performing a linear regression between *thermal offset* and TWI in unconsolidated soils and peat areas.

Once all the assumptions were tested, the expressions that relate the thermal offsets as a function of the TWI were determined, based on the empirical data gathered in our study area (Equation 15a and 15b). These functions were used for the spatialization of the thermal offset in next section all over the study area.

$$Toffset\ (bedrock) = 3.32x(TWI) - 0.54 \qquad Toffset\ \left({}^{uncons}/_{peat}\right) = -7.49x(TWI) - 2.26$$

R^2=0.81 R^2=0.98

Equation 15. a) Relationship function between *toffset* and Topographic Wetness Index (TWI) with the respective estimation adjustment value of R^2. b) Relationship function between *toffset* and Topographic Wetness Index (TWI) with the respective estimation adjustment value of R^2.

4.5 Spatial distribution of TTOP parameters and the TTOP spatial model.

Once determined the statistical relationships of the TTOP parameters with different terrain features, which results are presented in section 4.4, we computed the Equations 13 to 15 over the study area. The results are shown in Figures 55 to 59.

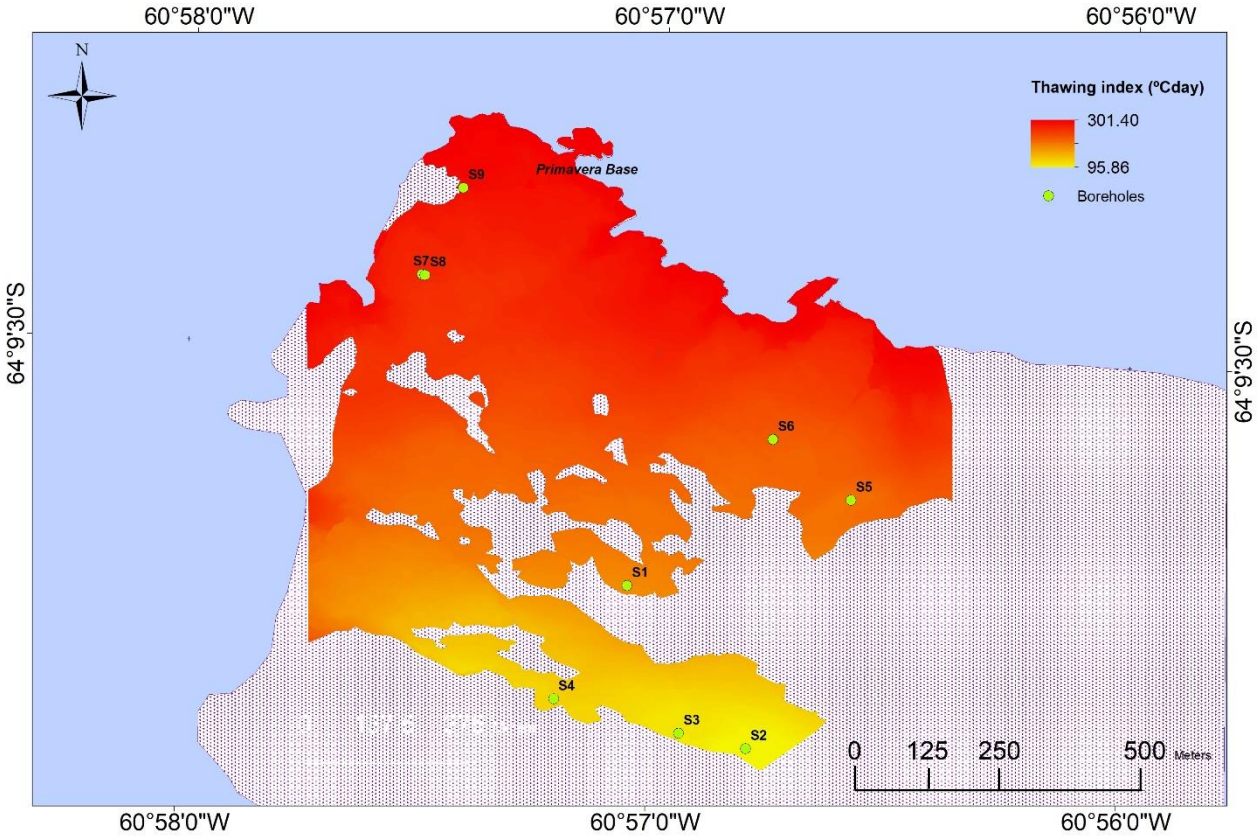

Figure 55. Modelled air thawing index *(It)* distribution in Cierva Point based on data from the years 1 and 2. White dotted region represents areas of permanent snow, ponds or topographic errors standing out of the model. Spatial resolution: 1m.

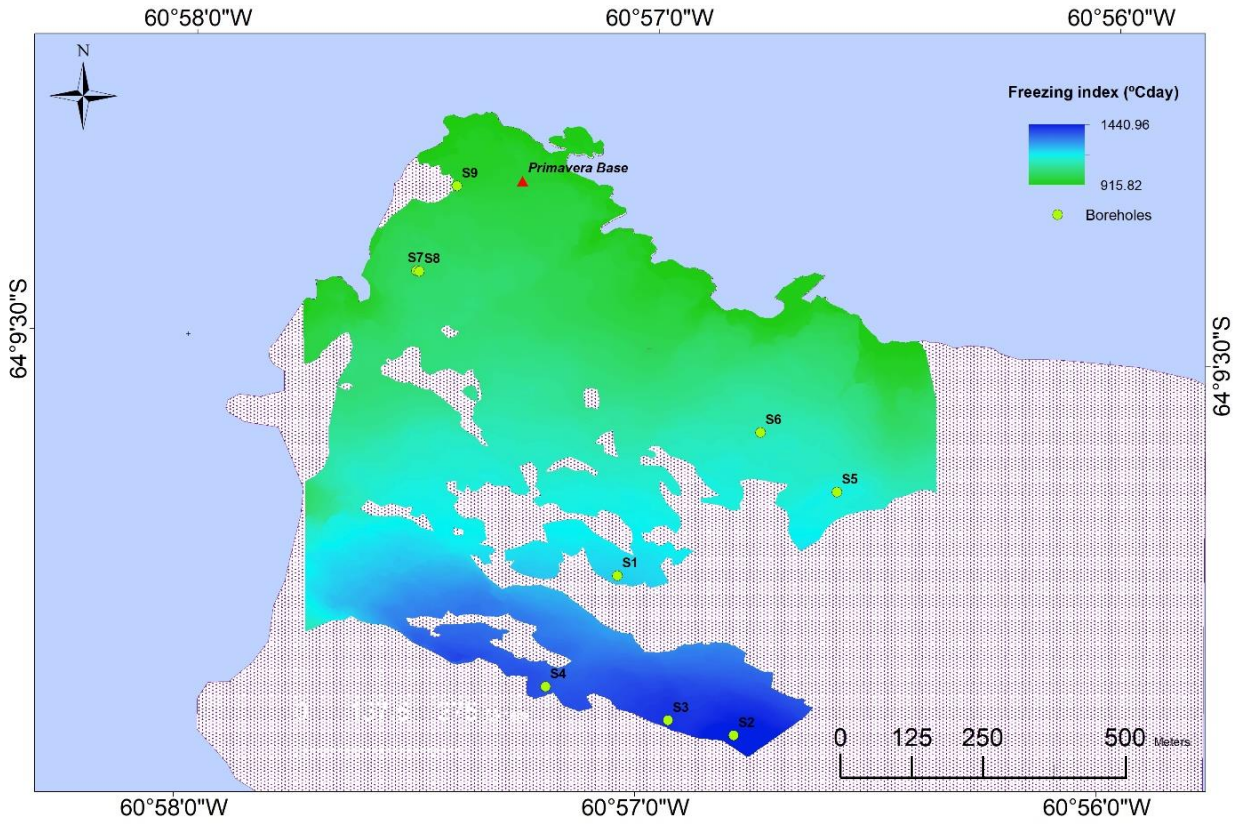

Figure 56. Modelled air freezing index *(If)* distribution in Cierva Point based on data from the years 1 and 2. White dotted region represents areas of permanent snow, ponds or topographic errors standing out of the model. Spatial resolution: 1m.

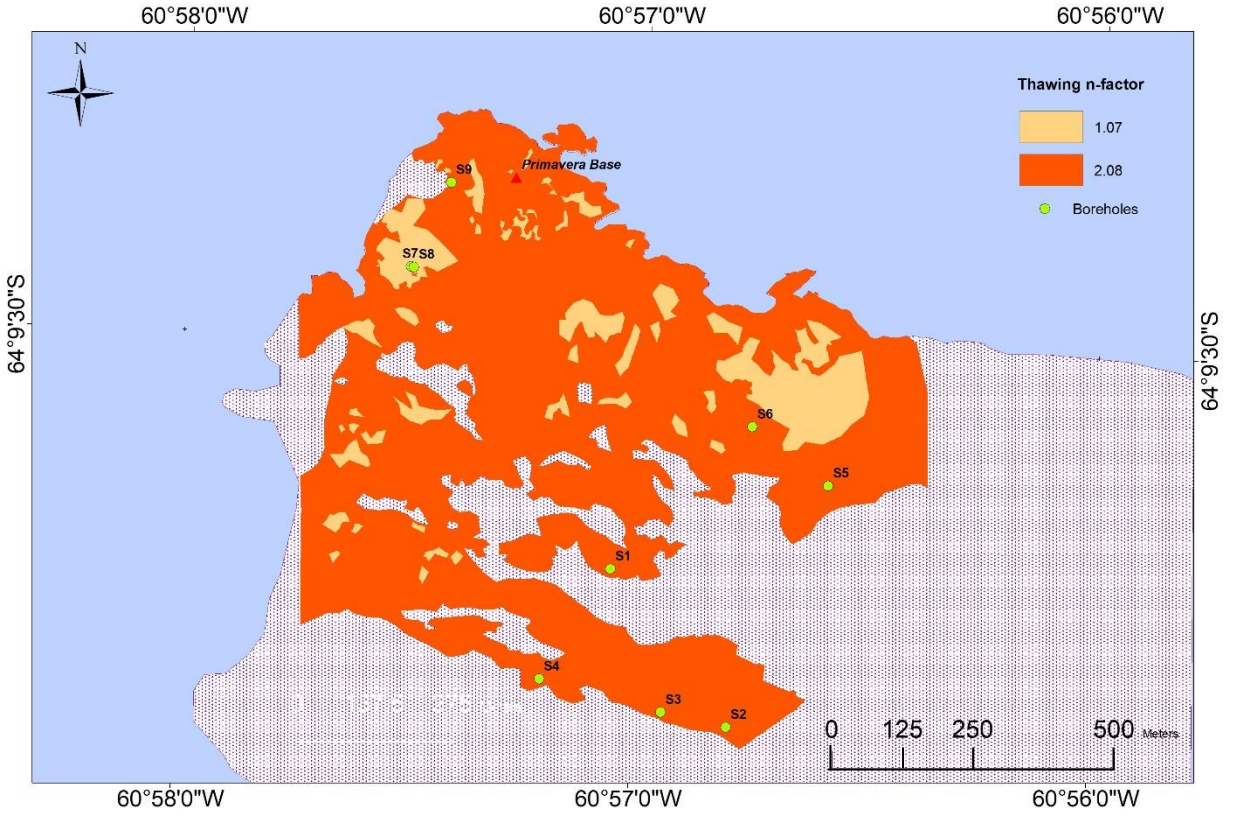

Figure 57. Modelled thawing n-factor *(nt)* distribution in Cierva Point based on data from the years 1 and 2. White dotted region represents areas of permanent snow, ponds or topographic errors standing out of the model. Spatial resolution: 1m.

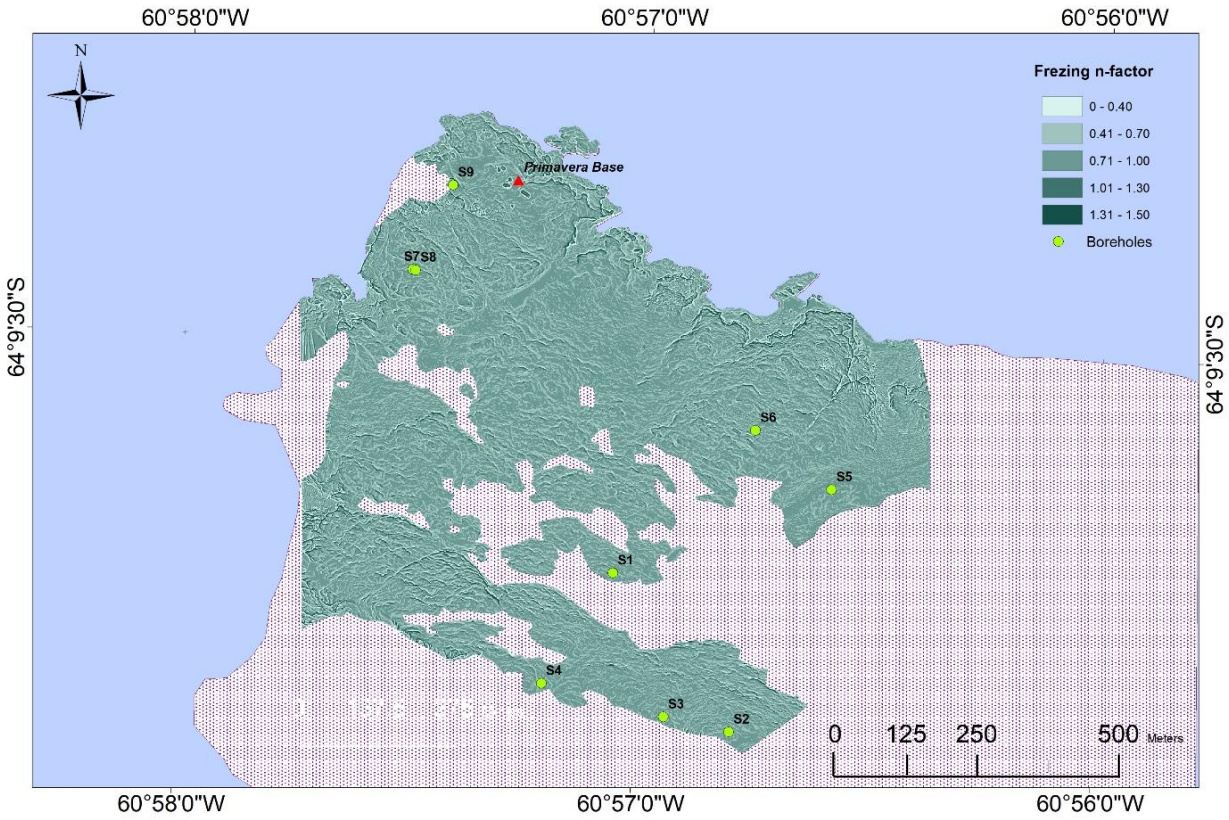

Figure 58. Modelled thawing n-factor (nt) distribution in Cierva Point based on data from the years 1 and 2. White dotted region represents areas of permanent snow, ponds or topographic errors standing out of the model. Spatial resolution: 1m.

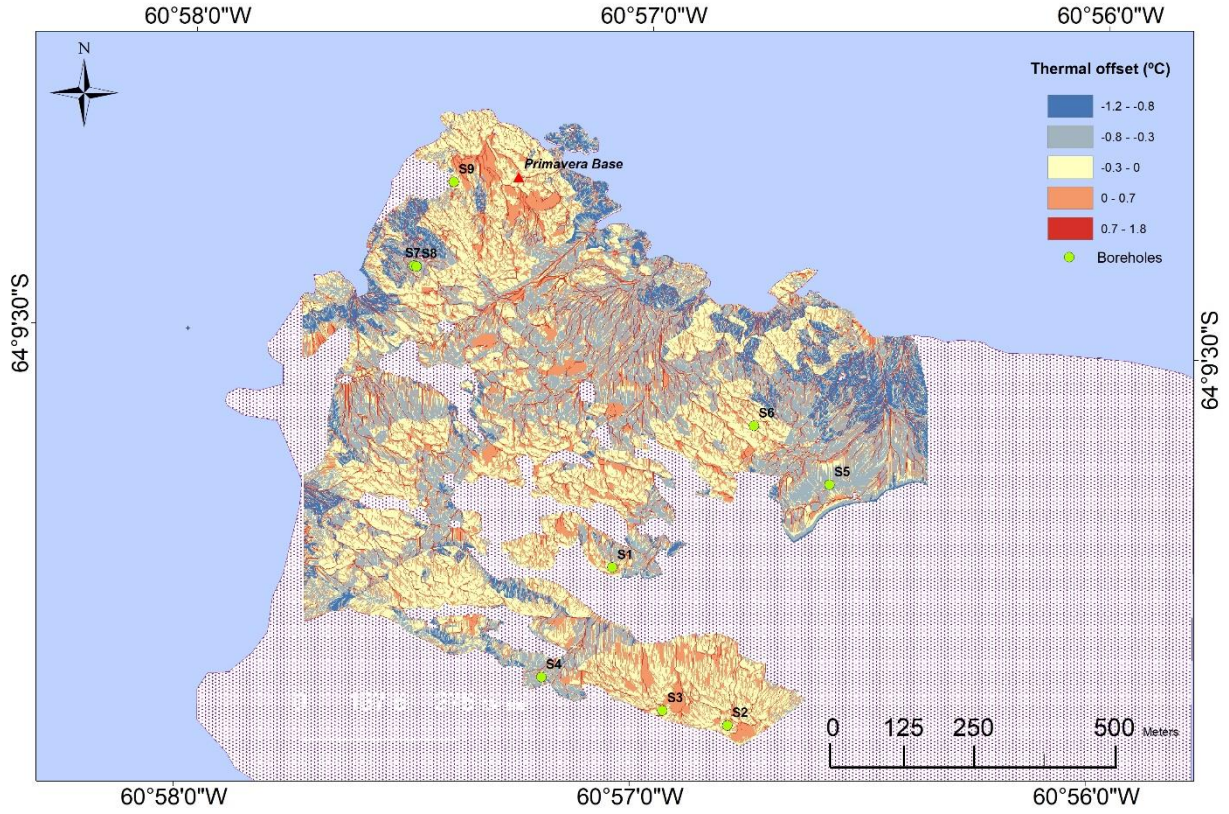

Figure 59. Modelled thermal offset *(toffset)* distribution in Cierva Point based on data from the years 1 and 2. White dotted region include areas of permanent snow, ponds or topographic errors standing out of the model. Spatial resolution: 1m.

Figures 55 to 59 show the spatial distribution models of the TTOP parameters based on statistical functions topo-climatic control factors over the area of study. As expected, the thawing and freezing air indexes decrease and increase respectively with the altitude in our area of study. N-thawing factor is mainly influenced by the presence or absence of moss. This factor's value gets an average value of 1.07 in the locations covered by at least 5 cm moss and gets an average value of 2.08 in the moss-free areas.

The n-freezing factor drops in the areas with higher propensity to snowpack accumulation (i.e. more concave areas), due to the insulator properties of the snowpack.

The thermal offset is the result of applying two different linear reggresion functions, one for each different kind of ground substrate (i.e bedrock or unconsolidated /peat soils). The absolute value of the thermal offset increases in wetter areas when the substrate is bedrock, but decreases in saturated areas when the substrates are unconsolidated soils or peats.

In the final distribution of the TTOP (Figure 60), values attain lower values in higher altitudes and at unconsolidated soils and peat deposits covered by moss, rather than at lower altitude and bare bedrock areas. Moreover, the TTOP shows its maximum values, higher than 0 ºC and up to 3.5°C, in potentially moist areas (matching with TWI≈1 values in Figure 34), characterized, as well, by a concave topography. This means that in these areas (accounting for aproximately 12% of the total area), permafrost is absent and the TTOP stands for the temperature at the base of the seasonally thawing layer. The reason is probably related to the high thermal conductivity of water (which encourage to total thaw of the saturated ground in the summer, when the air temperatures reach positive values) and with the higher potential for snowpack accumulation. The minimum values of the modelled TTOP (down to -6.33°C) were found in the most convex areas. In these areas, the total exposition of the ground to the winds and solar radiation minimizes the chances of snowpack accumulation during the winter season, leaving the bare surface exposed to heat loss during the freezing season. In summer, the buffer effect of the moss formations would insulate the frozen ground dificulting to gain heat from the solar radiation. This facts characterize these locations with high values of n-freezing fator and low values of n-thawing factor respectively, which in fact accounts negatively in the TTOP model equation (Equation 2), inducing lower lower values of TTOP.

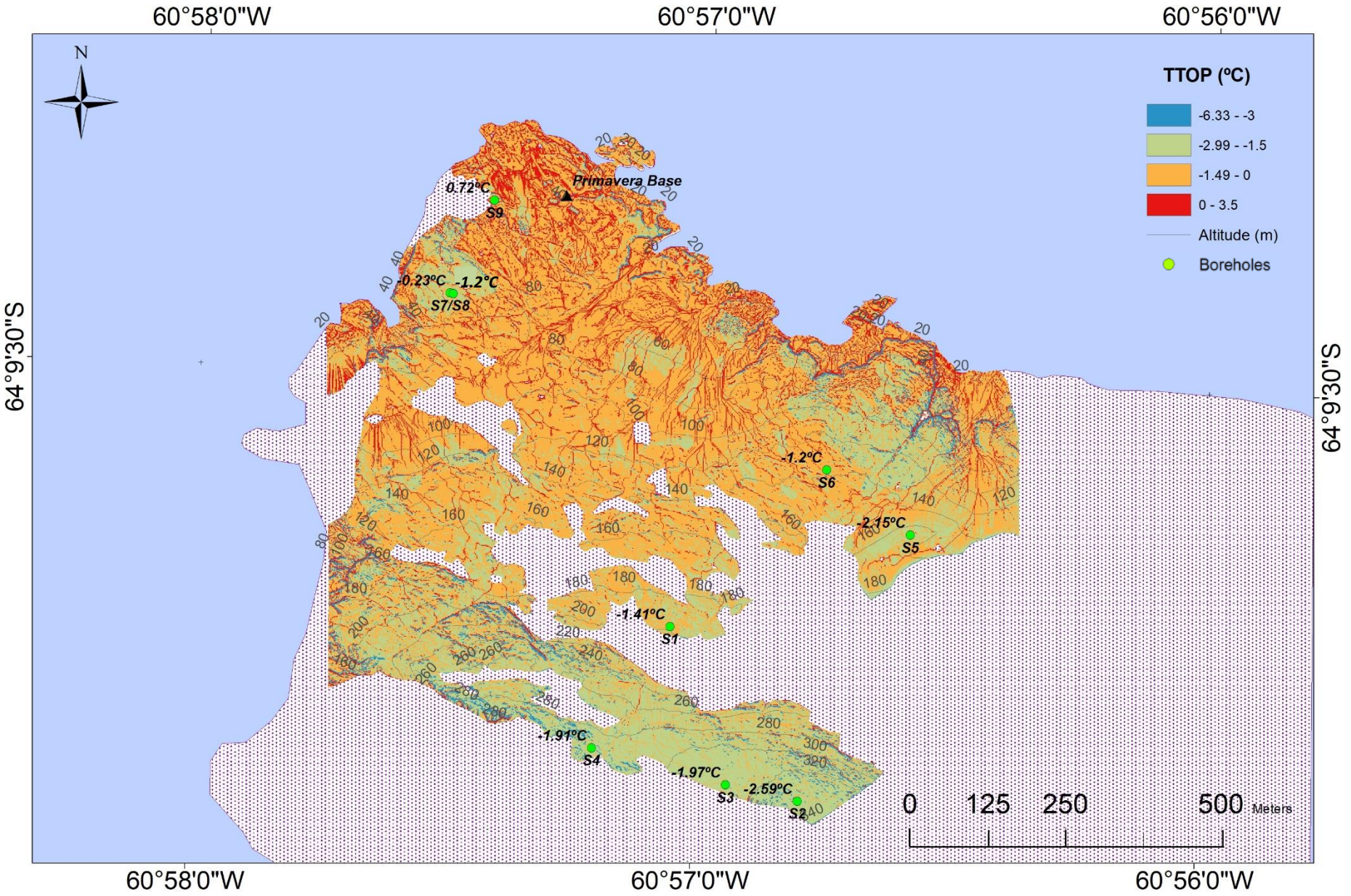

Figure 60. TTOP distribution over the area of study. Resulting TTOP values for each monitoring site are labelled. Altitude lines are expressed in meters above the ellipsoid WGS84. White dotted region represents areas of permanent snow, ponds or topographic errors standing out of the model. Spatial resolution: 1m.

4.6 Spatial model validation

For a better comparisons and validation of results, the Table 13 shows both the observed values and the modelled spatial results of air indexes (*Ita*, *Ifa*), n-factors (*nt*,*nf*), thermal offset (*toffset*) and TTOP, including the measurement uncertainties, which propagate from thermistor measurement (see Table 5) through the parameters functions. It shows, as well, the value of local error in the estimation of the spatial parameters for each monitoring site. The difference between the observed and modelled values of air thawing and freezing indexes (i.e. the error of spatialization of these parameters) ranged between approximately 6 and 122°Cdays in Site 4 and Site 1 respectively. The maximum error found in the spatial estimation of n-freezing factor was 2.24 in Site 2 and the best estimation of this parameter occurred in Sites 7 and 8 (nt error = 0.08). The higher error in the spatialization of the freezing n-factor is observed in Site 4 (nf error= 0.13) and the lowest occur in Site 2 with an error of 0.06.

Sites 1 and 6 present the poorest estimations of thermal offset (error of 0.33°C), being Site 4 characterized by the best estimation with an error of 0.02°C.

Finally, the maximum and minimum spatial estimation errors in the TTOP were found in Site 6 (0.51°C) and Site 1 (0.02°C), respectively.

On the other hand, Table 14 compiles the mean measurement uncertainties and show them in contrast with the mean estimation error of each parameter for all the boreholes. The mean error of the spatial estimation for all the parameters is, in general, smaller than the measurement uncertainty in the observed data, except for the *nt* factor, where the error exceeded the measurement uncertainty in 0.24 ºC. However, the overall estimation error of the spatial distribution of TTOP, after computing the Equation 2 all over the study area, was ±0.32 ºC, 0.18 ºC smaller than the mean thermistor measurement uncertainty of the observed TTOP (±0.50 ºC). As this magnitude of the mean overall spatial estimation error of the final TTOP model falls inside the margins of the measurement uncertainty, the estimation was considered good enough for the validation of the TTOP spatial model results.

		Site1	Site2	Site3	Site4	Site5	Site6	Site7	Site8	Site9
Ita (°C)	observed	118.40±54.50	112.50±54.50	121.47±54.50	133.81±54.50	147.82±54.50	334.90±54.50	304.71±54.50	304.71±54.50	230.64±54.50
	spatial estimation	185.62	99.31	110.57	128.15	206.00	224.87	265.02	264.91	286.31
	Absolute local error	67.22	13.19	10.90	5.66	58.18	110.03	39.69	39.80	55.67
Ifa (°C)	observed	1333.40±124.5	1422.11±124.5	1369.56±124.5	1368.48±124.5	1198.87±124.5	1049.60±124.5	988.20±124.5	988.20±124.5	1002.76±124.5
	spatial estimation	1211.62	1432.15	1403.37	1358.47	1159.55	1111.35	1008.74	1009.03	954.36
	Absolute local error	121.78	10.04	33.81	10.01	39.32	61.75	20.54	20.83	48.40
nt	observed	1.43±0.52	4.32±0.60	1.89±0.69	1.52±0.68	2.19±0.40	0.87±0.35	2.00±0.27	0.99±0.19	2.38±0.34
	spatial estimation	2.08	2.08	2.08	2.08	2.08	2.08	2.08	1.07	2.08
	Absolute local error	0.65	2.24	0.19	0.56	0.11	1.21	0.08	0.08	1.09
nf	observed	0.55±0.13	0.82±0.19	0.74±0.21	0.59±0.25	0.91±0.12	0.60±0.32	0.74±0.30	0.76±0.14	0.85±0.27
	spatial estimation	0.65	0.76	0.66	0.72	0.83	0.77	0.62	0.64	0.73
	Absolute local error	0.11	0.06	0.08	0.13	0.08	0.17	0.12	0.12	0.12
Toffset (°C)	observed/estimated	0.38±0.20	-0.35±1.00	-0.24±1.00	0.06±1.00	-0.7±1.00	0.23±1.00	0.15±1.00	-0.1±1.00	1.1±1.00
	spatial estimation	0.05	-0.04	-0.04	0.08	-0.67	-0.1	0.22	-0.07	1.02
	Absolute local error	0.33	0.31	0.2	0.02	0.03	0.33	0.07	0.03	0.08
TTOP (°C)	observed/estimated	-1.21±0.1	-2.25±0.50	-2.42±0.50	-1.61±0.50	-2.59±0.50	-0.69±0.50	-0.18±0.50	-1.35±0.50	0.32±0.50
	spatial estimation	-1.41	-2.59	-1.97	-1.91	-2.15	-1.2	-0.23	-1.2	0.72
	Absolute local error	0.2	0.34	0.45	0.3	0.44	0.51	0.05	0.15	0.4

Table 13. Values for the locally observed and spatial estimated results of air indexes (*Ita*, *Ifa*), n-factors (*nt*,*nf*), thermal offset (*toffset*) and *TTOP* model.

	Mean measurment uncertainity (±)	Mean estimation error (±)
Ita (°C)	54.50	44.48
Ifa(°C)	124.50	40.72
nt	0.45	0.69
nf	0.21	0.11
Toffset (°C)	0.72	0.16
TTOP (°C)	0.50	0.32

Table 14. Comparison between the mean measurement uncertainties and the error of the spatial estimation of each parameter for all the boreholes

4.7 Permafrost sensitivity to climate change in Cierva Point

In order to evaluate the potential permafrost spatial sensitivity to climate change, it was implemented a TTOP model for a hypothetical scenario, where long-term mean annual air temperatures increase 1 ºC disregarding changes in any other topo-climatic factor, such as the seasonal snow pack, moss distribution or soil moisture content, as explained in section 3.5. The results of the distribution of the new TTOP is shown in Figure 61.

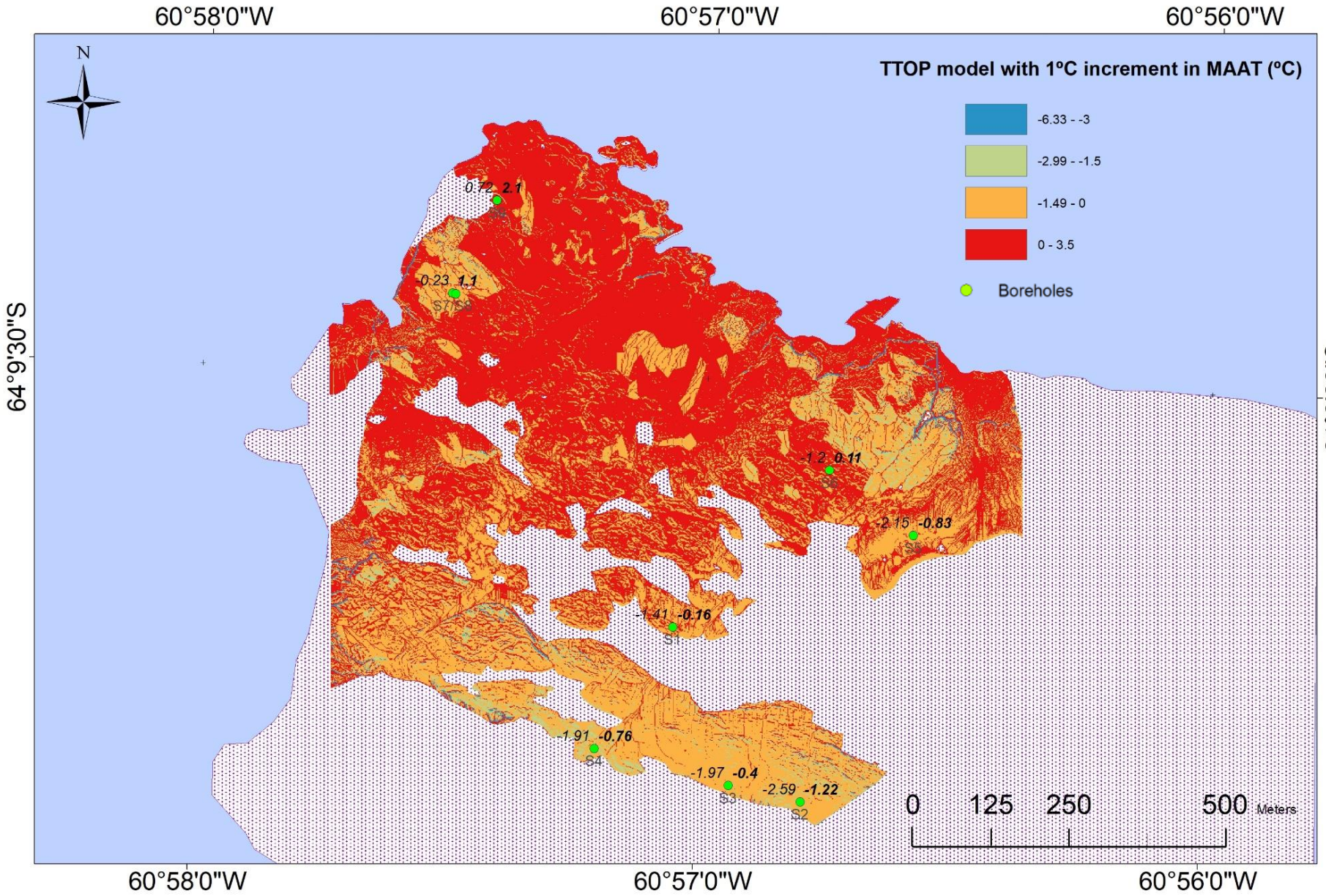

Figure 61. TTOP distribution on a hypothetical scenario of 1 ºC increase in the mean daily air temperature.

Labels in bold at the right top of each site show the resulting TTOP after a 1 ºC increment on the MAAT. Label at the left top of each site show the modelled TTOP values in the current scenario. White dotted region represents areas of permanent snow, ponds or topographic errors standing out of the model. Spatial resolution: 1m.

Figure 61 shows the new values of mean annual temperature at the TOP when a 1 ºC increase in the MAAT is considered. For each specific monitoring site, the TTOP values modelled in both different scenarios are labelled: 1. before the climate change (in the upper left of each site), and 2. After the MAAT increased 1 ºC (in bold to the right of each site). Sites 1,2,3,4,5 and 8, even though increased its values, still maintained negative temperatures at the permafrost table after the variance. However, the temperature at the top of permafrost in sites 6 and 7 increased above 0 ºC suggesting the potential disappearance of permafrost in these sites. Resulting positive TTOP values for these sites after the increment of the MAAT stand for the temperature at the base of the seasonal freezing and thawing layer (Way & Lewkowicz, 2016), under which the ground does not freeze anymore during the winter time. In site 9, permafrost was absent before the increment of temperature and still remained absent in the second scenario.

In order to simplify the visualization of the TTOP model distribution in both case scenarios, both maps where reclassified in two different sectors: areas with TTOP < 0 ºC and areas with TTOP > 0 ºC (Figures 62a and 62b). Even though the depth of the permafrost table is unknown in most of them, areas with TTOP < 0 ºC in both scenarios represent areas where permafrost is estimated to be present. Positive TTOP values correspond to cases where the ground still freezes and thaws seasonally, but where no permafrost occurs.

In the scenario 1, most of the study area (around 88%) shows negative values of TTOP and thus indicate presence of permafrost. Permafrost-free areas, where TTOP resulted positive, are a minority (around 12%), that mainly occur in areas characterized by higher Topographic Wetness Indexes and high moisture contents (characterized by higher thermal conductivities that dry soils).

When comparing with the second scenario (Figure 62b), a significant increase of the permafrost free areas is observed, almost the 50% of the permafrost in scenario 1 would disappear. Figure 63 shows the TTOP changes from scenario 1 to 2. Blue areas account for the 43% of the total area of interest and represent the regions where permafrost was found with TTOP < 0 ºC in scenario 1 and still remained negative after the warming. Red colour designates the permafrost free areas (TTOP > 0 ºC) in scenario 1 that remained permafrost-free (with positive TTOP) after the climate change, and account for the 12% of the area. Finally, brown areas represent the regions where permafrost was present (TTOP < 0 ºC) in scenario 1, but disappeared as a consequence of the climate warming in scenario 2 (45%).

The TTOP values in almost all the study area were estimated to increase in average 1.18 ºC as a consequence of the air temperature forcing.

The areas showing a higher increase in the TTOP, and thus the most sensitive to the air temperature change, were the ones at lower altitudes with bare ground surfaces and/or high concavity. The absence of moss covers makes these areas noticeably exposed to warming during the summer, when solar radiation is directly absorbed by the ground. The thicker snowpack associated to the concavity, provides better insulation during winter, reducing heat losses and contributing to ground warming. The areas which still maintained permafrost after the air temperature increase, were mainly those at higher altitudes or the areas with a moss bed insulating the ground from the summer warming. Permafrost remains present in areas of convex topography as well, where a low potential of snow cover, leaves the ground exposed to high of heat losses during the winter.

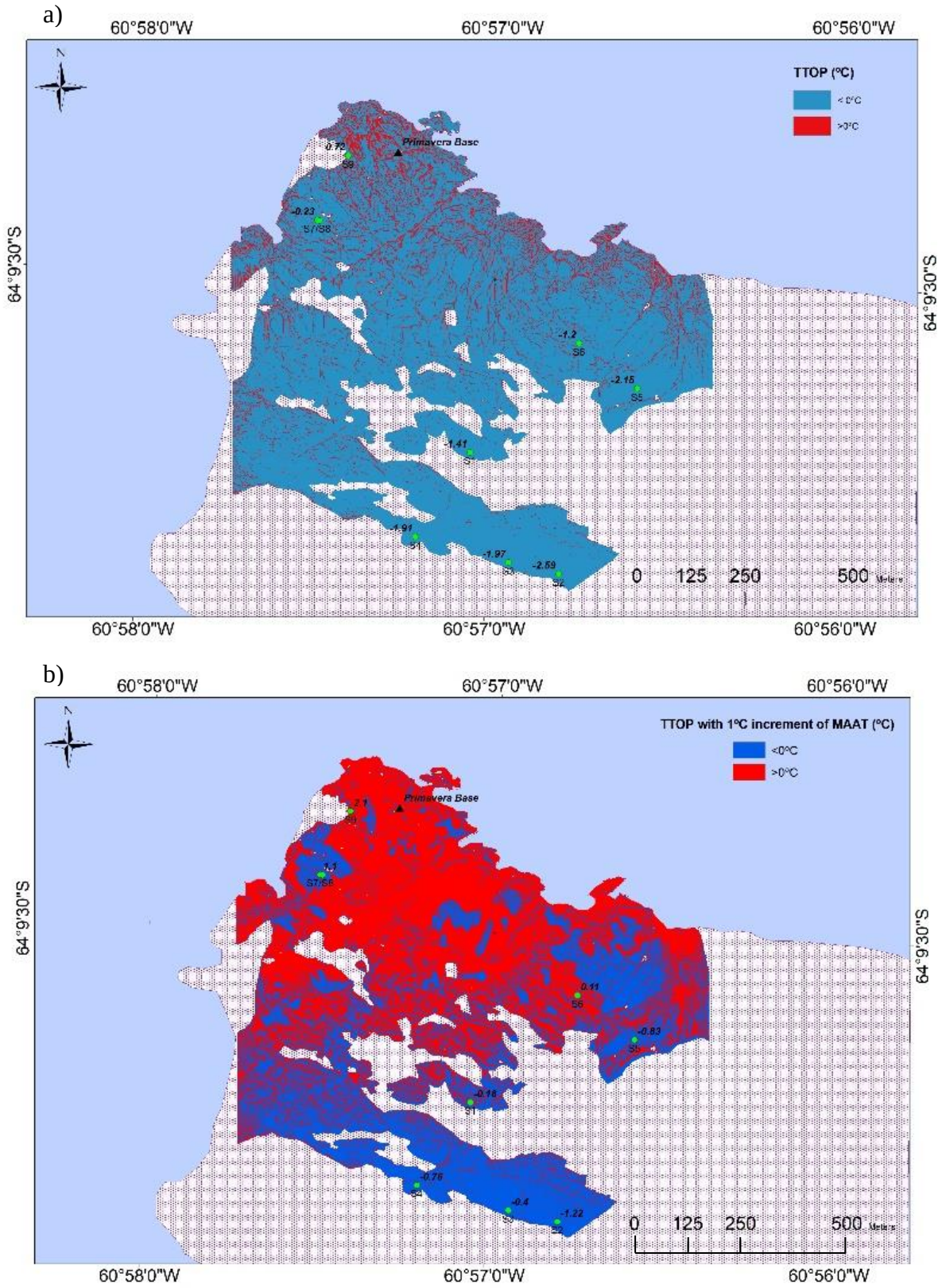

Figure 62. a) Spatial distribution of TTOP classified separately in positive and negative TTOPs. b) Spatial distribution of TTOP considering an increment of 1 ºC in the long-term MAAT. The map is classified in positive and negative TTOP. Spatial resolution: 1m.

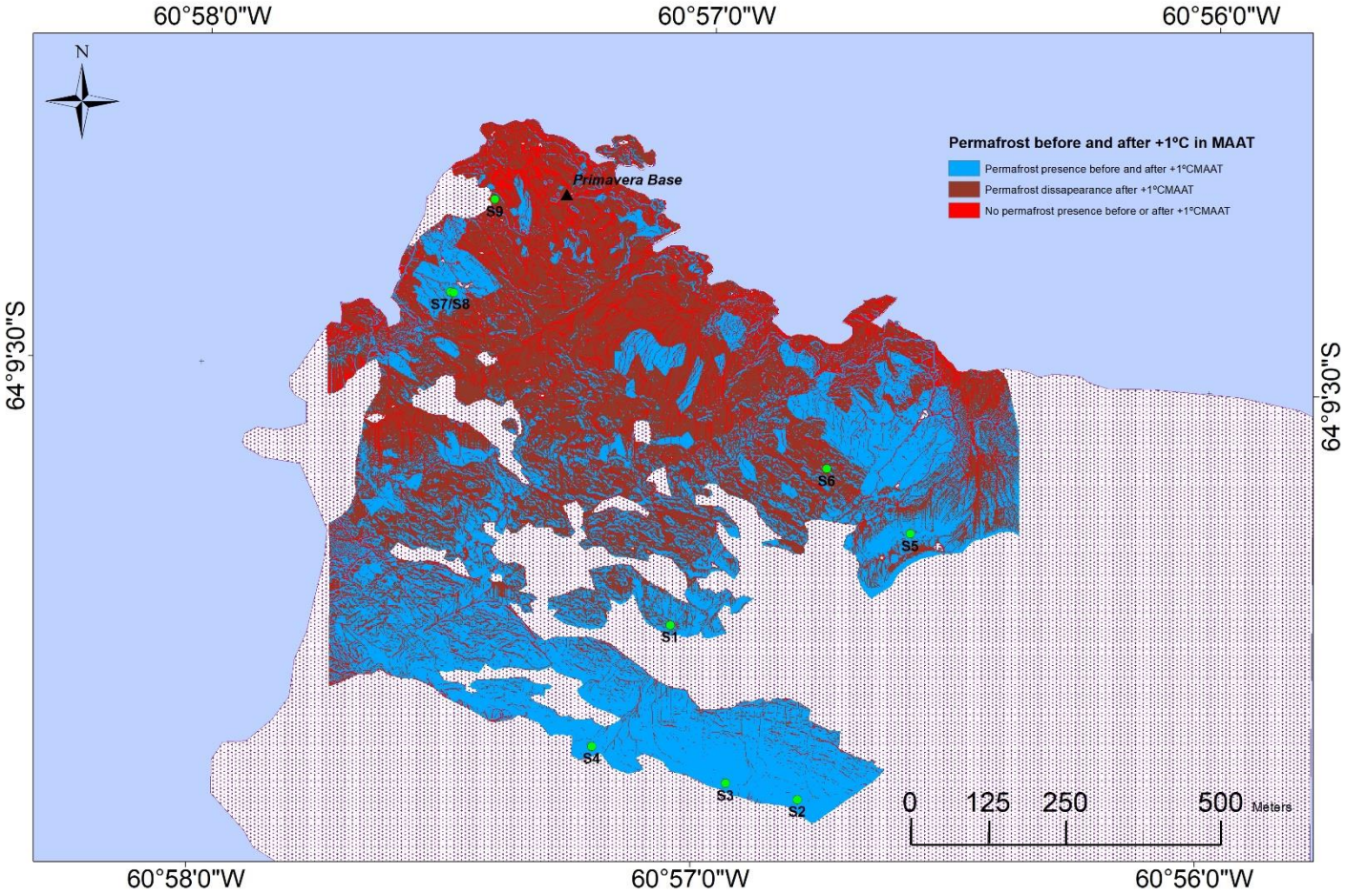

Figure 63. Change in permafrost distribution in Cierva Point due to a long-term increase of 1 ºC in the MAAT. Green dots represent the 9 monitoring boreholes. White dotted region represents permanent snow, ponds or topographic errors standing out of the model. Spatial resolution: 1m.

5. Conclusions

In order to evaluate permafrost climate sensitivity at Cierva Point, the ground temperature regimes in nine sites were analysed and the spatial distribution of the Temperature at the Top Of Permafrost (TTOP) was modelled.

By analysing the temperature regime for the sites where observational data was available thanks to nine boreholes, permafrost was observed at depths in the range from 0.4 to 5 m depending on substrate, topographical and vegetation characteristics. At the deepest borehole in bedrock, in a site with slightly convex terrain, north aspect and at 198 m altitude, permafrost was found at 5 m and showed a mean annual temperature of -1.2 ºC. In a convex moraine area, at 166 m and north aspect, permafrost was found at 1 m depth and the Temperature at the Top of Permafrost was -2.6 ºC. In a low elevation site at 72 m, characterized by 40 cm of moss cover over a peat substrate, permafrost was found at 0.4 m, right below the moss layer with a TTOP of -1.4 ºC.

In general, the estimated depths of the top of permafrost were found to be deeper (and the seasonal thawing layer thicker) in bedrock sites, followed by unconsolidated soils and peat substrates. In one of the monitored sites in bedrock and characterized by the highest wetness index value and located at the lowest elevation (36 m), the temperature profile suggests the absence of permafrost and sets the temperature at the top of the seasonally thawing and freezing layer at 0.32 °C.

The ground temperature profile of the deepest borehole (15m) and its comparison with the air temperature regime provided some insights on the thermal impact of the snowpack on the ground surface temperature in this representative site. Some differences were found in the thermal offset values between the air and the surface during the first monitoring period from 2012-2014 and the second monitoring period from 2016-2018. In the first period, the ground surface thermal regime showed a stronger decoupling from the cold air temperatures in the winter time, while from 2016-2018 the surface thermal regime was found to be strongly coupled with the atmosphere. Also, the zero-curtain effect was observed to be shorter in the spring of 2015 and 2017 in comparison with previous years. These observations may reflect a longer lasting and thicker snowpack accumulation during the winter seasons of 2012 and 2013, which would have provided a stronger insulation to the surface for longer than the thinner snowpack in 2016-2018. An observed reduction of the active layer thickness in this site during the first two years of the dataset could be also explained by this fact. This

observation is in agreement with previous observations in nearby regions reporting a reduction of the active layer thickness in ice-free areas of the South Shetland Islands between 2006 and 2014, linked with episodes of longer lasting and thicker snowpack accumulation the surface (Goyanes et al., 2014; Ramos et al., 2017; de Pablo et al., 2017).

The spatial modelling of the distribution of the TTOP parameters over Cierva Point, showed that the *air thawing* and *freezing* indexes were observed to decrease and increase respectively with the altitude, being somehow related with the adiabatic lapse rate. *N-thawing factor* values were lower in locations covered by moss formations than in bare soils and bedrock. The *n-freezing factor* was found to drop in the areas with higher potential snowpack accumulation (i.e. more concave areas). Both these results are explained by the buffer effect of the moss cover and the snowpack, which act as good thermal insulators (specially during the winter season in the case of the latter). The absolute values of the spatially modelled *thermal offsets* showed an increase (larger difference between TTOP and mean annual surface temperatures) in moist areas where the substrate is bedrock, but a decrease in saturated areas, where the substrate are unconsolidated soils or peats. Reasons for this, may be the higher thermal conductivity of peats and soils when they are wet, rather that dry, and of bedrock, when dry.

Values resulting from the final distribution of the Temperature in the Top of Permafrost *(TTOP)* were lower in higher altitudes and at unconsolidated soils and peat deposits covered by moss, rather than at lower altitude and bare bedrock areas. Moreover, the TTOP shows its maximum values (above 0 ºC and up to 3.5 °C), in potentially moist areas, characterized as well by concave topography. This means that in these areas, permafrost is absent and the TTOP will stand for the temperature at the base of the seasonal thawing layer. The reason is probably related to the high thermal conductivity of water (which promotes the total thaw of the saturated ground in the summer, when the air temperatures reach positive values) and with the higher potential for snowpack accumulation (which acts as a thermal insulator layer, reducing heat losses in winter).

Low values of TTOP were found, as well, in the most convex areas covered by moss formations. In these areas, the total exposition of the ground to the winds and solar radiation minimizes the chances of snowpack accumulation during the cold season, leaving the bare surface exposed to significant heat losses. In summer, the buffer effect of the moss formations insulates the frozen ground limiting heat gains from solar radiation. These characterize are typical of the locations with high values of n-freezing factor and low values of n-thawing

factor, respectively, which in fact, account negatively in the TTOP model equation (Equation 2), inducing its lower values.

The overall estimation error of the spatial distribution of TTOP after computing the TTOP model equation over the study area, was ±0.32 ºC, and hence 0.18 ºC below the mean thermistor measurement uncertainty of the observed TTOP (±0.50 ºC). As this magnitude of the mean overall spatial estimation error of the final TTOP model falls inside the margins of the measurement uncertainty, the estimation was considered good enough for the validation of the TTOP spatial model results. This estimation error magnitude accounts somehow for the high small-scale variability of terrain features combined with a small sample size of monitoring points (i.e. lack of repetition for observed data in moss-covered areas with underlying peats), that together with high temperature measurement uncertainties, creates a high probability of relation due to randomness in the estimation of statistical relationships. Consequently, continuous functions like the regression models used in this method, that do not account for this random variability at smaller scales, are sometimes likely to fail when trying to explain the variability of the TTOP parameters at the 1 m/pixel resolution local scale of the study area. Hence, in future developments, other less restrictive estimation methods such as regression tree analysis could be alternatively applied as included in other studies (Anderton et al., 2004; Watson et al., 2006).

Finally, analysing the TTOP distribution in the hypothetical scenario of climate change, with a long-term mean annual air temperature increase of 1 ºC and disregarding changes in any other topoclimatic factors, a significant reduction of the TTOP values in the area was observed. The results suggest the disappearance of nearly the 50% of the permafrost estimated to currently exist in Cierva Point.

The areas showing a higher increase in the TTOP, and resulted to be the most sensitive to the air temperature change, were the ones at lower altitudes, characterized by bare ground surfaces and/or high concavity. The absence of a moss cover makes these areas noticeably exposed to the increase of temperature during the summer, when solar radiation is directly absorbed by the ground. However, a thicker snowpack linked to the concave topography provides better insulation during the winter reducing heat loses and contributing ground warming. The areas which still maintained underlying permafrost after the air temperature increase, were those at high altitudes and or the areas counting with a top moss bed cover insulating the ground from the increment of temperature during the summer. Concave areas

also maintained underlain permafrost as a low potential of snow cover, leaves the ground exposed to high rates of heat loses during the winter.

The disappearance of permafrost areas in Cierva Point may lead to significant impacts in the area's ecosystem, especially on hydrology and consequently in flora and fauna. The results of a 1 ºC warming suggest the potential degradation of permafrost mainly at low and mid altitude areas, covering mostly all the areas with the greatest accumulation of moss and lichen colonies and penguin activity nowadays. Permafrost presence is of uppermost importance for the hydrology of the area, as the impermeable properties of the permanent frozen ground promote the pooling of rain and melt water on the surface making possible its existence. The thawing of permafrost in wetland areas would therefore increase the water infiltration through thicker soils and permeable joints, reducing the superficial water flow available for moss communities in the area as well. As an example, the three current existing temporary ponds located at the northwest side of the peninsula, situated at around 80 m altitude, may lower its water table resulting in possibly impacts on the penguin high activity occurring in these areas as well. Flora and fauna are consequently very vulnerable to changes in the permafrost distribution in Cierva Point.

The permafrost model developed in this dissertation provides interesting insights about the current situation and future scenarios of ground temperatures. However, it must be taken into account that the model implements parameterizations on soil, vegetation and climate data, which encompass broad uncertainties, as land cover, soil characteristics are estimated on a coarse scale and interpolated for large areas. Besides, using longer periods of dataset for the computation of the model may reflect a closer reality of TTOP values over the past years (as the final dataset used for the computation of the model was reduced to 2 years long due to the discontinuity of the records over the full period from 2012 to 2018). Moreover, permafrost is controlled by local topo-climatic factors, which may vary over small scales. The magnitude of the estimation error accounts somehow for the high small-scale variability of these topoclimatic features combined with a small sample size of monitoring points (i.e. lack of repetition for observed data in moss-covered areas with underlying peats). This creates a high probability of relation due to randomness in the estimation of statistical relationships between TTOP parameters and terrain features. Consequently, continuous functions like the regression models used in this method, that do not account for this random variability at smaller scales, are sometimes under the risk of failing when trying to explain the variability of the TTOP

parameters at small scales such as the 1m/pixel resolution local scale used in this project. Therefore, large sample datasets are crucial in order to reproduce the state of the art and future ground temperature regimes in permafrost regions (Solheim, 2016).

In order to improve the precision of the model carried out in this dissertation and increase the dataset quality in future investigation lines, still new monitoring sites could be set up to record temperatures over longer continuous time periods. However, this is a logistical complex issue and also costly, accounting for the very remote location of Cierva Point.

References

Aduda, B.O. (1996). Effective thermal conductivity of loose particulate systems. *J Mater Sci* (31), 6441–6448.

Anisimov, O.A., Shiklomanov, N.I., Nelson, F.E. (1997). Global warming and active layer thickness: results from transient general circulation models. *Global and Planetary Change,* (15), 61–77.

Ball, B. A. (2010, December 23). Patterns in Antarctic Soil [Blog post], Retrieved Jan 2, 2018, from: http://polarsoils.blogspot.com.es/2010/12/patterns-in-antarctic-soil.html

Bevington, A., and Lewkowicz, A.G. (2015). Assessment of a land cover driven TTOP model for mountain and lowland permafrost using field data, southern Yukon and northern British Columbia, Canada. In *Proceedings of GéoQuebec: 68th Canadian Geotechnical Conference and 7th Canadian Permafrost Conference. Québec City, Canada*, 9.

Bethan, D. (2017, June 22). "Periglacial Environments." *AntarcticGlaciers.org*. Retrieved Jan 2, 2018, from: http://www.antarcticglaciers.org/glacial-geology/glacial-landforms/antarctic-periglacial-environments/

Biskaborn, B. K., Lanckman, J., Lantuit, H., Elger, K., Streletskiy, D. A., & Cable, W. L. (2015). *The new database of the Global Terrestrial Network for Permafrost (GTN-P),* 245–259. https://doi.org/10.5194/essd-7-245-2015

Bockheim JG. (1995). Permafrost distribution in the Southern Circumpolar Region and its relation to the environment: a review and recommendations for further research. *Permafrost and Periglacial Processes,* (6), 27–45.

Bockheim, J., Vieira, G., Ramos, M., López-martínez, J., Serrano, E., & Guglielmin, M. (2012). Climate warming and permafrost dynamics in the Antarctic Peninsula region. *Elsevier journal*, *100* (2013), 215–223.

Böning, C.W., Dispert, A., Visbeck, M., Rintoul, S.R., Schwartzkopf, F.U. (2008). The response of the Antarctic Circumpolar Current to recent climate change. *Nature Geoscience, 1*, 864–869.

Brenning A, Gruber S, Hoelzle M. 2005. Sampling and statistical analyses of BTS measurements. *Permafrost and Periglacial Processes*, (16), 383–394. DOI: 10.1002/ ppp.541

Brown, J., Ferrians, O.J.Jr., Heginbottom, J.A., Melnikov, E.S. (1998, revised February 2001). Circum-Arctic map of permafrost and ground-ice conditions. Boulder, CO: National Snow and Ice Data Center/World Data Center for Glaciology. Digital Media

Brown, J., O.J. Ferrians, Jr., J.A. Heginbottom, E.S. Melnikov, (1997) Circum-Arctic map of permafrost and ground-ice conditions. Washington, DC: U.S. Geological Survey in Cooperation with the Circum-Pacific Council for Energy and Mineral Resources. Circum-Pacific Map Series CP-45, scale 1:10,000,000, 1 sheet. (https://ipa.arcticportal.org/products/gtn-p/ipa-permafrost-map

Burgess, M.M., Smith, S.L., Brown, J., Romanovsky, V., Hinkel, K. (2000). Global Terrestrial Network for Permafrost (GTNet-P) permafrost monitoring contributing to global climate observations. *Geological Survey of Canada, Current Research, 2000E*(14), 1–7.

Burn, C.R. (1998). Field investigations of permafrost and climatic change in Northwest North American. In *Proceedings of the 7th International Conference on Permafrost, Yellowknife, Canada, Nordicana, Quebec*, (55), 107–120.

Burn, C.R. and Smith, C.A.S. (1988). Observations of the "thermal offset" in near-surface mean annual ground temperatures at several sites near Mayo, Yukon Territory, Canada. *Arctic*, (41), 99-104.

Campbell, I.B. (2001). Soils and ice-free areas. In: *Waterhouse EJ (ed) Ross Sea region: a state of the environment, report for the Ross Sea Region of Antarctica* (pp 4.16–4.35). New Zealand Antarctic Institute, Christchurch.

Campbell, I.B., Claridge, G.G.C. (1969). A classification of Frigic soils – the zonal soils of Antarctica. *Soil Sci*, (107), 75–85.

Campbell, I. B., & Claridge, G. G. C. (2009). Antarctic Permafrost Soils. In *Permafrost Soils*, (16), pp. 17–31. Berlin: Springer. https://doi.org/10.1007/978-3-540-69371-0

Cassie, J. (n.d.). MAAT, Permafrost Characterization and Climate Warming [online presentation]. Retrieved Jun 15, 2018 from: http://slideplayer.com/slide/7451974/

Christiansen, H.H., Etzelmüller, B., Isaksen, K., Juliussen, H., Farbrot, H., Humlum, O., Johansson, M., Ingeman-Nielsen, T., Kristensen, L., Hjort, J., Holmlund, P., Sannel, A.B.K., Sigsgaard, C., Åkerman, H.J., Foged, N., Blikra, L.H., Pernosky, M.A., Ødegård, R.S., (2010). The thermal state of permafrost in the Nordic area during the International Polar Year 2007–2009. *Permafrost and Periglacial Processes*, (21), 156–181.

Cohen, J. (1988), *Statistical Power Analysis for the Behavioral Sciences, 2nd Edition.* Hillsdale: Lawrence Erlbaum.

Cook, A.J., Vaughan, D.G. (2010). Overview of areal changes of the ice shelves on the Ant- arctic Peninsula over the past 50 years. *The Cryosphere*, (4), 77–98.

Cooley, S. (2016a). Topographic Wetness Index (TWI). GIS 4 Geomorphology. Retrieved Apr 15, 2018 from: http://gis4geomorphology.com/topographic-index-model/

Cooley, S. (2016b). Hillslope Wetness Index. *GIS 4 Geomorphology*. Retrieved Apr 15, 2018 from: http://gis4geomorphology.com/hillslope-wetness-index/

de Pablo, M.A., Ramos,M.,Molina, A., 2014. Thermal characterization of the active layer at the Limnopolar Lake CALM-S site on Byers Peninsula (Livingston Island), Antarctica. *Solid Earth*, (5), 721–739.

de Schutter, P (2004). Thermokast. Retrieved Aug 30, 2018 from: http://www.ougseurope.org/index.php?id=39

Delisle, G. (2007). Near-surface permafrost degradation: How severe during the 21st century? *Geophysical Research Letters*, *34*(9), 4. https://doi.org/10.1029/2007GL029323

Desrochers, D. T. and Granberg, H. B. (1988). Scheferville snow-ground interface temperatures. In *Fifth International Conference on Permafrost, Trondheim, Norway*. Tapir, Trondheim, *1*, 67-72

Dick, L. (2012, October 5). Ice wedge polygons [Blog post], Retrieved Jan 2, 2018, from: http://www.alaskaphotoworld.com/alaska365/2012/10/05/ice-wedge-polygons/

Dong, Y., Mccartney, J. S., & Lu, N. (2015). Critical Review of Thermal Conductivity Models for Unsaturated Soils, (March). https://doi.org/10.1007/s10706-015-9843-2

Ducklow, H., Fraser, W., McClintock, J. (2008). Ecological responses to climate change on the Antarctic Peninsula: the peninsula is an icy world that is warming faster than anywhere else on Earth, threatening a rich but delicate biological community. *American Scientist*, (96), 302–310.

Erickson, T. A., Williams, M. W., & Winstral, A. (2005). Persistence of topographic controls on the spatial distribution of snow in rugged mountain terrain, Colorado , United States, 41, 1–17. https://doi.org/10.1029/2003WR002973

Etzelmüller, B., Flo Heggem, E. S., Sharkhuu, N., Frauenfelder, R., Kääb, A., & Goulden, C. (2006). Mountain permafrost distribution modelling using a multi-criteria approach in the Hövsgöl area, Northern Mongolia. *Permafrost and Periglacial Processes*, *17*(2), 91–104. https://doi.org/10.1002/ppp.554

Farouki, O.T. (1981).Thermal properties of soils. Cold Regions Science and Engineering. *CRREL Monograph*, *1*, 81–136.

Ferreira, A., Vieira, G., Ramos, M., & Nieuwendam, A. (2016). Ground temperature and permafrost distribution in Hurd Peninsula (Livingston Island, Maritime Antarctic): An assessment using freezing indexes and TTOP modelling. *Catena*, (149), 560–571. https://doi.org/10.1016/j.catena.2016.08.027

Fitzpatrick, R. (2006, Februalry 02). *The adiabatic atmosphere*. Retrieved 2018, May 15 from: http://farside.ph.utexas.edu/teaching/sm1/lectures/node56.html

Fox, A.J., Cooper, P.R. (1994). Measured properties of the Antarctic Ice Sheet derived from the SCAR digital database. *Polar Record*, 30-201.

Frauenfeld, O. W., Zhang, T., & Mccreight, J. L. (2007). Northern hemisphere freezing / thawing index variations over the twentieth century, *63*(July 2006), 47–63. https://doi.org/10.1002/joc

GNT-P (2018). The Global Terrestrial Network for Permafrost. *International Permafrost Association*. Retrieved Aug, 31 from: https://ipa.arcticportal.org/products/gtn-p.

Goodrich, L.E. 1982. The influence of snow cover on the ground thermal regime. *Canadian Geotechnical Journal*, (19), 421–432.

Goyanes, G., Vieira, G., Caselli, A.,Mora, C., Ramos, M., de Pablo,M.A., Neves, M., Santos, F., Bernardo, I., Gilichinsky, D., Abramov, A., Batista, V., Melo, R., Nieuwendam, A., Ferreira, A., Oliva, M. (2014). Régimen térmico y variabilidad espacial de la capa activa en isla Decepción, Antártida. *Rev. Asoc. Geol. Argent.*, *71* (1), 112–124.

Grosse, G., Goetz, S., McGuire, A. D., Romanovsky, V. E., & Schuur, E. A. G. (2016). Changing permafrost in a warming world and feedbacks to the Earth system. *Environmental Research Letters*, *11*(4). https://doi.org/10.1088/1748-9326/11/4/040201

Guglielmin, M., (2011). Advances in permafrost and periglacial research in Antarctica: a review. *Geomorphology*, (155-156), 1–6.

Guglielmin, M., Worland, M.R., Cannone, N. (2012). Spatial and temporal variability of ground surface temperature and active layer thickness at the margin of maritime Antarctica, Signy Island. *Geomorphology*, *(*155–156), 20–33.

Hallet, B. (2013). Stone circles: form and soil kinematics. *Philosophical transactions. Series A, Mathematical, physical, and engineering sciences, 371 2004*, 20120357.

Hansen; et al. (2007). "Viability, diversity and composition of the bacterial community in a high Arctic permafrost soil from Spitsbergen, Northern Norway". *Environmental Microbiology*, (9), 2870–2884. Retrieved from: doi:10.1111/j.1462-2920.2007.01403.x.

Harris SA. 1981. Climatic relationships of permafrost zones in areas of low winter snow-cover. *Arctic, 36*(1): 64–70.

Harris, S.A. (2001). Twenty years of data on climate-permafrost-active layer variations at the lower limit of alpine permafrost, Marmot Basin, Jasper National Park, Canada. *Geografiska Annaler, 83A* (1-2), 1-14.

Hauck C, Vieira G, Gruber S, Blanco JJ, Ramos M. (2007). Geophysical identification of permafrost in Livingston Island, Maritime Antarctic. *Journal of Geophysical Research,* (112), F02S19. doi:10.1029/2006JF000544.

Hugget RJ, Cheesman J. (2002). Topography and the Environment. Longman: London.

Humlum O. (1997). Active layer thermal regime at Three Rock Glaciers in Greenland. *Permafrost and Periglacial Processes, 8*, 383–408.

Humlum, O. (1998). Active layer thermal regime 1991-1996 at Qeqertarsuaq, Disko Island, central Greenland. *Arctic Alpine Res., 30*(3), 295-305.

Huschke RE (ed.). (1959). Glossary of Meteorology, 1st edn. *American Meteorological Society*. Boston, MA. 638.

Ingólfsson, O. (2008). Quaternary Geology. Retrieved Jan 2, 2018, from: https://notendur.hi.is/oi/quaternary_geology.htm

IPCC (2007). Summary for Policymakers. In: Climate Change 2007: The Physical Science Basis. Working Group I Contribution to the Fourth Assessment Report of the Intergovernmental Panel on Climate Change (eds Solomon, S., Qin, D., Manning, M., Chen, Z., Marquis, M., et al.). Cambridge University Press, Cambridge, United Kingdom and New York, NY, USA.

Jost, G., Weiler, M., Gluns, D. R., & Alila, Y. (2007). The influence of forest and topography on snow accumulation and melt at the watershed-scale, 101–115. https://doi.org/10.1016/j.jhydrol.2007.09.006

Karunaratne, K.C., and Burn, C.R. (2003). Freezing n-factors in discontinuous permafrost terrain, Takhini River, Yukon Territory, Canada. In *Proceedings of the 8th International Conference on Permafrost. University of Zurich-Irchel, Zürich, Switzerland*, 519–524.

Lachenbruch, A.H., Sass, J.H., Mrshal, B. V., Moses, T. H., Munroe, R. J., Smith, E. P. (1981). Geothermal studies in Alaska; conditions at Prudhoe Bay In *The United States Geological Survey in Alaska*, 19-20.

Lanouette, F., Doré, G., & Lemieux, C. (2015). Influence of snow cover on the ground thermal regime along an embankment built on permafrost: In-situ measurements. https://doi.org/10.13140/RG.2.1.2482.1848

Lewkowicz, A. G., Bonnaventure, P. P., Smith, S. L., and Kuntz, Z. (2012). Spatial and thermal characteristics of mountain permafrost, Northwest Canada, *Geogr. Ann. A*, (94), 195–215. https://doi.org/10.1111/j.1468-0459.2012.00462.x.

Ling, F. and Zhang, T. (2003). Impact of the timing and duration of seasonal snow cover on the active layer and permafrost in the Alaskan, Arctic, *Permafrost Periglac., (*14), 141–150. https://doi.org/10.1002/ppp.445, 2003.

Lopez-Terrill, V. (Last updated: 2014, Nov 10). Tundra Biome. Colorado State University Libraries. Retrieved 2018, Jan 13 from: http://lib2.colostate.edu/wildlife/tundra-biome.html

Maslanik, J., Yu, Y. (2010). Collavorative research: The impact of Arctic storms on land fast ice variations. *Polar Science Center*. Retrieved Feb 12, 2018 from: http://psc.apl.washington.edu/nonwp_projects/landfast_ice/freezing.php

Mitchell, J.K., Soga, K. (2005). Fundamentals of soil behaviour. Wiley, New York.

Muralikrishna, I. V., Manickam, V. (2017). Air Pollution Control Technologies. *ScienceDirect*. Retrieved Sept 3, 2018 from: https://www.sciencedirect.com/topics/earth-and-planetary-sciences/adiabatic-lapse-rate

Papale, D., Agarwal, D. A., Baldocchi, D., Cook, R. B., Fisher, J. B., and van Ingen, C. (2012). Database maintenance, data sharing policy, collaboration, in: *Eddy Covariance, Springer, the Netherlands*.

Peduzzi, P., Concato, J.,Kemper, E., Holford, T., Feinstein, A. (1996). A simulation study of the number of events per variable in logistic regression analysis. *Journal of Clinical Epidemiology*, *49* (12), 1373–1379. doi:10.1016/s0895-4356(96)00236-3.

Péwé, T. (2016). Permafrost. In *Encyclopaedia Britannica*. Encyclopædia Britannica, inc. Retrieved from https://www.britannica.com/science/permafrost

Péwé, T.L. (1979). Permafrost and its Effects on Human Activities in Arctic and Subarctic Regions. *GeoJournal*, 3 (333). https://doi.org/10.1007/BF00221235

Ramos M, Hassler A, Vieira G, Hauck C, Gruber S. (2009a). Setting up boreholes for permafrost thermal monitoring on Livingston Island in the Maritime Antarctic. *Permafrost and Periglacial Processes*, (20), 57–64. DOI: 10.1002/ppp.635.

Ramos M, Vieira G, Gilichinsky D, De Pablo MA. (2009b). Establecimiento de estaciones de medida del régimen térmico del permafrost en el área de 'Crater Lake'. Isla Decep- ción (Antártida). *II Iberian Congress of the International Permafrost Association, Siguenza, Spain*, 21-23 June.

Ramos M, Vieira G. (2009). Evaluation of the ground surface enthalpy balance from bedrock shallow borehole temperatures (Livingston Island, Maritime Antarctic). *The Cryosphere*, (3), 133–145. www.the-cryosphere.net/3/ 133/2009

Ramos, M., de Pablo, M.A., Vieira, G., Molina, A., Abramov, A., Goyanes, G. (2017). Recent shallowing of the thaw depth at Crater Lake, Deception Island, Antarctica (2006–2014). *CATENA*, *149* (2), 519-528.

Riseborough, D. W. (2003). Thawing and freezing indices in the active layer. *Geological Survey of Canada*, 953-958.

Romanovsky, V.E. and Osterkamp, T.E. (1995). Interannual variations of the thermal regime of the active layer and near-surface permafrost in northern Alaska. *Permafrost and Periglacial Processes*, (6), 313-335.

Romanovsky, V.E., Smith, S.L., and Christiansen, H.H. (2010). Permafrost Thermal State in the Polar Northern Hemisphere during the International Polar Year 2007-2009: a synthesis. *Permafrost Periglacial Proc.*, (21), 106- 116.

Schaefer, K. , Lantuit, H. , Romanovsky, V. and Schuur, E. A. G. (2012). *Policy Implications of Warming Permafrost* (United Nations Environment Programme Special Report). Retrieved from: http://epic.awi.de/33086/1/permafrost.pdf

Schaefer, K., Lantuit, H., Romanovsky, V. E., Schuur, E.A.G., Witt, R. (2014). The impact of the permafrost carbon feedback on global climate. *Environmental Research Letters*, 9(8), 085003. DOI: 10.1088/1748-9326/9/8/085003

Schuur, E. A. G., et al. (2015). Climate change and the permafrost carbon feedback. *Nature*, (520), 171–9.

Shaw, D. V. (2015, July 3). Tundra Polygons: The Key to Arctic Diversity [Blog post], Retrieved Jan 2, 2018, from: http://www.david-w-shaw.com/tundra-polygons-the-key-to-arctic-diversity/

Shur, Y.L., and Jorgenson, M.T. (2007). Patterns of permafrost formation and degradation in relation to climate and ecosystems. *Permafrost Periglacial Processes*, *18*(1), 7–19. doi:10.1002/ppp.582.

Smith, C.A.S., Burn, C.R., Tarnocai, C. and Sproule, B. (1998). Air and soil temperature relations along an ecologi- cal transect through the permafrost zones of northwestern Canada. In *Proceedings 7th International Conference on Permafrost, Yellowknife, Canada*. *Nordicana, QuŽbec,* 1009-1016.

Smith, L. C., Y. Sheng, G. M. MacDonald, and L. D. Hinzman (2005), Disappearing Arctic Lakes, *Science, 308*(5727), 1429.

Smith, M. W., & Riseborough, D. W. (1996). Permafrost Monitoring and Detection of Climate Change. *Permafrost and Periglacial Processes, 7*, 301-309.

Smith, S.L., Romanovsky, V.E., Lewkowicz, A.G., Burn, C.R. Allard, M., Clow, G.D., Yoshikawa, K. and Throop, J. (2010). Thermal State of Permafrost in North America – A Contribution to the International Polar Year. *Permafrost Periglacial Proc., 21*, 117-135.

Staff (2014). What is permafrost). International Permafrost Association. Retrieved 2014, Feb 28.

Stammerjohn, S.E., Martinson, D.G., Smith, R.C., Yuan, X., Rind, D., 2008. Trends in Ant- arctic annual sea ice retreat and advance and their relation to El Niño–Southern Oscillation and Southern Annular Mode variability. *Journal of Geophysical Research*, 113, C03S90. http://dx.doi.org/10.1029/2007JC004269.

Statistical Solutions (2018a). Correlation (Pearson, Kendall, Spearman). StatisticsSolutions. Retrieved Apr 20, 2018, from: http://www.statisticssolutions.com/correlation-pearson-kendall-spearman/

Statistical Solutions (2018b). Assumptions of Multiple Linear Regression. StatisticsSolutions. Retrieved Apr 20, 2018, from: http://www.statisticssolutions.com/assumptions-of-multiple-linear-regression

Statistical Solutions (2018c). Testing assumptions of Multiple Linear Regression in SPSS. StatisticsSolutions. Retrieved Apr 20, 2018, from: http://www.statisticssolutions.com/testing-assumptions-of-linear-regression-in-spss/

Stocker-Mittaz, C., Hoelzle, M. and Haeberli, W. (2002). Modelling alpine permafrost distribution based on energy-balance data: a first step. *Permafrost Periglacial Proc., 13*(4), 271-282.

Sulebak JR, Tallaksen LM, Erichsen B. 2000. Estimation of areal soil moisture by use of terrain data. *Geografiska Annaler, 82A*, 89–105.

Taylor, A.E. (1995). Field measurements of n-factors for natur- al forest areas, Mackenzie Valley, Northwest Territories. In *Current Research, Geological Survey of Canada, 1995-B*, 89-98.

Turner, J., Bindschadler, R., Convey, P., et al. (2009). Antarctic climate change and the environment. Scientific Committee on Antarctic Research. Cambridge, England.

Turner, J., Colwell, S.R., Marshall, G.J., Lachlan-Cope, T.A., Carleton, A.M., Jones, P.D., Lagun, V., Reid, P.A., Iagovkina, S. (2005). Antarctic climate change during the last 50 years. *International Journal of Climatology, 25*, 279–294.

Turner, J., Lu, H.,White, I., King, J.C., Phillips, T., Scott Hosking, J., Bracegirdle, T.J.,Marshall, G.J.,Mulvaney, R., Deb, P. (2016). Absence of 21st century warming on Antarctic Pen- insula consistent with natural variability. *Nature*, 535. http://dx.doi.org/10.1038/ nature18645.

U.S. Army/Air Force. 1966. Arctic and subarctic construction: general provisions. U.S. Government Printing Office: Washington, DC., USA. Technical Manual TM-852-1/AFM, (48), 88-19.

Ullrich, C. (2016, July). Permafrost. *National Geographic*. Retrieved Jan 3, 2018 from: http://ngm.nationalgeographic.com/geopedia/Permafrost

Umweltbundesamt (2016). Climate of the Antarctic. Retrieved on Aug 31, 2018 from: https://www.umweltbundesamt.de/en/climate-of-the-antarctic

UNEP (2012). United Nations Environment Programme. Thawing of permafrost expected to cause significant additional global warming, not yet accounted for in climate predictions. *ScienceDaily*. Retrieved December 24, 2017 from www.sciencedaily.com/releases/2012/11/121127094250.htm

Vaughan, D.G., Marshall, G.J., Connolley, W.M., Parkinson, C., Mulvaney, R., Hodgson, D.A., King, J.C., Pudsey, C.J., Turner, J. (2003). Recent rapid regional climate warming on the Antarctic Peninsula. Climatic Change., (60), 243–274.

Vieira, G., Lopez-Martinez, J., Serrano, E., Ramos, M., Gruber, S., Hauck, C., Blanco, J.J. (2008). Geomorphological observations of permafrost and ground-ice degradation on Deception and Livingston Islands, Maritime Antarctica. In Proceedings of the 9th International Conference on Permafrost, 29 June–3 July 2008, Fairbanks, Alaska, Extended Abstracts, Vol. 1, Kane D, Hinkel K (eds). University of Alaska Press: Fair- banks, 1839–1844.

Vieira, G., Ramos, M., Gruber, S., Hauck, C., Blanco, J. (2007). The permafrost environment of northwest Hurd Peninsula (Livingston Island, maritime Antarctic): Preliminary results. USGS OF-2007-1047, Extended Abstract 2, U.S. Geological Survey and the National Academies.

Vieira, G., Ramos, M., Trindade, A., Gruber, S., Hauck, C., Mora, C., Batista, V., Neves, M., Pimpirev, C., Kenderova, R., De Pablo, M.A. (2009). Spatial distribution and characteristics of permafrost in Hurd Peninsula, Livingston Island, Maritime Antarctic. Geophysical Research Abstracts, European Geosciences Union: Vienna.

Vieira, G. (2009). The International Polar Year 2007–08 and the development of Portuguese research on Antarctic permafrost. Finisterra- Revista Portuguesa de Geografia, (87), 83–94.

Vieira,G., Bockheim,J., Guglielmin,M., Balks,M., Abramov,A.A., Boelhouwers, J.,Cannone,N., Ganzert, L., Gilichinsky, D.A., Goryachkin, G., López-Martínez, J., Meiklejohn, J., Raffi,R., Ramos, M.,Schaefer, C., Serrano,E., Simas, F., Sletten,R., Wagner,D. (2010). Thermal state of permafrost and active-layer monitoring in the Antarctic: advances during the International Polar Year 2007–2009. Permafrost and Periglacial Processes, (21), 182–197.

Way, R. G., Lewkowicz, A. G., & Gajewski, K. (2016). Modelling the spatial distribution of permafrost in Labrador–Ungava using the temperature at the top of permafrost. Canadian Journal of Earth Sciences, 53(10), 1010–1028. https://doi.org/10.1139/cjes-2016-0034

Wilhelm, K. R., Bockheim, J. G., & Haus, N. W. (2016b). Geoderma Properties and processes of recently established soils from deglaciation of Cierva Point , Western Antarctic Peninsula, (277), 10–22. https://doi.org/10.1016/j.geoderma.2016.05.001

Wilhelm, K., & Bockheim, J. (2016a). Influence of soil properties on active layer thermal propagation along the western Antarctic Peninsula. https://doi.org/10.1002/esp.3926

Williams, P. J., and M. W. Smith (1989), The Frozen Earth: Fundamentals of Geocryology, (pp. 306). Cambridge Univ. Press, New York.

Wu, Q., & Shi, B. (2003). Application of models for calculating thermal offset and annual mean permafrost-surface temperature (AMPST). In Permafrost research on the Qinghai-Tibet Plateau, 1–6.

Yun, T.S., Santamarina, J.C. (2008). Fundamental study of thermal conduction in dry soils. *Granular Matter*, (10),197.

Zhang, T. (2005). Influence of the seasonal snow cover on the ground thermal regime: An overview, *Reviews of Geophysics*, (43), RG4002. doi:10.1029/2004RG000157.

Zhang, T., Barry, R.G., Knowles, K. Heginbottom, J.A., and J. Brown, J. (1999). Statistics and characteristics of permafrost and ground ice distribution in the Northern Hemisphere. *Polar Geography*, *23*(2), 147-169.

Zhao, Y., Peth, S., Horn, R. (2010). Modeling of coupled water and heat fluxes in both unfrozen and frozen soils. In *19th World Congress of Soil Science*, 113–116.

Zoltikov, I.A. (1962), Heat regime of the central Antarctic glacier, In *Antarctica, Reports of the Commission, 1961* (pp. 27–40), Publishing House of the Academy of Sciences of the USS.

ANNEX

A.1 Tables with Maximum, Minimum and Mean annual ground temperatures in complete years 1 and 2 (from Mar2012 to Mar 2014) for the 9 boreholes.

Site 1- PERMAFROST

Ground Annual Temperatures (ºC)

Natural Year	Period Range	Depth	-5cm	-20cm	-40cm	-80cm	-120cm	-160cm	-200cm	-250cm	-300cm	-350cm	-400cm	-500cm	-550cm	-600cm	-700cm	-800cm	-1000cm	-1250cm	-1500cm
Year 1: 2012/13	23-Mar-12	Max 1	-	6.461	5.851	4.259	3.106	2.400	1.885	1.339	1.071	0.838	0.643	0.202	0.002	-0.198	-0.542	-0.662	-0.927	-0.982	-1.035
	-	Mean 1	-	-1.594	-1.700	-1.543	-1.456	-1.461	-1.431	-1.410	-1.447	-1.421	-1.331	-1.288	-1.287	-1.286	-1.300	-1.254	-1.250	-1.171	-1.161
	22-Mar-13	Min 1	-	-5.804	-5.478	-4.572	-3.948	-3.490	-3.135	-2.887	-2.747	-2.597	-2.408	-2.141	-2.052	-1.971	-1.862	-1.730	-1.554	-1.359	-1.287
Year 2: 2013/14	23-Mar-13	Max 2	-	4.485	3.727	2.887	2.152	1.871	1.650	1.370	0.899	0.548	0.320	0.080	-0.237	-0.429	-0.458	-0.646	-0.840	-0.894	-0.926
	-	Mean 2	-	-1.583	-1.636	-1.461	-1.483	-1.268	-1.375	-1.386	-1.259	-1.278	-1.264	-1.083	-1.185	-1.251	-1.154	-1.158	-1.135	-1.090	-1.056
	10-Mar-14	Min 2	-	-4.086	-4.007	-3.657	-3.469	-3.093	-3.024	-2.874	-2.588	-2.471	-2.358	-1.947	-1.992	-1.998	-1.705	-1.651	-1.395	-1.296	-1.303
Average Years 1&2		Max	6.00	5.47	4.79	3.57	2.63	2.14	1.77	1.35	0.99	0.69	0.48	0.14	-0.12	-0.31	-0.50	-0.65	-0.88	-0.94	-0.98
		Mean	-1.60	-1.59	-1.67	-1.50	-1.47	-1.36	-1.40	-1.40	-1.35	-1.35	-1.30	-1.19	-1.24	-1.27	-1.23	-1.21	-1.19	-1.13	-1.11
		Min	-5.05	-4.95	-4.74	-4.11	-3.71	-3.29	-3.08	-2.88	-2.67	-2.53	-2.38	-2.04	-2.02	-1.98	-1.78	-1.69	-1.47	-1.33	-1.30

Site 2- SUMMIT

Ground Annual Temperatures (ºC)

Natural Year	Period Range	Depth	-5cm	-15cm	-40cm	-60cm	-80cm	-100cm	-120cm	-140cm	-160cm	-180cm
Year 1: 2012/13	23-Mar-12	Max 1	13.08	12.76	10.28	8.91	7.21	5.98	5.23	4.13	3.17	2.47
	-	Mean 1	-1.70	-1.65	-1.68	-1.70	-1.79	-1.92	-1.81	-1.85	-2.02	-2.00
	22-Mar-13	Min 1	-8.47	-8.08	-7.08	-6.39	-5.96	-5.75	-5.38	-5.12	-5.07	-4.76
Year 2: 2013/14	23-Mar-13	Max 2	12.00	13.01	10.16	8.34	6.84	5.60	4.49	3.72	3.18	2.69
	-	Mean 2	-2.10	-1.84	-1.82	-1.87	-1.97	-1.95	-1.95	-1.90	-1.96	-1.98
	10-Mar-14	Min 2	-10.32	-9.63	-8.64	-8.13	-7.62	-7.14	-6.74	-6.25	-5.98	-5.79
Average Years 1&2		Max	12.54	12.88	10.22	8.62	7.03	5.79	4.86	3.93	3.17	2.58
		Mean	-1.90	-1.74	-1.75	-1.79	-1.88	-1.93	-1.88	-1.88	-1.99	-1.99
		Min	-9.39	-8.85	-7.86	-7.26	-6.79	-6.45	-6.06	-5.69	-5.53	-5.27

Site 3- BELOW SUMMIT

Ground Annual Temperatures (ºC)

Natural Year	Period Range	Depth	-5cm	-15cm	-40cm	-60cm	-80cm	-100cm	-120cm	-140cm	-160cm	-180cm
Year 1: 2012/13	23-Mar-12	Max 1	8.30	7.21	5.05	3.95	2.81	2.16	1.74	1.36	1.07	0.72
	-	Mean 1	-2.09	-2.07	-2.09	-2.12	-2.24	-2.28	-2.23	-2.21	-2.24	-2.28
	22-Mar-13	Min 1	-6.03	-5.74	-5.25	-4.99	-4.93	-4.81	-4.66	-4.54	-4.48	-4.35
Year 2: 2013/14	23-Mar-13	Max 2	7.96	8.45	6.13	4.74	3.65	0.86	0.88	0.83	1.03	0.60
	-	Mean 2	-2.27	-2.00	-2.08	-2.15	-2.25	0.21	0.29	0.30	-2.25	-2.28
	10-Mar-14	Min 2	-8.70	-8.16	-7.45	-7.01	-6.75	0.03	0.15	0.18	-5.57	-5.38
Average Years 1&2		Max	8.13	7.83	5.59	4.34	3.23	2.16	1.74	1.36	1.05	0.66
		Mean	-2.18	-2.04	-2.09	-2.13	-2.25	-2.28	-2.23	-2.21	-2.25	-2.28
		Min	-7.37	-6.95	-6.35	-6.00	-5.84	-4.81	-4.66	-4.54	-5.02	-4.87

Site 4- SADDLE

Ground Annual Temperatures (ºC)

Natural Year	Period Range	Depth	-5cm	-15cm	-40cm	-60cm	-80cm	-100cm	-120cm
Year 1: 2012/13	23-Mar-12	Max 1	8.68	7.35	4.09	2.32	1.39	0.73	0.23
	-	Mean 1	-2.13	-2.08	-2.11	-2.07	-2.03	-2.03	-2.13
	22-Mar-13	Min 1	-8.31	-7.73	-5.95	-5.05	-4.70	-4.42	-4.31
Year 2: 2013/14	23-Mar-13	Max 2	6.09	5.46	4.22	3.59	3.08	2.63	2.18
	-	Mean 2	-1.21	-1.14	-1.17	-1.13	-1.10	-1.12	-1.18
	10-Mar-14	Min 2	-4.47	-4.36	-4.17	-3.97	-3.81	-3.66	-3.54
Average Years 1&2		Max	7.39	6.40	4.15	2.95	2.23	1.68	1.21
		Mean	-1.67	-1.61	-1.64	-1.60	-1.56	-1.58	-1.65
		Min	-6.39	-6.04	-5.06	-4.51	-4.26	-4.04	-3.93

Site 5- MORAINE

Ground Annual Temperatures (ºC)

Natural Year	Period Range	Depth	-5cm	-15cm	-40cm	-60cm	-80cm	-100cm	-120cm	-140cm	-160cm	-180cm
Year 1: 2012/13	23-Mar-12	Max 1	10.00	8.35	4.07	2.82	1.19	0.23	0.28	0.14	0.17	0.08
	-	Mean 1	-1.81	-1.74	-2.02	-2.11	-2.21	-2.32	-2.26	-2.29	-2.23	-2.26
	22-Mar-13	Min 1	-13.19	-10.69	-7.88	-6.84	-5.95	-5.37	-5.05	-4.88	-4.67	-4.57
Year 2: 2013/14	23-Mar-13	Max 2	6.78	6.16	5.10	2.96	1.88	0.22	0.23	0.10	0.04	-0.01
	-	Mean 2	-1.69	-1.68	-2.09	-2.22	-2.40	-2.55	-2.51	-2.54	-2.50	-2.55
	10-Mar-14	Min 2	-13.19	-10.69	-7.88	-6.84	-5.95	-5.37	-5.05	-4.88	-4.67	-4.57
Average Years 1&2		Max	8.39	7.25	4.58	2.89	1.53	0.23	0.26	0.12	0.10	0.04
		Mean	-1.75	-1.71	-2.05	-2.17	-2.31	-2.44	-2.38	-2.42	-2.37	-2.41
		Min	-13.19	-10.69	-7.88	-6.84	-5.95	-5.37	-5.05	-4.88	-4.67	-4.57
		Max modified	8.24	7.10	4.43	2.74	1.38	0.00	0.00	0.00	0.00	0.00
		Mean modified	-1.89	-1.86	-2.20	-2.31	-2.46	-2.59	-2.53	-2.56	-2.52	-2.55
		Min modified	-13.34	-10.84	-8.03	-6.98	-6.10	-5.52	-5.20	-5.02	-4.82	-4.72

Site 6- MIDSLOPE										
Ground Annual Temperatures (ºC)										
Natural Year	Period Range	Depth	-5cm	-15cm	-40cm	-60cm	-80cm	-100cm	-120cm	-140cm
Year 1: 2012/13	23-Mar-12	Max 1	9.18	8.55	6.47	5.79	4.84	4.36	3.91	3.42
	-	Mean 1	-0.92	-0.66	-0.73	-0.68	-0.70	-0.69	-0.68	-0.79
	22-Mar-13	Min 1	-6.65	-5.71	-4.76	-4.05	-3.42	-3.21	-2.96	-2.87
Year 2: 2013/14	23-Mar-13	Max 2	-	-	-	-	-	-	-	-
	-	Mean 2	-	-	-	-	-	-	-	-
	10-Mar-14	Min 2	-	-	-	-	-	-	-	-
Average Years 1&2		Max	9.18	8.55	6.47	5.79	4.84	4.36	3.91	3.42
		Mean	-0.92	-0.66	-0.73	-0.68	-0.70	-0.69	-0.68	-0.79
		Min	-6.65	-5.71	-4.76	-4.05	-3.42	-3.21	-2.96	-2.87

Site 7- MOSS-ROCK												
Ground Annual Temperatures (ºC)												
Natural Year	Period Range	Depth	-5cm	-15cm	-40cm	-60cm	-80cm	-100cm	-120cm	-140cm	-160cm	-180cm
Year 1: 2012/13	23-Mar-12	Max 1	11.50	10.03	6.80	5.48	4.40	3.67	3.08	2.60	2.08	1.77
	-	Mean 1	-0.27	-0.28	-0.42	-0.63	-0.59	-0.63	-0.69	-0.67	-0.74	-0.73
	22-Mar-13	Min 1	-10.37	-9.29	-6.98	-5.91	-4.70	-4.16	-3.83	-3.54	-3.35	-3.08
Year 2: 2013/14	23-Mar-13	Max 2	10.75	9.69	6.80	5.23	4.27	3.46	2.86	2.39	2.05	1.77
	-	Mean 2	-0.40	-0.46	-0.66	-0.75	-0.78	-0.84	-0.87	-0.90	-0.88	-0.85
	10-Mar-14	Min 2	-8.76	-8.04	-7.04	-6.37	-5.74	-5.29	-4.88	-4.56	-4.17	-3.84
Average Years 1&2		Max	11.13	9.86	6.80	5.35	4.34	3.57	2.97	2.49	2.06	1.77
		Mean	-0.33	-0.37	-0.54	-0.69	-0.69	-0.74	-0.78	-0.79	-0.81	-0.79
		Min	-9.56	-8.67	-7.01	-6.14	-5.22	-4.73	-4.36	-4.05	-3.76	-3.46

Site 8- MOSS-MOSS												
Ground Annual Temperatures (ºC)												
Natural Year	Period Range	Depth	-5cm	-15cm	-40cm	-60cm	-80cm	100cm	-120cm	-140cm	-160cm	-180cm
Year 1: 2012/13	23-Mar-12	Max 1	6.77	3.29	0.28	0.24	0.22	0.28	0.34	0.25	0.36	0.32
	-	Mean 1	-0.66	-0.82	-0.99	-0.96	-0.93	-0.86	-0.82	-0.89	-0.80	-0.81
	22-Mar-13	Min 1	-9.06	-6.89	-4.62	-3.97	-3.63	-3.37	-3.15	-3.03	-2.78	-2.63
Year 2: 2013/14	23-Mar-13	Max 2	6.90	4.27	0.21	0.23	0.15	0.22	0.22	-	0.23	0.26
	-	Mean 2	-1.34	-1.16	-1.22	-1.11	-1.20	-1.10	-1.04	-	-1.02	-0.93
	10-Mar-14	Min 2	-10.00	-7.65	-5.68	-4.81	-4.54	-4.22	-3.97	-	-3.56	-3.33
Average Years 1&2		MaxAGT	6.83	3.78	0.25	0.24	0.19	0.25	0.28	0.25	0.29	0.29
		MAGT	-1.00	-0.99	-1.10	-1.03	-1.06	-0.98	-0.93	-0.89	-0.91	-0.87
		MinAGT	-9.53	-7.27	-5.15	-4.39	-4.08	-3.79	-3.56	-3.03	-3.17	-2.98
		Max modified	6.58	3.52	0.00	0.00	0.00	0.00	0.00	0.00	0.00	0.00
		Mean modified	-1.25	-1.24	-1.35	-1.27	-1.25	-1.23	-1.21	-1.15	-1.20	-1.16
		Min modified	-9.78	-7.53	-5.40	-4.63	-4.27	-4.04	-3.84	-3.28	-3.47	-3.27

Site 9- LOW-DEEP																	
Ground Annual Temperatures (ºC)																	
Natural Year	Period Range	Depth	-5cm	-15cm	-40cm	-60cm	-80cm	-100cm	-120cm	-140cm	-160cm	-180cm	-200cm	-250cm	-300cm	-350cm	-400cm	-430cm
Year 1: 2012/13	23-Mar-12	Max 1	-	11.86	10.94	10.25	9.63	8.88	8.00	7.44	6.94	6.50	6.00	4.50	3.75	3.13	2.81	2.77
	-	Mean 1	-	-0.99	-1.00	-1.01	-0.65	-0.74	-0.69	-0.84	-0.66	-0.48	-0.38	-0.81	-0.65	-0.49	-0.44	-0.43
	22-Mar-13	Min 1	-	-12.92	-11.13	-9.81	-8.13	-7.19	-6.38	-6.00	-5.00	-4.50	-4.00	-4.00	-3.06	-2.50	-2.00	-2.00
Year 2: 2013/14	23-Mar-13	Max 2	-	11.86	11.40	10.51	9.84	8.89	7.82	7.12	6.46	5.99	5.60	4.78	4.03	3.20	2.85	2.63
	-	Mean 2	-	-0.64	-0.36	-0.43	-0.32	-0.31	-0.32	-0.37	-0.36	-0.34	-0.32	-0.36	-0.31	-0.29	-0.11	-0.13
	10-Mar-14	Min 2	-	-10.41	-9.11	-8.38	-7.48	-6.76	-6.15	-5.70	-5.30	-4.95	-4.64	-4.08	-3.51	-2.90	-2.30	-2.14
Average Years 1&2		Max	12.32	11.86	11.17	10.38	9.73	8.88	7.91	7.28	6.70	6.25	5.80	4.64	3.89	3.16	2.83	2.70
		Mean	-0.87	-0.81	-0.68	-0.72	-0.48	-0.52	-0.51	-0.60	-0.51	-0.41	-0.35	-0.59	-0.48	-0.39	-0.28	-0.28
		Min	-12.00	-11.67	-10.12	-9.10	-7.80	-6.97	-6.26	-5.85	-5.15	-4.72	-4.32	-4.04	-3.29	-2.70	-2.15	-2.07